


12-2014

# Indirect Matrix Converter as Standard Power Electronic Interface

Andrés Escobar-Mejía  
*University of Arkansas, Fayetteville*

Follow this and additional works at: <http://scholarworks.uark.edu/etd>

 Part of the [Electronic Devices and Semiconductor Manufacturing Commons](#), and the [Power and Energy Commons](#)

---

## Recommended Citation

Escobar-Mejía, Andrés, "Indirect Matrix Converter as Standard Power Electronic Interface" (2014). *Theses and Dissertations*. 2003.  
<http://scholarworks.uark.edu/etd/2003>

This Dissertation is brought to you for free and open access by ScholarWorks@UARK. It has been accepted for inclusion in Theses and Dissertations by an authorized administrator of ScholarWorks@UARK. For more information, please contact [scholar@uark.edu](mailto:scholar@uark.edu), [ccmiddle@uark.edu](mailto:ccmiddle@uark.edu).

Indirect Matrix Converter  
as Standard Power Electronic Interface

Indirect Matrix Converter  
as Standard Power Electronic Interface

A dissertation submitted in partial fulfillment  
of the requirements for the degree of  
Doctor of Philosophy in Electrical Engineering

by

Andres Escobar Mejia  
Universidad Tecnologica de Pereira  
Bachelor in Electrical Engineering, 2002  
Universidad Tecnologica de Pereira  
Master of Science in Electrical Engineering, 2006

December 2014  
University of Arkansas

This dissertation is approved for recommendation to the Graduate Council.

---

Dr. Juan Carlos Balda  
Dissertation Director

---

Dr. Roy McCann  
Committee Member

---

Dr. UcheWejinya  
Committee Member

---

Dr. Simon Ang  
Committee Member

## ABSTRACT

The increase in the penetration levels of distributed generation in the modern power grid and its importance in future energy systems have accelerated the interest of developing new power electronic interfaces for the energy conversion process. The feasibility of applying the indirect matrix converter as the standard power electronic interface for applications with power ratings from several kW to few MW is addressed in this dissertation. Special attention is given to those applications where space dominates the power electronic requirements. The main motivation for using the indirect matrix converter is that eliminates the energy storage component in the way of a dc-link capacitor for the energy conversion process. This contributes to reduce size and weight, and potentially, increase reliability of the power electronic interface. Two main new contributions are presented. First, a new power electronic interface that allows the connection of two ac power grids through a medium- or high-voltage dc system is proposed. The new topology contemplates the use of two high-voltage dc-link converters based on the modular multilevel converter, two indirect matrix converters and two medium-frequency transformers. Second, a new sensorless control technique working in the  $d - q$  reference is developed. The controller is used to interface a distributed generation unit to the power grid when the indirect matrix converter is used as the power electronic interface. The design and performance of the proposed power electronic interface is validated through time-domain simulations and a laboratory prototype is built to experimentally validate the sensorless controller.

## **ACKNOWLEDGEMENTS**

First, I would like to thank my wife, Claudia Lorena Grisales, who shared with me 3 years of her life here in Fayetteville. I would like to extend my sincere regards to Dr. Juan Carlos Balda and the members of my committee for the comments and support during this process. I would like to thank also to my friend and mentor Didier Giraldo Buitrago. Thanks also to the Steiner family: Jere, Jennifer, Caleb, Tyler and Grace because they hosted me for five years and I really felt like a family member. I would also like to thank my lab mates: Arthur K. Barnes, Austin Curbow, Corris Stewart, David Guzman, Dereck Trowler, Jonathan Hayes, Kenny George, Luciano Andres Garcia, Luis Mogollon, Mahmood Saadeh, Manuel Sanchez, Roderick Garcia, Ross Liederbach, Samuel Garcia and Yusi Liu. Advice to those who have not finished: Never perish, there is always light at the end of the tunnel.

## **DEDICATION**

All this effort goes to the person who has supported me for more than a decade and has seen how I have grown as a person and as a professional. Thank you Claudia Lorena Grisales Arango, because you are my inspiration, the motor that moves my life and makes my heart beat.

## TABLE OF CONTENTS

CHAPTER ONE .....	1
INTRODUCTION.....	1
1.1 Distributed Generation .....	1
1.2 Power Electronic Interfaces for Distributed Generation Units.....	5
1.3 Overview of Controllers for Grid-Connected Voltage Source Converters .....	10
1.4 Dissertation Motivation .....	11
1.5 Dissertation Objectives.....	13
1.6 Dissertation Organization .....	13
1.7 Dissertation Contributions.....	15
References .....	16
CHAPTER TWO.....	24
AN INDIRECT MATRIX CONVERTER FOR CCHP MICROTURBINES IN.....	24
DATA CENTER POWER SYSTEMS .....	24
Abstract.....	24
2.1 Introduction .....	25
2.2 Indirect Matrix Converter as a PEI for DCs.....	28
2.2.1 <i>IMC Loss Calculations</i> .....	29
2.3 Indirect Matrix Converter Control Strategy .....	31
2.3.1 <i>Rectifier Stage</i> .....	32
2.3.2 <i>Inverter Stage</i> .....	33
2.4 Proposed Control Strategy for the IMC.....	34
2.5 Simulations Results .....	36
2.6 Conclusions .....	39
Acknowledgments .....	40
References .....	40
APPENDIX A.1.....	44
PERMISSIONS .....	44

CHAPTER THREE.....	47
NEW CONTROL STRATEGY FOR INDIRECT MATRIX CONVERTERS OPERATING IN BOOST MODE.....	47
Abstract.....	47
3.1 Introduction .....	47
3.2 IMC-Based DG System Description .....	50
3.3 Indirect Matrix Converter Control Strategy .....	51
3.3.1 VSR and CSI Modulation .....	51
3.3.2 Proposed Sensorless Controller.....	53
3.4 Experimental Results.....	55
3.5 Conclusions .....	61
Acknowledgments .....	61
References .....	62
APPENDIX B.1.....	65
PERMISSIONS .....	65
CHAPTER FOUR.....	68
NEW POWER ELECTRONIC INTERFACE COMBINING DC TRANSMISSION, A MEDIUM-FREQUENCY BUS AND AN AC-AC CONVERTER TO INTEGRATE DEEP-SEA FACILITIES WITH THE AC GRID .....	68
Abstract.....	68
4.1 Introduction .....	69
4.2 Proposed Topology Overview .....	72
4.2.1 Modular Multilevel Converter Stage.....	72
4.2.2 Medium-Frequency Transformer Stage .....	73
4.2.3 AC-AC Converter Stage .....	75
4.3 Proposed Topology for Subsea Power Systems .....	76
4.4 Passive Components Size Evaluation.....	79
4.4.1 MMC Capacitor and Arm Inductor Ratings .....	79
4.4.2 MF Transformer Core and Winding Size .....	81
4.5 Topology Loss Analysis .....	84
4.5.1 MF Transformer Losses .....	84
4.5.2 IMC Conduction and Switching Losses .....	84



4.5.3	<i>MMC Switching Losses</i> .....	85
4.6	Proposed PEI Topology Case Study .....	85
4.7	Conclusions .....	89
	Acknowledgments .....	89
	References .....	90
	APPENDIX C.1 .....	96
	PERMISSIONS .....	96
CHAPTER FIVE	.....	99
A SENSORLESS GRID SYNCHRONIZATION METHOD FOR MODULAR MULTILEVEL CONVERTERS IN HVDC SYSTEMS .....		
	Abstract.....	99
5.1	Introduction .....	99
5.2	MMC AC-Side Current Control Conventional Approach.....	103
5.3	Proposed Sensorless Control Technique .....	105
5.3.1	<i>Balanced Operating Conditions</i> .....	105
5.3.2	<i>Distorted and Unbalanced Operating Conditions</i> .....	108
5.3.3	<i>Controller Parameter Selection</i> .....	110
5.4	Proposed Controller Validation .....	112
5.4.1	<i>Grid-Lock and Operation under Ideal Conditions</i> .....	113
5.4.2	<i>Harmonic-Voltage Pollution Condition</i> .....	117
5.4.3	<i>Grid-Frequency Variation Condition</i> .....	118
5.4.4	<i>Grid Voltage-Magnitude Variation Condition</i> .....	119
5.5	Conclusions .....	121
	References .....	122
CHAPTER SIX	.....	128
CONCLUSIONS AND SUGGESTIONS FOR FUTURE WORK .....		
6.1	Conclusions .....	128
6.1.1	<i>BBC and IMC Efficiency Comparison</i> .....	128
6.1.2	<i>IMC New Sensorless Controller</i> .....	129
6.1.3	<i>IMC in Boost Operation Mode</i> .....	129
6.1.4	<i>New PEI Involving the IMC</i> .....	132

6.1.5	<i>Proposed Sensorless Controller for a High Power Rating Converter</i> .....	132
6.2	Recommendations for Future Work .....	133
	References .....	134

## LIST OF FIGURES

Fig. 1.1. A facility with a DG unit having a central control system determining the amount of power supplied from the CCHP to increase overall efficiency .....	5
Fig. 1.2. PEI schematic for DG units. Two-headed arrows indicate bidirectional power flow which is required for some applications [22], [26] .....	6
Fig. 1.3. AC-AC converter classification (IMC have other sub-categories that are the result of reducing the number of semiconductor devices).....	7
Fig. 1.4. CMC including snubber circuit for a safe operation (a), and IMC with reduced snubber requirements (b) .....	9
Fig. 2.1. Power distribution system for a DC with CCHP [3], [6].....	26
Fig. 2.2. IMC interfacing a high-frequency PMSG with the power grid .....	28
Fig. 2.3. Comparison between BBC and IMC calculated efficiencies based on a 15-kVA converter at 480-V <sub>rms</sub> output voltage.....	31
Fig. 2.4. Rectifier (a) and inverter (b) space vector diagram in sector I [29].....	33
Fig. 2.5. Proposed control block diagram for the IMC inverter.....	36
Fig. 2.6. $d$ and $q$ current variations for changes of the reference current.....	38
Fig. 2.7. Inverter output line voltage .....	38
Fig. 2.8. Output currents of the IMC .....	39
Fig. 3.1. Configuration of the IMC in boost mode as the PEI for a DG unit .....	51
Fig. 3.2. VSR (a) and CSI (b) space vector diagrams [12], [25].....	52
Fig. 3.3. Proposed control block diagram for the IMC .....	54
Fig. 3.4. Overall control scheme .....	56
Fig. 3.5. Step response of (3.3) used to determine $B$ .....	57

Fig. 3.6. Input current THD as a function of  $L_{fi}$ .....59

Fig. 3.7. Generator output voltage (top), VSR input voltage and virtual dc-link voltage (middle), grid voltage (bottom) - Voltage scale is 100 V per division with a time scale of 5 ms per division .....60

Fig. 3.8. Generator output current (top), injected grid current (bottom). The current scale is 5 A per division with a time scale of 5 ms per division.....60

Fig. 4.1. Proposed dc-ac PEI connecting two ac systems with .....70

Fig. 4.2. Proposed PEI components (IMC rectifier and inverter stages are interleaved to reduce parasitics, and the IMC input and output filters are not shown) .....73

Fig. 4.3. Proposed PEI applicable to subsea facilities.....78

Fig. 4.4. Capacitor size comparison as function of the fundamental frequency .....81

Fig. 4.5. Transformer volume for different fundamental frequencies.....83

Fig. 4.6. MMC output line-to-line voltages (a) at 10 kV/div and output currents (b) at 20 A/div. MF-XFMR output voltages (c) at 2 kV/div and output currents (d) at 200 A/div. All figures with a time scale of 1ms per division .....88

Fig. 5.1. HVdc terminal based on the MMC concept. Thyristors within the SM are used for bypassing the SM in case switch failure ..... 101

Fig. 5.2. Proposed control block diagram in the  $d$  axis (a) and  $q$  axis (b)..... 106

Fig. 5.3. Outer control loop to determine the gains of the conductance vector  $[g^d g^q]^T$  ..... 108

Fig. 5.4. Proposed control block diagram in the  $d$  and  $q$  axes with ROGI and SOGI controllers ..... 110

Fig. 5.5. Gains  $A$  and  $B$  variations for 10%, 20% and 30% current overshoots when  $CB_1$  is closed ..... 112

Fig. 5.6. Grid voltage (top), MMC output voltage (middle) and grid current during locking up for a time scale of 2 ms ..... 115

Fig. 5.7. MMC terminal line-to-line voltage (top) with  $2N+1$  number of levels and grid currents (bottom) under variations of the power references for a time scale of 10 ms ..... 115

Fig. 5.8. Active power (top) and reactive power (bottom) under ideal grid conditions for a time scale of 20 ms ..... 116

Fig. 5.9. Grid voltages (top), MMC output voltage (middle) and grid current (bottom) under harmonic pollution for a time scale of 20 ms ..... 117

Fig. 5.10. Active power (top) grid currents (bottom) under grid-frequency variations for a time scale of 10 ms ..... 119

Fig. 5.11. Grid voltage decreases by 5%: voltage in the  $d$  axis (top), active power (middle) and grid currents (bottom) for a time scale of 20 ms ..... 120

Fig. 5.12. Grid voltage increases by 5%: voltage in the  $d$  axis (top), active power (middle), grid currents (bottom) for a time scale of 20 ms ..... 121

## LIST OF TABLES

Table 2.1. Semiconductor Device Parameters .....	30
Table 2.2. Parameters of the MT-PMSG System.....	37
Table 3.1. System parameters .....	56
Table 4.1. Comparison between different magnetic materials [26], [27] .....	75
Table 4.2. General parameters for the case study .....	87
Table 4.3. MMC Capacitor and inductor size reduction .....	87
Table 4.1. Estimated global efficiency for the PEI .....	87
Table 5.1. System parameters [41] .....	111

## LIST OF PAPERS

Chapter Two. A. Escobar, J.C. Balda, C.A. Busada, D. Christal, “An indirect matrix converter for CCHP microturbines in data center power systems,” in *Proceedings of the 34<sup>th</sup> IEEE International Telecommunications Energy Conference*, pp. 1–6, October, 2012.

Chapter Three. A. Escobar, J.K. Hayes, J.C. Balda, C.A. Busada, “New control strategy for indirect matrix converters operating in boost mode,” in *Proceedings of the IEEE Energy Conversion Congress and Exposition, ECCE 2013*, pp. 2715–2720, September, 2013.

Chapter Four. A. Escobar, Yusi Liu, J.C. Balda, K. George, “New power electronic interface combining dc transmission, a medium-frequency bus and an ac-ac converter to integrate deep-sea facilities with the ac grid,” in *Proceedings of the IEEE Energy Conversion Congress and Exposition, ECCE 2014*, pp. 4335–4344, September, 2014.

Chapter Five. A. Escobar, J.K. Hayes, J.C. Balda, C.A. Busada, “A sensorless grid synchronization method for modular multilevel converters in HVdc systems,” submitted to *IEEE Transaction on Industry Applications*, in review.

# CHAPTER ONE

## INTRODUCTION

### 1.1 Distributed Generation

In years past, the ac grid has been dominated by large-scale centralized power plants (e.g., fossil<sup>1</sup>-, hydro- and nuclear-based power plants) often located far from the load consumption centers and close to the primary power sources requiring long-distance transmission lines to transmit the bulk power. The concept of a central-based bulk generation system is considered cost effective and reliable for consumers and utilities; however, the motivation to exploit local resources and follow new government policies to reduce high-levels of CO<sub>2</sub> emissions (the target is to reduce greenhouse gases emissions to 17% of current levels by 2050 [1]) creates the need to change this concept. This allows for the introduction of distributed generation (DG), leading to a more controllable, robust, secure and sustainable electric power system [2].

Contrary to centralized power plants, DG—often called on-site generation with power ratings from several kW up to 10 MW [3]—is defined as a cluster of small generation units, located on the customer side of the grid to provide power when it is needed. Examples of DG include:

- Photovoltaic systems<sup>2</sup>
  - Wind systems<sup>2</sup>
  - Fuel cells
  - Internal combustion engines
  - Microturbines
  - Energy storage
- } Environmental friendly
- } Require a fuel source
- } Limited energy resource

---

<sup>1</sup> Fossil-based generation includes coal-fired, oil and natural gas.

<sup>2</sup> Large-scale solar and wind farms are usually considered bulk generation.



The DG concept emerged from the need of the industrial sector to improve power quality indices like voltage distortion index, flicker factor, and imbalance factor [5], [6] by installing their own generation units [6]. Its multiple advantages when compared with a central power supply (i.e., the utility) led to its adoption in buildings, hospitals, hotels, data centers (DCs) and residential areas [7].

Distributed generation units have been extensively proposed to be part of future power grids as the conventional grid moves to an efficient, reliable and smarter grid [8], [9]. Issues like new environmental policies to reduce fossil-fuel dependency and the increase of energy prices force utilities to think about new alternatives for generating electricity and encourage consumers to make proper use of it. New concepts like microgrids are presented as part of future energy systems to overcome the problems associated with centralized grids. Microgrids are defined as the smart relationship between a collection of DG units operating in parallel to meet the local load demand at voltage levels from a range of 1 kV to 69 kV. Furthermore, microgrids include a controller capable of regulating frequency and voltage to allow the operation in both grid-tied and islanding modes [10]. Unlike the central power approach, microgrids tend to be more efficient and flexible given their reduced size and the shorter distance between the generator and the consumption centers, which allows for the integration of multiple DG units [11].

Although new large central power plants have technical benefits over smaller systems, several advantages make DG units relevant for future electric energy grids [12]:

Congestion relief: Distributed generation can potentially bring power to local loads during peak periods when electricity prices are higher, alleviating the congestion in transmission lines when distribution feeders are heavy loaded. It can also help to reduce overall interconnection cost and

the requirement for new power plants. Surplus power can be injected to the grid, reducing the payback period.

Diversity: A large variety of fuels can be used by DG units to reduce the dependence on a single environmentally harmful source, such as coal. As an example, microturbines using natural gas—or gas produced by a biodegradation process—as a fuel source are commercially available for power ratings from a few kW up to 1 MW [13], [14].

Economy: Distributed generation units require less initial capital cost when compared to large power plants that have long payback periods. Mass production of small power units should enable economy of scale to reduce costs.

Efficiency: Around 7% of the electricity generated by centralized power plants is lost in distribution and transmission lines. Reducing distances reduces the losses associated with the transportation process.

Heat production: In addition to electricity, some DG units have the capability to provide heat to thermal loads. This heat, a byproduct of the electricity generation process could be beneficial to supply space heating and hot water to hospitals, hotels, residential areas, etc., improving overall system efficiency.

Power quality: When placed at a specific location, DG units can potentially provide ancillary services to mitigate power quality problems [15], such as the low-voltage profile across long feeders or loads connected far from a power distribution substation.

Reliability: A centralized distribution system is subjected to hazards that could leave thousands (or even millions) of customers without electricity for long periods of time. In the case of

hurricane Sandy, which hit the East coast area in 2012, affecting the transmission grid, millions of residents were left without electricity for days. Distributed generators operating in islanding mode, located in buildings or local distribution substations, could have provided support to those areas reducing the total time without electricity. For example, natural gas lines are buried so they are less prone to suffer damage during severe conditions.

Upgradability: Distributed generation units are easy to update and increase power ratings by connecting several of them in parallel to serve large loads or provide electric power during peak demand periods. This reduces the need to build new transmission lines to serve power distribution substations.

Microturbines with power ratings from 15 kW to 1 MW [16] that achieve power densities of about 15 kW/m<sup>3</sup> [17] have been proposed for many applications because they possess several of the previously mentioned advantages when compared with other types of DG units [18], [19]. Their capability of generating electricity as well as meeting cooling or heating demands, best known as combined cooling heat and power (CCHP), in a small-size unit with low-noise level makes them convenient for multiple applications such as the ones previously mentioned as well as others with limited space.

The following example compares the energy requirements of a traditional power supply system with a microturbine-based system. Figure 1.1 considers a facility (e.g., building, data center, hospital, mall, residential complex, etc. [16]) where the total demanded power, 1.67 pu<sup>3</sup>, could be delivered from a DG unit or from the utility plus another primary source (e.g., natural gas), for the furnace to serve the heat throughout the facility.

---

<sup>3</sup> Base values depend on the load power requirements (e.g., a few kW for residential areas up to several MW for larger facilities).

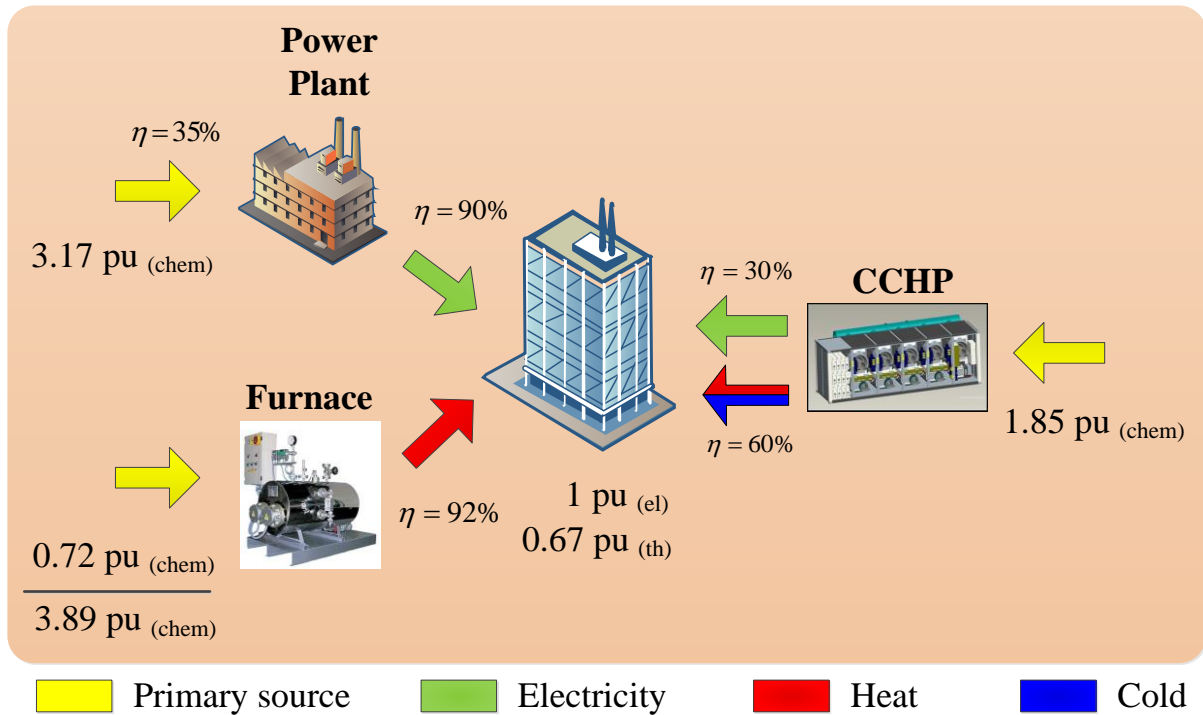


Fig. 1.1. A facility with a DG unit having a central control system determining the amount of power supplied from the CCHP to increase overall efficiency

One pu out of the total are used to produce electricity and the remaining 0.67 pu are used to produce thermal power. As shown, 3.89 pu of primary fuel (i.e., coal, natural gas, etc.) would be required to supply the demand with the conventional centralized concept and a local heat unit [20]. With the CCHP system, a cluster of microturbines connected in parallel satisfy the demand requiring only 1.85 pu of primary fuel to supply the same load, indicating a significant reduction in the primary fuel and improving overall efficiency.

## 1.2 Power Electronic Interfaces for Distributed Generation Units

Unlike internal combustion engines that are usually connected directly to the grid, most of the previously mentioned DG units require power electronic interfaces (PEIs) to convert the power generated to grid levels [21], [22]. As illustrated in Fig. 1.2, PEIs facilitate the interconnection of

the DG unit at the point of connection with the grid or point of common coupling (PCC). The main components of the interface are the power electronics and the output interface, consisting of an LC or an LCL filter used to filter out the high-order harmonics resulting from the switching process (other schemes may include an isolating transformer). The control unit consists of a dedicated algorithm that generates the required gate signals, and serves to synchronize the DG's generated voltages to those of the grid and to regulate the power flow exchange. To this end, current and voltage sensors are normally required to extract information from the grid and the DG unit.

There are two main types of three-phase ac-ac converters as illustrated in Fig. 1.3 [23]–[25]: those with an intermediate dc link, which facilitates the connection of an energy storage component, and those not requiring one for the ac-ac conversion process.

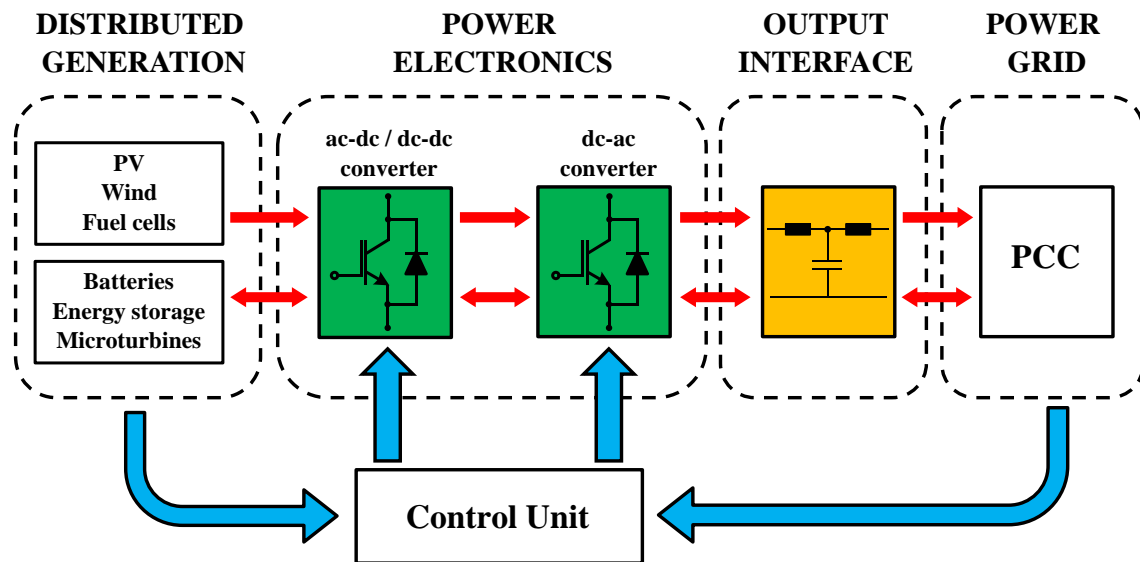


Fig. 1.2. PEI schematic for DG units. Two-headed arrows indicate bidirectional power flow which is required for some applications [22], [26]

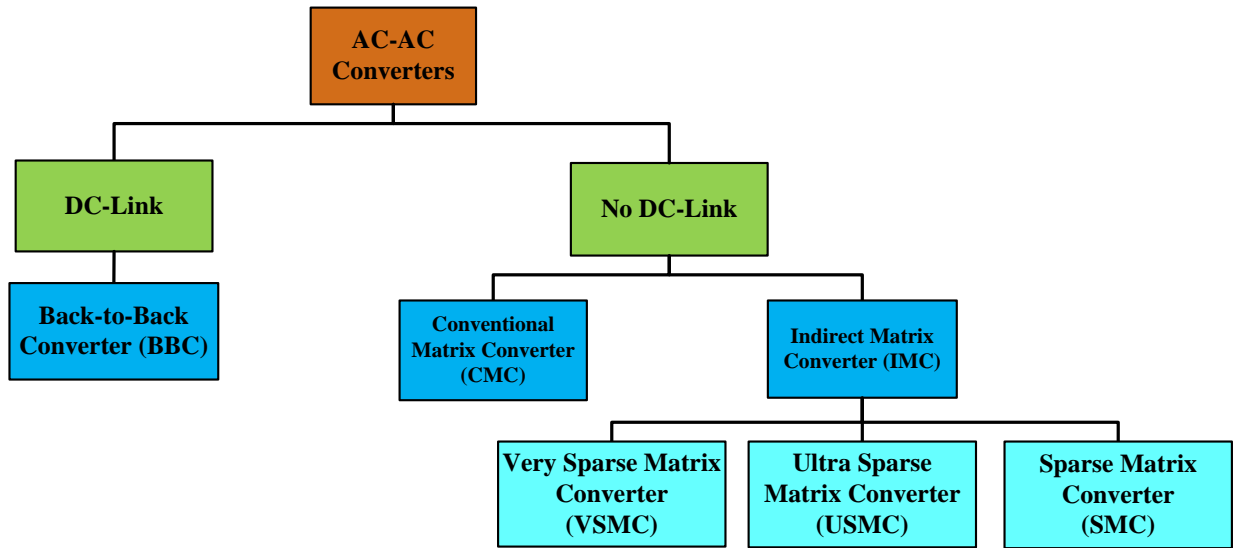


Fig. 1.3. AC-AC converter classification (IMC have other sub-categories that are the result of reducing the number of semiconductor devices)

The “dc-link” branch includes the conventional back-to-back converter in a voltage source converter configuration (BBC-VSC), considered the work horse of the motor drive industry, and the standard for the ac-ac conversion process with power ratings from a few MW up to hundreds of MW. Its technical advantages make it preferable over other types of power converters for applications like motor drives and wind turbine-based generation, among others [27]. This converter includes the intermediate dc-link stage where a capacitor is used as an energy storage component, decoupling the input from the output, and absorbing discontinuities caused by the switching process in the ac-dc and dc-ac stages. The dc-link capacitor is, in most applications, of the electrolytic type, although film capacitors could be implemented under certain design considerations [28].

An electrolytic capacitor is a passive component that brings multiple functionalities to the ac-ac conversion process. Unfortunately due to its constructive characteristics, its volume can be up to 50% of the power converter total size [29], and thus it is considered one of the bulkiest and

weakest components in power converters. Many manufacturers have evaluated the life time expectancy of this component [30]–[34] concluding that its aging process is highly affected by operating conditions such as ambient temperature, ripple current and voltage variations [30], [35]. It has been demonstrated in [30] that if an electrolytic capacitor operates at temperature ranges between 40°C and its maximum operating temperature (85°C~105°C), its life time expectancy is reduced by half for each 10°C above 40°C. The operating temperature is calculated using the ambient temperature and the temperature rise caused by the power loss due to the ripple current [30]. Thus, the BBC failure rate can be reduced by connecting several electrolytic capacitors in parallel to reduce the ripple current flowing through each one, but with the penalty of a more bulky and heavy converter [36]. Since this is not a feasible solution for application with space limitation, the electrolytic capacitor remains responsible for most of the breakdown failures [37], with one of the lowest mean times between failures when compared with other components.

Several studies have evaluated the impact of reducing its size by using a different technology (e.g., film capacitors and hybrid capacitors) [38], [39], or eliminating this component in order to increase overall system reliability, as in the case of power factor correctors [40], ac-ac converters [41], static VAR compensators [42] and microinverters for photovoltaic applications [43].

The “no dc-link” branch includes converters, widely known as a matrix converter (MC), not involving a large energy storage component in the dc-link. Without a bulky capacitor, the MC becomes more attractive as a power converter for applications demanding reliability and size/weight savings, such as the aerospace industry or motor drives integrated with the motor frame, which is not possible with the conventional BBC [44]. However, some disadvantages associated with the absence of the dc capacitor, such as low input/output voltage ratio (limited to 86%), lack of ride-through capability, and the complexity of the control technique to guarantee

proper waveforms and safe operation, have prevented the MC from becoming a standard off-the-shelf converter for many applications such as motor drives.

There are two types of MC: conventional matrix converters (CMCs) and indirect matrix converters (IMCs). As shown in Fig. 1.4(a), the CMC uses nine bidirectional switches (two semiconductors in antiparallel configuration) allowing a direct connection between the input and the output. The IMC shown in Fig. 1.4(b), also called the dual-bridge topology [45], separates the ac-ac conversion into two stages allowing separate control of the rectifier and the inverter. The fact that the IMC has two separate stages allows the IMC to be more flexible and reliable than the CMC [46].

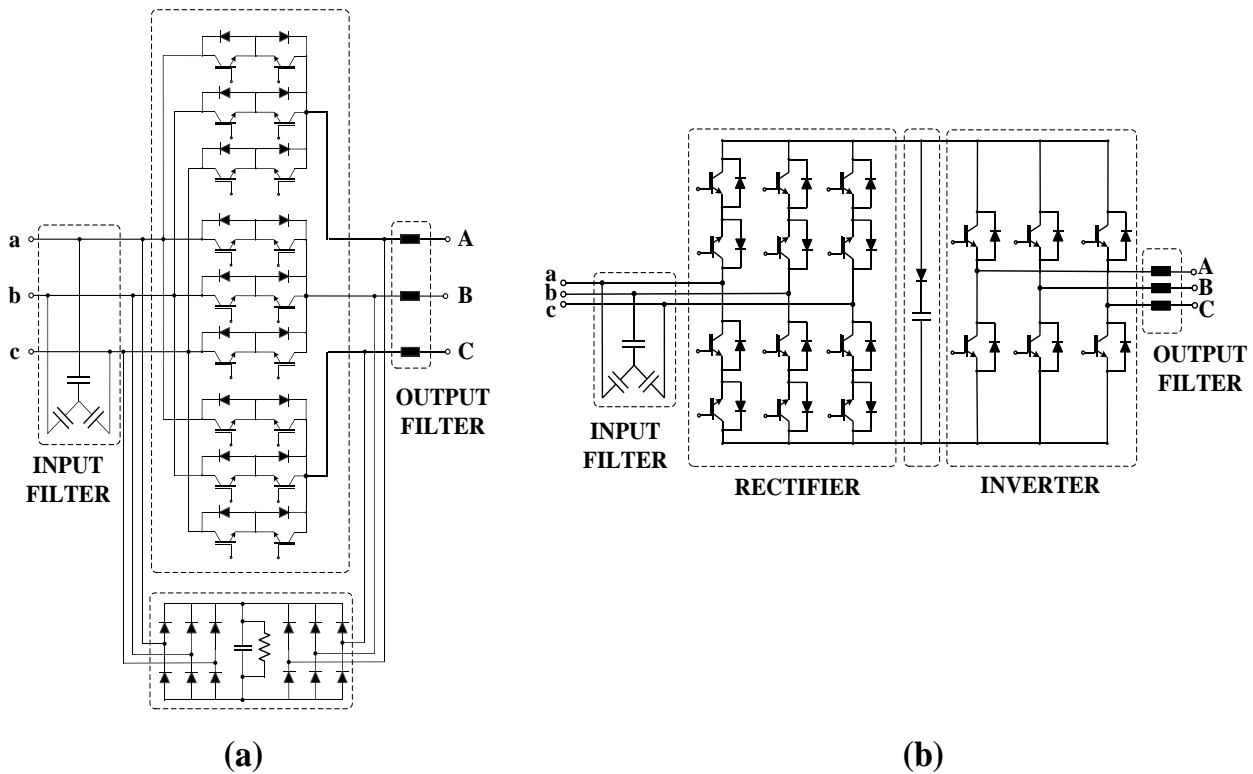


Fig. 1.4. CMC including snubber circuit for a safe operation (a), and IMC with reduced snubber requirements (b)



Matrix converters have been widely studied for several years and proposed as an alternative to the BBC, to connect a fixed/variable-frequency fixed/variable-voltage ac power supply with any load requiring fixed/variable-frequency fixed/variable-voltage (e.g., electric motors), without using a large component in the dc link. Advantages including unity input/output power factor, bidirectional power flow, sinusoidal input current and sinusoidal output voltage [47], [48] make this converter attractive for particular applications, especially those where volume and weight dominate the PEI requirements.

### **1.3 Overview of Controllers for Grid-Connected Voltage Source Converters**

Over the last decades several controllers for grid-connected applications have been presented in the literature to control the amount of current that DG units can inject into the grid with minimum harmonic content [49]–[53]. Most of these controllers follow the same approach, thus they can be applied to a wide power range starting from low-power DG units up to wind turbines generating several MW. Also, the existing controllers are able to operate the VSC as desired even during severe power quality disturbances such as harmonics and grid imbalances [54]–[57].

Most of these controllers make use of the information gathered from current and voltage sensors located on either side of the converter. In general, two voltage and two current sensors are required on the ac side of the filter inductor for a three-wire system, while one voltage sensor is placed on the dc link (an extra current sensor in the dc-link may be required for load compensation [58]). Even though these sensors are accurate and highly reliable, the conditioning circuit for the analog to digital conversion process may be exposed to EMI that creates noise on the captured signals [59]. This can lead to a misreading of the sensed variables and false triggering of the semiconductor devices in the PEI.

To reduce the converter's cost and potentially increase system reliability, the number of elements involved in the ac-ac process could be reduced without affecting the PEI performance. Several control schemes have been successfully proposed to diminish the number of voltage sensors on the grid side [60]–[63]. The general idea of the proposed schemes is to estimate the grid voltages (amplitude, frequency and phase) based on the information coming from the current sensors located at the output of the converter. The design parameters allow fast transient responses with almost zero steady-state errors and high bandwidths.

#### **1.4 Dissertation Motivation**

The seeking of a more efficient, reliable and sustainable electric power generation, transmission, and distribution system has changed the concept of the power grid as it is known today. Future energy systems will have high penetration levels of renewables and will be dominated by a large number of electrically self-sufficient areas, or the so-called microgrids, which will be interconnected together to accomplish a “smart grid”.

Distributed generation units, interfaced to the grid by a power converter, from a few tens to hundreds of kW have been successfully deployed in conventional power grids and will become more common in future grids due to the advantages previously mentioned [64]. As an example, the existence of buried natural gas pipelines in the commercial, industrial and residential sectors, and the interest to generate electricity locally by using small generating units such as natural gas-based microturbines [65] will increase the demand for compact, efficient and reliable PEIs—accomplishing the requirements set in [1]—particularly in, but not limited to, residential areas, small commercial buildings and urban cores, where space comes at a premium. For the PEI of some DG units, manufacturers provide a lifetime expectancy of 20 years with an initial cost of

\$700 to \$1,100 per kW and maintenance intervals between 5,000 and 8,000 hours (limited by the life time expectancy of electrolytic capacitors [66]) at a cost of \$0.005-\$0.016 per kWh [64]. In most cases, the dc-link capacitor is the component in the PEI that requires replacement due to its reduced lifetime expectancy under rated conditions, accounting for up to 60% of the failures in power converters [67].

In the case renewable energy resources, the growth in the installed capacity of offshore wind turbines, operating at a few MW, and the promising scenario for the coming years, [68] has pushed the demand for multilevel PEI such as the cascade H-bridge, neutral-point-clamped, flying capacitor topologies [69] and most recently the modular multilevel converter (MMC), which are commonly used in medium-voltage adjustable-speed drives [70]. These topologies are equipped with a series connection of electrolytic capacitors in the dc-link to satisfy voltage level ratings. In some cases, balancing resistors are used to equally balance the dc voltage. The heat generated due to the resistor losses could be radiated to the electrolytic capacitor [71] reducing even more its life expectancy when not properly cooled.

The need of a compact and reliable PEI, motivates the implementation of converters that do not involve energy storage components for the ac-ac process. In the case of the IMC, most of the obstacles that keep it away from been an appealing solution in real world applications have been solved. In terms of losses, [72] demonstrated than the IMC becomes more efficient than the BBC for frequencies above 10 kHz. This is due to the fact that the IMC's rectifier switches when a null voltage vector is applied to the inverter stage. Also, [73] overcame the voltage ratio limitation by operating the IMC in the so-called "boost mode". This is experimentally tested in a 5-kVA SiC-based IMC prototype used as the PEI to interface a variable-frequency voltage source with the power grid.

## 1.5 Dissertation Objectives

The main objectives of this dissertation are to develop an IMC-based PEI that can become a standard PEI for DG units and grid-interconnected applications including those demanding higher power ratings. This will be accomplished through the following specific objectives:

- To evaluate if the IMC could be more efficient than the BBC in terms of conduction and switching losses for certain operating conditions.
- To establish if it is viable to reduce controller complexity by not requiring sensing of the grid voltages to interface with the grid (and thus eliminating the need for a “grid connecting point”).
- To determine if it is possible to overcome the voltage ratio limitation commonly presented in the IMC, without using extra components.
- To demonstrate if the proposed ideas are feasible by fabricating an IMC prototype based on IMC SiC JFETs.
- To evaluate if the IMC-based PEI could be considered a standard ac-ac PEI for different applications where space is a constraint.
- To evaluate if the earlier-proposed sensorless controller could be extended to other converter topologies like a modular multilevel converter terminal.

## 1.6 Dissertation Organization

This dissertation is organized as a collection of papers that have been published in IEEE Conferences and are in the process of revision for IEEE Transaction publications. The dissertation includes the following five main chapters:

- The reader is introduced to IMCs in Chapter Two, which suggests its application to interface a high-frequency microturbine with critical loads such as data centers (DCs). A comparison in terms of conduction and switching losses between the BBC and the IMC is also presented. A novel voltage sensorless control scheme to interconnect a DG unit with the power grid through an IMC is proposed. The chapter ends with time-domain simulations in the Matlab/Simulink™ environment to validate the proposed ideas.
- A 5-kVA scaled-down SiC-JFET based IMC is developed in Chapter Three to validate experimentally the controller proposed in the previous chapter. The power and voltage ratings of the scaled-down prototype is based on the power capabilities of the Smart Sustainable Electrical Energy Systems (SSEES) laboratory. The prototyped IMC, operating in boost mode to overcome the poor voltage ratio limitation typical of IMCs, is used as the PEI for a medium-frequency low-voltage VSC and the power grid. Experimental results are presented validating the proposed control scheme.
- The concept of IMCs as a standard power electronic interface for applications with high power ratings is extended in Chapter Four. A new PEI involving an IMC, a medium-frequency (or high-frequency) transformer, and a MMC, is proposed to interconnect dc-ac systems. The PEI's main operating principles, design equations, and overall control scheme are described. Size and efficiency are evaluated for the proposed topology for different operating frequencies and compared with the conventional approach. A case study is illustrated through time-domain simulations considering different operating conditions to demonstrate the validity of the proposed topology.
- The voltage sensorless controller proposed Chapter One is extended to a MMC terminal in Chapter Five. The controller is able to control the active and reactive power flow exchanges

between the MMC and the power grid. Resonant controllers are added to the controller to overcome abnormal grid conditions such as imbalances and harmonics. Extensive time-domain simulations in the Matlab/Simulink™ environment are carried out to validate the proposed controller.

- Finally, a summary of the research work, conclusions, and recommendations for future work is provided in Chapter Six.

## 1.7 Dissertation Contributions

The main original contributions are:

- A new ac-ac or dc-ac PEI that can be implemented in different applications, especially in those where volume is a constraint. The analysis of the proposed idea includes losses and volume of the converter stages [74].
- A new controller that does not require sensing the DG output voltages to synchronize it with the power grid [72]. The sensorless controller is developed in the  $d - q$  frame and validated through experimental results in a 5 kVA SiC-JFET based indirect matrix converter [73]. An improved version of the sensorless controller is validated through simulations in a 400 MVA MMC terminal [75]. The enhanced version has the capability of regulating the active and reactive power flows between the two power sources even during abnormal grid conditions.

## References

- [1] United States Department of Energy, “Projected Greenhouse Gas Emissions,” in U.S. Climate Action Report 2010, Washington: Global Publishing services, June, 2010, chapter 5, pp. 76–85.
- [2] B. Kroposki, P.K. Sen, K. Malmedal, “Selection of distribution feeders for implementing distributed generation and renewable energy applications,” *IEEE Transactions on Industry Applications*, vol. 49, no. 6, pp. 2825–2834, November/December 2013.
- [3] IEEE Standard for Interconnecting Distributed Resources with Electric Power Systems, IEEE Standard 1547, July, 2003.
- [4] T. Lin, A. “On power quality indices and real time measurement,” *IEEE Transactions on Power Delivery*, vol. 20, no. 4, pp. 2552–2562, October, 2005.
- [5] A. Bracale, P. Caramia, G. Carpinelli, A. Russo, P. Verde, “Site and system indices for power-quality characterization of distribution networks with distributed generation,” *IEEE Transactions on Power Delivery*, vol. 26, no. 3, pp. 1304–1316, July, 2011.
- [6] United States Department of Energy, “The potential benefits of distributed generation and rate-related issues that may impede their expansion,” [Online]. Available: <https://www.ferc.gov/legal/fed-sta/exp-study.pdf>. [Accessed July 2014].
- [7] M.H. Nazari, M. Ilić, “Potential for efficiency improvement of future electric energy systems with distributed generation units,” in *Proceedings of the IEEE Power and energy Society General Meeting*, pp. 1–9, July, 2010.
- [8] G. Adinolfi, V. Cigolotti, G. Graditi, G. Ferruzzi, “Grid integration of distributed energy resources: Technologies, potentials contributions and future prospects,” in *Proceedings of the IEEE International Conference on Clean Electrical Power*, ICCEP, pp. 509–515, June, 2013.
- [9] B. Kroposki, P.K. Sen, K. Malmedal, “Optimum sizing and placement of distributed and renewable energy sources in electric power distribution systems,” *IEEE Transactions on Industry Applications*, vol. 49, no. 6, pp. 2741–2752, November/December, 2013.
- [10] K. Ravindra, B. Kannan, N. Ramappa, “Microgrids: A value-based paradigm: The need for the redefinition of microgrids,” in *Proceedings of the IEEE Electrification Magazine*, vol. 2, no. 1, pp. 20–29, March, 2014.

- [11] P.C. Loh, D. Li, Y.K. Chai, F. Blaabjerg, “Hybrid AC–DC microgrids with energy storages and progressive energy flow tuning,” *IEEE Transactions on Power Electronics*, vol. 28, no. 4, pp. 1533–1543, April, 2013.
- [12] Resource Dynamic Corporation, “Assessment of Distributed Generation Technological Applications,” [Online]. Available: <http://www.distributed-generation.com/Library/Maine.pdf>. [Accessed July 2014].
- [13] Capstone Turbine Corporation, “Solutions – Resource Recovery: Biogas,” [Online]. Available: <http://www.capstoneturbine.com/prodsol/solutions/rrbiogas.asp>. [Accessed July 2014].
- [14] Volvo Aereo Corporation, “Small scale biogas fired combined cycle power plant,” Online]. Available: <http://www.enef.eu/history/2002/en/pdf/Torssander-AJ.pdf>. [Accessed July 2014].
- [15] Oak Ridge National Lab, “Microturbine power conversion technology review,” [Online]. Available: [Online]. Available: [http://www1.eere.energy.gov/manufacturing/distributedenergy/pdfs/microturbine\\_conversion.pdf](http://www1.eere.energy.gov/manufacturing/distributedenergy/pdfs/microturbine_conversion.pdf). [Accessed July 2014].
- [16] Capstone Turbine Corporation, “Energy efficiency the cool way,” [Online]. Available: [www.capstoneturbine.com/prodsol/solutions/cchp.asp](http://www.capstoneturbine.com/prodsol/solutions/cchp.asp). [Accessed July 2014].
- [17] —, “Power: Reliable, efficient and clean,” [Online]. Available: <http://www.capstoneturbine.com/prodsol/solutions/chp.asp>. [Accessed July 2014].
- [18] S. Grillo, S. Massucco, A. Morini, A. Pitto, F. Silvestro, “Microturbines control modeling to investigate the effect of distributed generation in electric energy networks,” *IEEE System Journal*, vol. 4, no. 3, pp. 303–312, September, 2010.
- [19] D.N. Gaonkar, S. Nayak, “Modeling and performance analysis of microturbine based distributed generation systems: A review,” in *Proceedings of the IEEE Conference EnergyTech*, pp. 1–6, May, 2011.
- [20] Whitby Hydro Energy Services Corporation: Engineering and Construction services, “Co-Generation,” [Online]. Available: [www.whitbyhydro.on.ca/pdf/5.2.B\\_CoGenWorkshop.pdf](http://www.whitbyhydro.on.ca/pdf/5.2.B_CoGenWorkshop.pdf). [Accessed July 2014].



- [21] A.K. Barnes, J.C. Balda, C.M. Stewart, “Selection of converter topologies for distributed energy resources,” in *Proceedings of the 27<sup>th</sup> IEEE Applied Power Electronics Conference and Exposition*, APEC 2012, pp. 1418–1423, February, 2012.
- [22] W. Kramer, S. Chakraborty, B. Kroposki, H. Thomas, “Advanced power electronic interfaces for distributed energy systems part 1: Systems and topologies,” [Online]. Available: <http://www.nrel.gov/docs/fy08osti/42672.pdf>. [Accessed July 2014].
- [23] J.W. Kolar, T. Friedli, F. Krismer, S.D. Round, “The essence of three-phase ac/ac converter systems,” in *Proceedings of the 13<sup>th</sup> IEEE Power Electronics and Motion Control Conference*, EPE-PEMC 2008, pp. 27–42, September, 2008.
- [24] T. Friedli, J.W. Kolar, J. Rodriguez, P.W. Wheeler, “Comparative evaluation of three-phase ac-ac matrix converter and voltage dc-link back-to-back converter systems,” *IEEE Transactions on Industrial Electronics*, vol. 59, no. 12, pp. 4487–4515, December, 2012.
- [25] J.W. Kolar, T. Friedli, “Comprehensive comparison of three-phase AC-AC matrix converter and voltage DC-link back-to-back converter systems,” in *Proceedings of the 2010 IEEE International Power Electronics Conference*, IPEC, pp. 2789–2798, June, 2010.
- [26] H. Chaoyong, H. Xuehao, H. Dong, “Plug and play power electronics interface applied in microgrid,” in *Proceedings of the 4<sup>th</sup> IEEE International Conference on Electric Utility Deregulation and Restructuring and Power Technologies*, DRPT 2011, pp.719–723, July, 2011.
- [27] J.W. Kolar, T. Friedli, T. Rodriguez, P.W. Wheeler, “Review of three-phase PWM ac-ac topologies,” *IEEE Transactions on Industrial Electronics*, vol. 58, no. 11, pp. 4988–5006, November, 2011.
- [28] Cornell Dubilier, “Power film capacitors versus aluminum electrolytic capacitors for dc link applications,” [Online]. Available: <http://www.apec-conf.org/wp-content/uploads/2013/09/is1.3.2.pdf>. [Accessed July 2014].
- [29] P. Szcześniak, “Review of ac-ac frequency converters,” in *Three-Phase AC-AC Power Converters Based on Matrix Converter Topology, Matrix-Reactance Frequency Converters Concept*, Springer, 2013, chapter 2, section 2.2, pp. 20, 21.
- [30] Nichicon, “General description of aluminum electrolytic capacitors,” [Online]. Available: <http://www.nichicon.co.jp/english/products/pdf/aluminum.pdf>. [Accessed July 2014].

- [31] ELNA America Inc. “Reliability of Aluminum Electrolytic Capacitors,” [Online]. Available: <http://www.mouser.com/pdfdocs/ELNAReliabilityAlumElecCaps.pdf>. [Accessed July 2014].
- [32] Panasonic, “Reliability of Aluminum Electrolytic Capacitors,” [Online]. Available: <http://industrial.panasonic.com/www-data/pdf/ABA0000/ABA0000TE4.pdf>. [Accessed July 2014].
- [33] Illinois Capacitors Inc. “Aluminum Electrolytic Capacitors,” [Online]. Available: [http://www.lintronicstech.com/index%20pdf/reliability\\_of\\_capacitors\\_general.pdf](http://www.lintronicstech.com/index%20pdf/reliability_of_capacitors_general.pdf). [Accessed July 2014].
- [34] Cornel Dubilier, “Aluminum Electrolytic Capacitor Application Guide,” [Online]. Available: <http://www.cde.com/catalogs/AEappGUIDE.pdf>. [Accessed July 2014].
- [35] S.K. Maddula, J.C. Balda, “Lifetime of electrolytic capacitors in regenerative induction motor drives,” in *Proceedings of the 36<sup>th</sup> IEEE Power Electronics Specialists Conference, PESC05*, pp. 153–159, June, 2005.
- [36] J.L Stevens, J.S. Shaffer, J.T. Vandenharn, “The service life of large aluminum electrolytic capacitors: effects of construction and application,” in *Proceedings of the 36<sup>th</sup> IEEE IAS Annual Meeting on Industry Applications Conference*, vol. 4, pp. 2493–2499, September, 2001.
- [37] M.A. Vogelsberger, T. Wiesinger, H. Ertl, “Life-cycle monitoring and voltage managing unit for dc-link electrolytic capacitors in PWM converters,” *IEEE Transactions on Power Electronics*, vol. 26, no. 2, pp. 493–503, February, 2011.
- [38] H. Yoo, S.-K. Sul, H. Jang, Y. Hong, “Design of a variable speed compressor drive system for air-conditioner without electrolytic capacitor,” in *Proceedings of the 42<sup>nd</sup> IEEE Annual Meeting Industry Application Conference*, pp. 305–310, September, 2007.
- [39] H.-S. Jung, S.-J. Chee, S.-K. Sul, Y.-J. Park, H.-S. Park, W.-K. Kim “Control of three-phase inverter for ac motor drive with small dc-link capacitor fed by single-phase ac source,” *IEEE Transactions on Industry Applications*, vol. 50, no. 2, pp. 1074–1081, March/April, 2014.
- [40] H. Wang, H. Chung, “A novel concept to reduce the dc-link capacitor in PFC front-end power conversion systems,” in *Proceedings of the 27<sup>th</sup> IEEE Applied Power Electronics Conference and Exposition, APEC 2012*, pp. 1192–1197, February, 2012.

- [41] G.S. Konstantinou, V.G. Agelidis, “Bidirectional rectifier-inverter multilevel topology without dc-link passive components,” in *Proceedings of the IEEE Energy Conversion Congress and Exposition, ECCE 2010*, pp. 2578–2583, September, 2010.
- [42] D. Balakrishnan, R.S. Balog, “Capacitor-less VAR compensator based on matrix converter,” in *Proceedings of the IEEE North America Power Symposium, NAPS 2010*, pp. 1–7, September, 2010.
- [43] G.S. Seo, B.H. Cho, K.C. Lee, “Electrolytic capacitor-less PV converter for full lifetime guarantee interfaced with dc distribution,” in *Proceedings of the 7<sup>th</sup> IEEE International Power Electronics and Motion Control Conference, ECCE ASIA*, pp. 1235–1240, June, 2012.
- [44] S. Bernet, S. Ponnaluri, R. Teichmann, “Design and loss comparison of matrix converters and voltage-source converters for modern AC drives,” *IEEE Transactions on Industrial Electronics*, vol. 49, no. 2, pp. 304–314, April, 2002.
- [45] L. Wei, T.A. Lipo, H. Chan, “Matrix converter topologies with reduced number of switches,” in *Proceedings of the 33<sup>rd</sup> IEEE Annual Power Electronics Specialists Conference, PESC02*, pp. 57–63, November, 2002.
- [46] J.W. Kolar, T. Friedli, F. Krismer, S.D. Round, “The essence of three-phase AC/AC converter systems,” in *Proceedings of the 13<sup>th</sup> IEEE Power Electronics and Motion Control Conference, 2008. EPE-PEMC 2008*, pp. 27–42, September, 2008.
- [47] J.W. Kolar, F. Schafmeister, S. Round, H. Ertl, “Novel three-phase AC–AC sparse matrix converters,” *IEEE Transactions on Power Electronics*, vol. 22, no. 5, pp. 1649–1661, September, 2007.
- [48] P.W. Wheeler, J. Rodríguez, J.C. Clare, L. Empringham, A. Weinstein “Matrix converters: A technology review,” *IEEE Transactions on Industrial Electronics*, vol. 49, no. 2, pp. 276–288, April, 2002.
- [49] D. Krug, S. Bernet, S. Dieckerhoff, “Comparison of state-of-the-art voltage source converter topologies for medium voltage applications,” in *Proceedings of the 38<sup>th</sup> IEEE Annual Meeting Industry Application Conference*, pp. 168–175, October, 2003.
- [50] F. Blaabjerg, R. Teodorescu, M. Liserre, A.V. Timbus, “Overview of control and grid synchronization for distributed power generation systems,” *IEEE Transactions on Industrial Electronics*, vol. 53, no. 5, pp. 1398–1409, October, 2006.

- [51] A. Timbus, M. Liserre, R. Teodorescu, P. Rodriguez, F. Blaabjerg, "Evaluation of current controllers for distributed power generation systems," *IEEE Transactions on Power Electronics*, vol. 24, no. 3, pp. 654–664, March, 2009.
- [52] M. Cespedes, J. Sun, "Adaptive control of grid-connected inverters based on online grid impedance measurements," *IEEE Transactions on Sustainable Energy*, vol. 5, no. 2, pp. 516–523, April, 2014.
- [53] B. Bouaziz, F. Bacha, "Direct power control of grid-connected converters using sliding mode controller," in *Proceedings of the IEEE International Conference on Electrical Engineering and Software Applications*, ICEESA 2013, pp. 1–6, March, 2013.
- [54] B. Parkhideh, S. Bhattacharya, "Vector-controlled voltage-source-converter-based transmission under grid disturbances," *IEEE Transactions on Power Electronics*, vol. 28, no. 2, pp. 661–672, February, 2013.
- [55] P. Rodríguez, A. Luna, R.S. Muñoz-Aguilar, I. Etxeberria-Otadui, R. Teodorescu, F. Blaabjerg, "A stationary reference frame grid synchronization system for three-phase grid-connected power converters under adverse grid conditions," *IEEE Transactions on Power Electronics*, vol. 27, no. 1, pp. 99–112, January, 2012.
- [56] P. Rodríguez, A. Luna, I. Candela, R. Mujal, R. Teodorescu, F. Blaabjerg, "Multiresonant frequency-locked loop for grid synchronization of power converters under distorted grid conditions," *IEEE Transactions on Industrial Electronics*, vol. 58, no. 1, pp. 127–138, January, 2011.
- [57] E.M. Adzic, D.P. Marcetic, V.A. Katic, M.S. Adzic, "Grid-connected voltage source converter operation under distorted grid voltage," in *Proceedings of the 14<sup>th</sup> IEEE International Power Electronics and Motion Control Conference*, EPE/PEMC, pp. T11-44–T11-51, September, 2010.
- [58] A.E. Leon, I.A Solsona, M.I Valla, "Control of three-phase voltage-source converters with reduced number of sensors," in *Proceedings of the 34<sup>th</sup> Annual IEEE Conference on Industrial Electronics*, IECON 2008, pp. 641–646, November, 2008.
- [59] T. Noguchi, H. Tomiki, S. Kondo, I. Takahashi, "Direct power control of PWM converter without power-source voltage sensors," *IEEE Transactions on Industry Applications*, vol. 34, no. 3, pp. 473–479, May/June, 1998.

- [60] Y.A.-R.I. Mohamed, E.F. El-Saadany, M.M.A. Salama, "Adaptive grid-voltage sensorless control scheme for inverter-based distributed generation," *IEEE Transactions on Energy Conversion*, vol. 24, no. 3, pp. 683–694, September, 2009.
- [61] R.G. Tonin, T. Bernardes, J.R. Massing, H. Pinheiro, "Sliding mode observer for voltage sensorless current control of grid-connected converters," in *Proceedings of the IEEE Brazilian Power Electronics Conference*, COBEP 2013, pp. 387–392, October, 2013.
- [62] K.H. Ahmed, A.M. Massoud, S.J. Finney, B.W. Williams, "Sensorless current control of three-phase inverter-based distributed generation," *IEEE Transactions on Power Delivery*, vol. 24, no. 2, pp. 919–929, April, 2009.
- [63] J.A. Suul, A. Luna, P. Rodriguez, T. Undeland, "Voltage-sensor-less synchronization to unbalanced grids by frequency-adaptive virtual flux estimation," *IEEE Transactions on Industrial Electronics*, vol. 59, no. 7, pp. 2910–2923, July, 2012.
- [64] B.L. Capehart, "Microturbines," [Online]. Available: <http://www.wbdg.org/resources/microturbines.php>. [Accessed July 2014].
- [65] K. Kamdar, G.G. Karady, "Optimal capacity and location assessment of natural gas fired distributed generation in residential areas," in *Proceedings of the IEEE Clemson University Power Systems Conference*, PSC 2014, pp. 1–5, March, 2014.
- [66] Cornell Dubilier, "Aluminum electrolytic capacitors," [Online]. Available: <http://www.cde.com/products/aluminum-electrolytic/#screw-terminal>. [Accessed July 2014].
- [67] O. Ondel, E. Boutleux, P. Venet, "A decision system for electrolytic capacitors diagnosis," in *Proceedings of the 35<sup>th</sup> IEEE Annual Power Electronics Specialist Conference*, PESC04, vol. 6, pp. 4360–4364, June, 2004.
- [68] F. Blaabjerg, M. Liserre, K. Ma, "Power electronics converters for wind turbine systems," *IEEE Transactions on Industry Applications*, vol. 48, no. 2, pp.708–719, March/April, 2012.
- [69] J.A. Alves, G. Cunha, P. Torri, "Medium voltage industrial variable speed drives," [Online]. Available: <http://ecatalog.weg.net/files/wegnet/WEG-medium-voltage-industrial-variable-speed-drives-technical-article-english.pdf>. [Accessed July 2014].

- [70] J. Rodriguez, S. Bernet, B. Wu, J.O. Pontt, S. Kouro, "Multilevel voltage-source-converter topologies for industrial medium-voltage drives," *IEEE Transactions Industrial Electronics*, vol. 54, no. 6, pp. 2930–2945, December, 2007.
- [71] H. Ertl, T. Wiesinger, J.W. Kolar, "Active voltage balancing of DC-link electrolytic capacitors," in *Proceedings of the IET Power Electronics*, vo. 1.1, no. 4, pp. 488–496, December, 2008.
- [72] A. Escobar, J.C. Balda, C.A. Busada, D. Christal, "An indirect matrix converter for CCHP microturbines in data center power systems," in *Proceedings of the 34<sup>th</sup> IEEE International Telecommunications Energy Conference*, pp. 1–6, October, 2012.
- [73] A. Escobar, J.K. Hayes, J.C. Balda, C.A. Busada, "New control strategy for indirect matrix converters operating in boost mode," in *Proceedings of the IEEE Energy Conversion Congress and Exposition, ECCE 2013*, pp. 2715–2720, September, 2013.
- [74] A. Escobar, Yusi Liu, J.C. Balda, K. George, "New power electronic interface combining dc transmission, a medium-frequency bus and an ac-ac converter to integrate deep-sea facilities with the ac grid," in *Proceedings of the IEEE Energy Conversion Congress and Exposition, ECCE 2014*, in Press.
- [75] A. Escobar, J.K. Hayes, J.C. Balda, C.A. Busada, "A sensorless grid synchronization method for modular multilevel converters in HVdc systems," submitted to *IEEE Transaction on Industry Applications*, in review.

## CHAPTER TWO

### AN INDIRECT MATRIX CONVERTER FOR CCHP MICROTURBINES IN DATA CENTER POWER SYSTEMS

A. Escobar, J.C. Balda, C.A. Busada, D. Christal, “An indirect matrix converter for CCHP microturbines in data center power systems,” in *Proceedings of the 34<sup>th</sup> IEEE International Telecommunications Energy Conference*, pp. 1–6, October, 2012.

#### **Abstract**

Data centers (DCs) are considered critical loads that require premium power from utilities to ensure reliability at all times. Microturbine (MT) generation systems are becoming important in DCs, not only as distributed generation (DG) for supplying electricity, but also for providing cooling and heating functions, which is known as combined cooling, heat and power (CCHP) or tri-generation.

This paper considers the use of an indirect matrix converter (IMC) as the power electronic interface (PEI) to connect a permanent magnet synchronous generator (PMSG) with the power grid in a DC. First, the paper analyzes the semiconductor losses for the IMC and the conventional back-to-back converter (BBC) as a function of the switching frequency in order to determine the favorable operating conditions for the IMC. It then presents a new control strategy that does not require measuring the grid voltages to inject the commanded power into the grid at unity power factor. Simulation results of a 15-kVA, 480-Vrms IMC-based MT generation system show the effectiveness of the proposed control technique for this particular application.

## 2.1 Introduction

Data centers are computational centers storing large amounts of information and equipment securely. They run efficiently and provide secure access to applications for users such as social network enterprises, government, financial institutions, news media, universities, etc. To operate without any interruptions, DCs require large amounts of premium power to ensure reliability [1], [2]. Thus, most DC installations have backup power generation systems (i.e., on-site generation and batteries) to provide redundancy when the main power supply fails. Besides electric power, information technology (IT) equipment requires proper cooling to prevent over-heating which may lead to early failures. The cooling system operates continuously and represents a major power consumer in DCs [3]–[5].

Microturbine units are used to drive high-speed PMSG and are becoming more attractive for on-site generation, in particular for loads under 5 MW that also require cooling and heating [6]. In a CCHP process, the wasted heat, a bi-product of the generating process, is used to produce the necessary cooling required by various pieces of equipment to operate safely, and thus, to improve system efficiency. MT-generator sets use different types of fuels to generate electricity (e.g., natural gas), their power range varies from 15 kW up to 1 MW, and operate at high speeds (e.g., 50,000~120,000 rpm). High rotational speeds produce high-frequency voltages that require an ac-ac converter to reduce the generator frequency to the grid frequency [7]. Many reasons are influencing the use of CCHP in DCs: efficiency increases, fossil-fuel energy consumption reductions, distribution line loading reductions, ability to produce cooling using an absorption chiller [6], [8], demand-side management capabilities, and reductions of CO<sub>2</sub> emissions into the atmosphere by a factor of 2 [9]. Fig. 2.1 shows a typical power distribution system for a DC that uses CCHP.



Conventionally, a BBC is used as the PEI to connect the high-frequency voltages generated by a PMSG driven by the MT with the power grid. The BBC consists of two stages that are connected via a dc link having electrolytic capacitors which are well known for their reduced lifetime [10], limiting the BBC mean time between failures. These capacitors are bulky, heavy and unreliable, so they are considered one of the main failure causes in BBCs [11]. Furthermore, grid-connected applications require synchronizing the generator with the grid using a phase-locked loop (PLL) algorithm sensing the grid voltages [12], [13]. The PLL algorithm produces the magnitude, phase and frequency of the grid voltages to synchronize the generator.

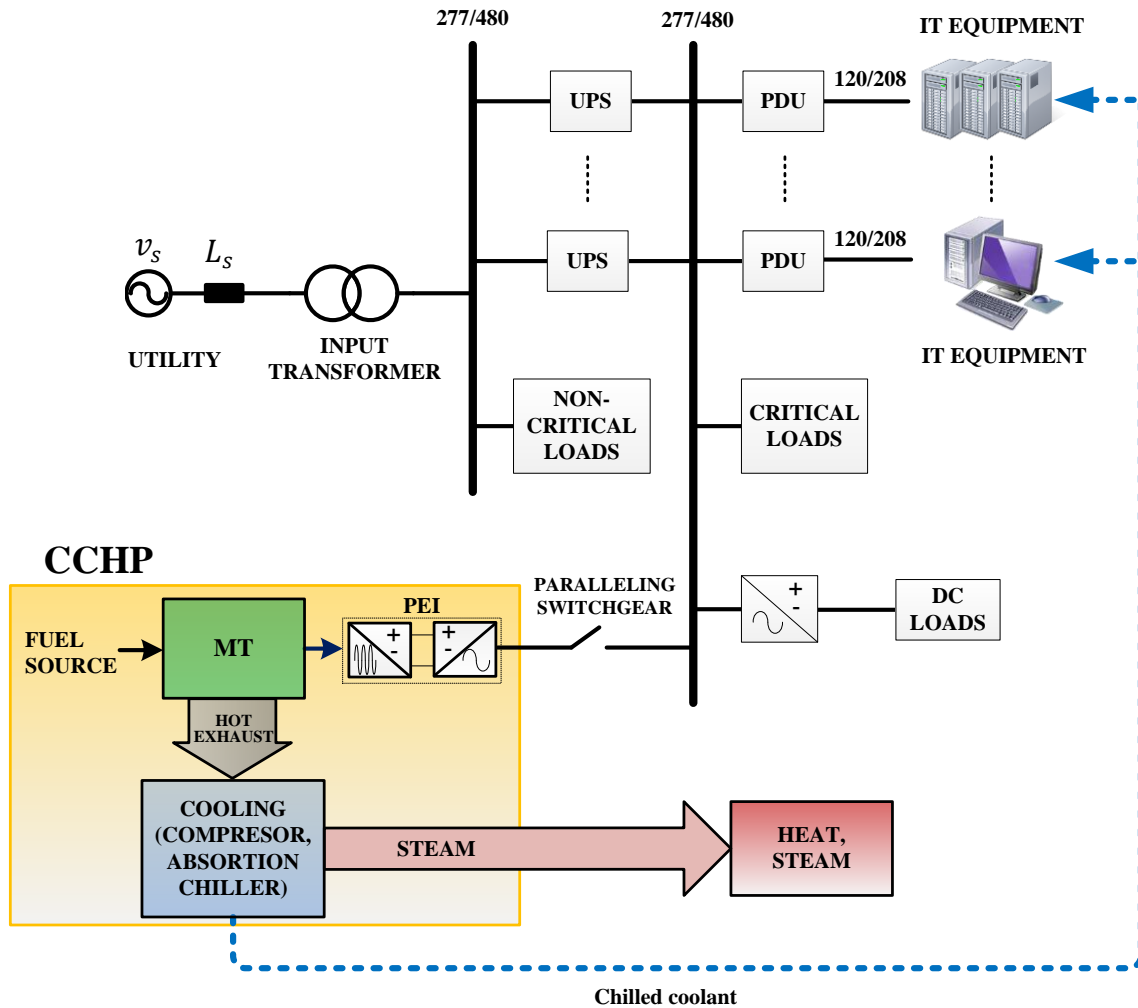


Fig. 2.1. Power distribution system for a DC with CCHP [3], [6]

In the last two decades, the IMC has been widely analyzed as adjustable-speed drives for motor applications; however, some disadvantages such as the low input/output voltage ratio limited to 86%, the complexity of the control techniques to guarantee proper waveforms and safe operation, and the lack of ride-through capabilities have kept the IMC from being adopted by industry [14]–[19]. Despite these disadvantages, IMC may be an alternative for particular applications [18], [19] such as low power, low voltage/fixed frequency ac-to-ac generation where it is possible to adjust the output voltage of a generator to meet grid voltage requirements. Indirect matrix converters have been proposed as a PEI to connect a variable-speed PMSG with a load operating at grid frequency [20]–[22]. The IMC does not have bulky and lifetime-limited dc-link electrolytic capacitors [14], [18]; thus, the converter life span can be improved while facilitating a compact PEI.

Taking into account the above, the paper presents first an analysis of the semiconductor losses in both the IMC and BBC to identify those operating conditions which are more favorable to the IMC. The paper then develops a new control strategy for the inverter stage of the IMC that does not require sensing the grid voltages to connect the IMC inverter stage with the grid. Instead, the IMC output currents, decomposed in the  $d - q$  synchronous frame, are used to calculate the inverter output voltages.

This paper is divided into the following sections: Section 2.2 presents the implementation of an IMC as a PEI for a DC, and compares the BBC and the IMC in terms of efficiency. Section 2.3 provides an introduction to the space vector modulation (SVM) control technique used to control the IMC inverter and rectifier. Section 2.4 presents the proposed new control strategy for the IMC inverter to regulate the injected currents. Lastly, Section 2.5 analyzes results from

simulations to demonstrate the capability of the IMC to connect a high-frequency generating unit with the power grid.

## 2.2 Indirect Matrix Converter as a PEI for DCs

Figure 2.2 depicts a DG system based on a MT that uses an IMC as a PEI. For simplicity, the PMSG is modeled as ideal three-phase voltage sources in series with synchronous inductances, and filters are placed at the input and output of the IMC to filter high-order harmonics that otherwise could affect the PMSG operation and the power quality delivered to the load. In all cases, the total harmonic distortions (THD) for input currents and output voltages should be less than 5% [23]. The grid is also modeled as inductors in series with ideal three-phase voltage sources. The rectifier is made of IGBTs connected in back-to-back configuration to provide IMC bidirectional capability required during start up when the MT operates as a motor drawing power from the grid (motor mode). Once the MT speed threshold is reached, the MT injects power back into the grid (generator mode). The inverter has the same structure as a conventional inverter “brick”.

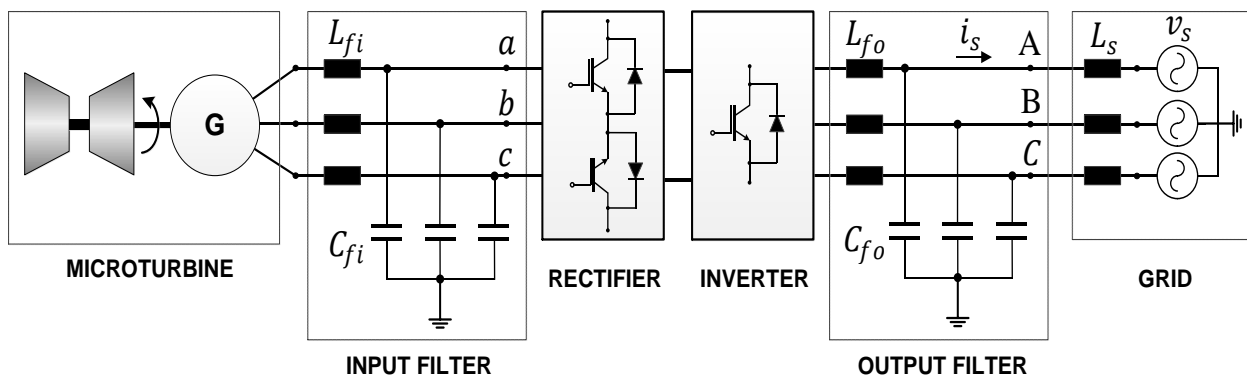


Fig. 2.2. IMC interfacing a high-frequency PMSG with the power grid

### 2.2.1 IMC Loss Calculations

Converter loss calculations are very important to estimate the overall efficiency of the power converter, and to help sizing the cooling system required for the application. In general, the total semiconductor losses of the converters are calculated as the sum of conduction and switching losses. Conduction losses are predominant at low switching frequencies, and switching losses are more significant at high frequencies. The conduction losses are caused mainly by the on-state resistance and on-state voltage across each switch or diode while conducting. The switching losses are due to the commutation process of the semiconductor device depending on the switching frequency as well as the turn-on and turn-off energies dissipated by each device [24].

As shown in Fig. 2.2, the IMC contains two bridges: the rectifier that is treated as a current source bridge (CSB) and the inverter treated as a voltage source bridge (VSB) [25].

For the rectifier, the conduction losses  $P_{c\_CSB}$  are calculated as:

$$P_{c\_CSB} = \frac{9}{2\pi} (V_{CEo} + V_{Do}) m_r I_o \cos\varphi_o + \frac{3\sqrt{3}}{2\pi^2} (r_{CE} + r_D) m_r I_o^2 (1 + 4\cos^2\varphi_o) \quad (2.1)$$

where  $m_r$  is the rectifier modulation index,  $I_o$  the peak output current and  $\varphi_o$  the output angular displacement. No switching losses are present in this stage since it switches when a zero-voltage state is applied to the inverter [26].

For the inverter, the switching losses  $P_{sw\_VSB}$  and the conduction losses  $P_{c\_VSB}$  are calculated as follows:

$$P_{sw\_VSB} = \frac{27}{\pi^2} f_{sw} (E_{on} + E_{off} + E_{rr}) \frac{V_i}{V_{dcnom}} \frac{I_o}{I_{cnom}} \cos\varphi_i \quad (2.2)$$

$$P_{c\_VSB} = 6 \left[ \frac{(V_{CEo} + V_{Do})I_o}{2\pi} + \frac{(V_{CEo} - V_{Do})I_o}{8} m_i \cos \varphi_o + \frac{(r_{CE} + r_D)I_o^2}{8} + \frac{(r_{CE} - r_D)I_o^2}{3\pi} m_i \cos \varphi_o \right] \quad (2.3)$$

where  $m_i$  is the inverter modulation index,  $V_i$  the peak input phase voltage,  $\varphi_i$  the input angular displacement and  $f_{sw}$  the switching frequency.

The methods described in [25]–[27] are used to calculate the losses for the IMC considering the discrete IKW40N120H3 IGBTs from Infineon. Table 2.1 lists IGBT and diode parameters. Figure 2.3 shows the BBC and IMC efficiencies for switching frequencies up to 40 kHz and output currents from 0 A to 30 A. The IMC becomes more efficient for switching frequencies higher than 10 kHz; this is mainly caused due to the capability of commutating the IMC rectifier during the zero-current periods of the dc link (zero-voltage vector applied to the inverter), which reduces rectifier switching losses.

Table 2.1. Semiconductor Device Parameters

Parameter	Symbol	Nominal value
IGBT zero-current voltage drop	$V_{CEo}$	1.05 V
IGBT on-state resistance	$r_{CE}$	25 m $\Omega$
IGBT conduction current under nominal conditions	$I_{cnom}$	40 A
IGBT dc-bus voltage under nominal conditions	$V_{dcnom}$	600 V
IGBT turn-on switching loss under nominal conditions	$E_{on}$	3.20 mJ
IGBT turn-off switching loss under nominal conditions	$E_{off}$	1.20 mJ
Diode zero-current forward voltage drop	$V_{Do}$	1.65 V
Diode on-state forward resistance	$r_D$	22 m $\Omega$

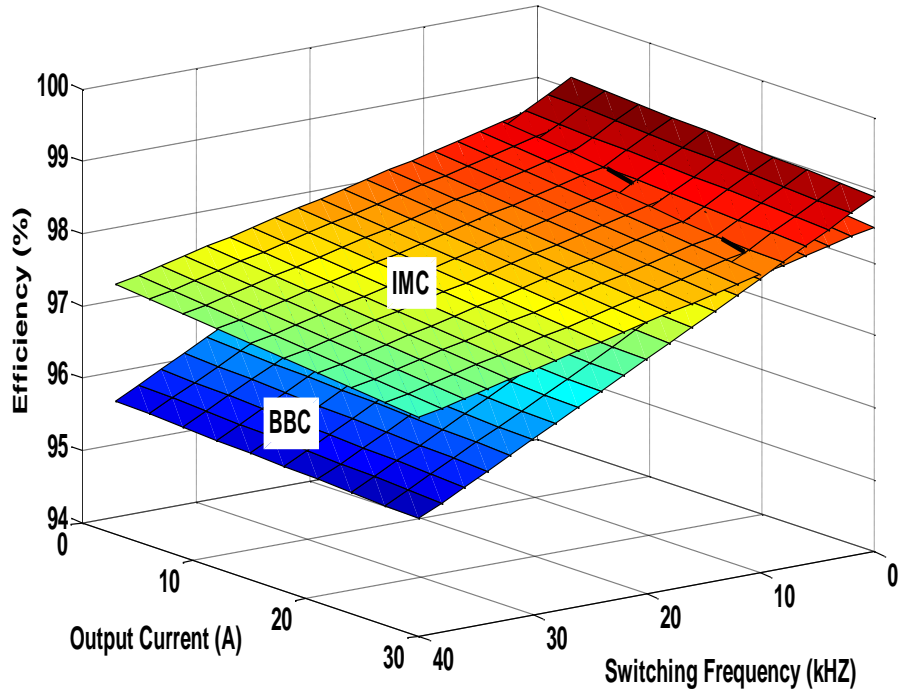


Fig. 2.3. Comparison between BBC and IMC calculated efficiencies based on a 15-kVA converter at 480-Vrms output voltage

The selection of the switching frequency is a trade-off between IMC passive components size and system efficiency, and has an impact on the electromagnetic interference (EMI) and THD [28]. When the  $f_{sw}$  changes from 20 kHz to 30 kHz there is a 50% reduction in the value of the input inductance  $L_{fi}$  (assuming  $C_{fi}$  equals to 50  $\mu$ F for both cases). Based on this result, the switching frequency  $f_{sw}$  for the proposed PEI using an IMC is selected to be 30 kHz since it is beyond the audible noise range and the calculated converter efficiency is above 96%.

### 2.3 Indirect Matrix Converter Control Strategy

To control the IMC rectifier and inverter, a SVM control technique has been traditionally proposed to produce the desired input/output current/voltage sinusoidal waveforms [29]. The

duty cycles in each stage are synchronized in order to provide safe commutation for the rectifier; i.e., rectifier commutates when a null vector is applied to the inverter.

### 2.3.1 Rectifier Stage

It is well known that there are 8 possible combinations for the rectifier switches: 6 active or non-zero vectors; so the desired IMC input currents can be synthesized by making use of the two adjacent active vectors defining any of the SVM six sectors to realize the commanded current vector  $I_{in}$  [30].

Fig. 2.4(a) depicts the current vector  $I_{in}$  in sector I. The duty cycles  $d_\alpha^r$ ,  $d_\beta^r$  and  $d_o^r$  that are used to synthesize this vector are calculated as follows [29]:

$$\begin{aligned} d_\alpha^r &= m_r \sin(\pi/3 - \theta_{in}) \\ d_\beta^r &= m_r \sin(\theta_{in}) \\ d_o^r &= 1 - d_\alpha^r - d_\beta^r \end{aligned} \quad (2.4)$$

where  $\theta_{in}$  is the reference current angle with respect to the considered sector. The IMC input currents can be represented as:

$$\begin{bmatrix} i_a \\ i_b \\ i_c \end{bmatrix} = \begin{bmatrix} d_\alpha^r + d_\beta^r \\ -d_\alpha^r \\ -d_\beta^r \end{bmatrix} I_{dc}, \quad (2.5)$$

and taking into account that  $\theta_{in} = (\omega_i t - \varphi_i + \pi/6)$  yields

$$\begin{bmatrix} i_a \\ i_b \\ i_c \end{bmatrix} = m_r \begin{bmatrix} \cos(\omega_i t - \varphi_i) \\ \cos(\omega_i t - \varphi_i - 2\pi/3) \\ \cos(\omega_i t - \varphi_i + 2\pi/3) \end{bmatrix} I_{dc} \quad (2.6)$$

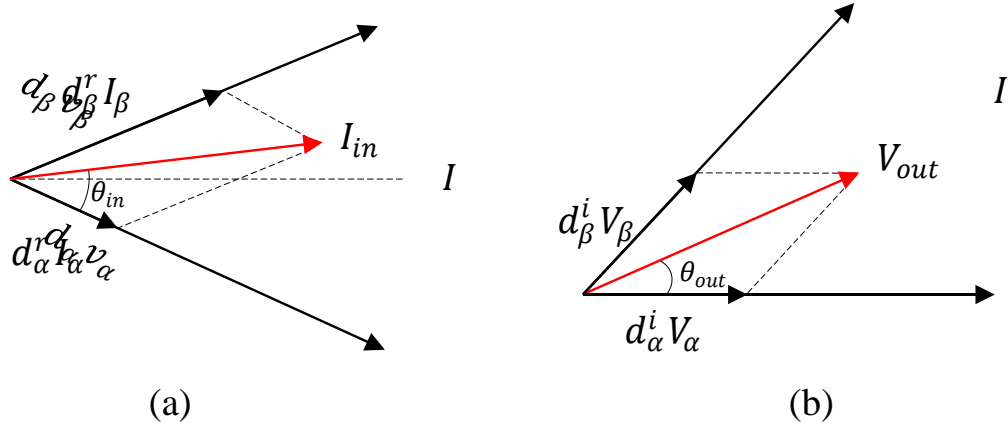


Fig. 2.4. Rectifier (a) and inverter (b) space vector diagram in sector I [29]

with  $0 \leq m_r = I_{in}/I_{dc} \leq 1$  and  $\omega_i$  the input angular frequency. Thus, the input currents can be represented as:

$$\begin{bmatrix} i_a \\ i_b \\ i_c \end{bmatrix} = I_{in} \begin{bmatrix} \cos(\omega_i t - \varphi_i) \\ \cos(\omega_i t - \varphi_i - 2\pi/3) \\ \cos(\omega_i t - \varphi_i + 2\pi/3) \end{bmatrix} \quad (2.7)$$

### 2.3.2 Inverter Stage

The inverter stage must always switch in such a manner that provides a path for the current; otherwise, the semiconductor devices could be destroyed due to undesired overvoltages [30]. In this stage, there are also 6 possible combinations that produce non-zero output voltages and 2 combinations that produce a zero or null output voltage. Likewise for the rectifier stage, the desired output voltage can be determined by using the duty cycles  $d_\alpha^i$ ,  $d_\beta^i$  and  $d_o^i$  in any considered sector [29].

For sector I,

$$\begin{aligned} d_\alpha^i &= m_i \sin(\pi/3 - \theta_{out}) \\ d_\beta^i &= m_i \sin(\theta_{out}) \end{aligned} \quad (2.8)$$



$$d_o^i = 1 - d_\alpha^i - d_\beta^i$$

where  $\theta_{out}$  is the reference voltage angle with respect to this sector. As presented in Fig 2.4(b), the line-to-line voltages can be written as follows:

$$\begin{bmatrix} v_{AB} \\ v_{BC} \\ v_{CA} \end{bmatrix} = \begin{bmatrix} d_\alpha^i + d_\beta^i \\ -d_\alpha^i \\ -d_\beta^i \end{bmatrix} V_{dc,ave} \quad (2.9)$$

For sector I,  $\theta_{out} = (\omega_o t - \varphi_o + \pi/3)$  then,

$$\begin{bmatrix} v_{AB} \\ v_{BC} \\ v_{CA} \end{bmatrix} = m_i \begin{bmatrix} \cos(\omega_o t - \varphi_o + \pi/6) \\ \cos(\omega_o t - \varphi_o + \pi/6 - 2\pi/3) \\ \cos(\omega_o t - \varphi_o + \pi/6 + 2\pi/3) \end{bmatrix} V_{dc,ave} \quad (2.10)$$

with  $0 \leq m_i = \sqrt{3}V_{out}/V_{dc,ave} \leq 1$ ,  $V_{dc,ave}$  the average dc-link voltage [31] and  $\omega_o$  the output angular frequency. Then, the output line-to-line voltages can be represented as:

$$\begin{bmatrix} v_{AB} \\ v_{BC} \\ v_{CA} \end{bmatrix} = \sqrt{3}V_{out} \begin{bmatrix} \cos(\omega_o t - \varphi_o + \pi/6) \\ \cos(\omega_o t - \varphi_o + \pi/6 - 2\pi/3) \\ \cos(\omega_o t - \varphi_o + \pi/6 + 2\pi/3) \end{bmatrix} \quad (2.11)$$

## 2.4 Proposed Control Strategy for the IMC

Applying Kirchhoff's voltage law to the equivalent per-phase circuit of the three phase inverter of the IMC and the grid, the voltages in the  $d - q$  frame can be written as:

$$p i_s^{dq} = \frac{1}{L_s} (v_{inv}^{dq} - v_s^{dq} - j\omega_o L_s i_s^{dq}) \quad (2.12)$$

where vectors like  $v_s^{dq} = v_s^d + jv_s^q$  are constant and rotate at the inverter synchronous speed (i.e., the grid frequency) under steady-state conditions. It is observed that the current is dependent on the cross-coupling terms  $\omega_o L_s i_s^d$  and  $\omega_o L_s i_s^q$ . Eliminating this cross-coupling through the control algorithm should improve the system response.

Conventionally, the voltage oriented control technique (VOC) is used to regulate the active and reactive currents injected by the inverter [32], [33]. For this technique, it is required to sense the grid voltages to determine the required inverter output voltages. To avoid sensing the grid voltages and decoupling the dynamics of the  $d - q$  axes, the following control technique is proposed:

$$v_{inv}^{dq} = -\frac{p\tau + 1}{pC + g} i_s^{dq} + j\omega_o L_s i_s^{dq} \quad (2.13)$$

where  $p$  represents the derivative operator,  $C$  the forward indirect gain,  $\tau$  the forward direct gain, and  $g$  is the conductance gain used to determine the currents injected into the grid at unity displacement power factor and resulting from higher-level controller not shown here [34].

The feed-forward terms  $j\omega_o L_s i_s^{dq}$  are used to decouple the cross-coupling terms, and thus, to improve the dynamic response of the system. Substituting (2.13) into (2.12) yields,

$$p i_s^{dq} = \frac{1}{L_s} \left( -\frac{p\tau + 1}{pC + g} i_s^{dq} - v_s^{dq} \right), \quad (2.14)$$

and,

$$i_s^{dq} = -\frac{pC + g}{p^2 L_s C + (L_s g + \tau)p + 1} v_s^{dq} \quad (2.15)$$

If the transfer function in (2.15) is stable, then, under steady-state conditions ( $p \rightarrow 0$ ):

$$i_s^{dq} = -g v_s^{dq} \quad (2.16)$$

From (2.16), the currents are in phase with the grid voltages. If the conductance  $g$  is positive, the inverter draws power from the grid; and if negative, the inverter injects power into the grid. The schematic of the proposed control strategy is presented in Fig. 2.5.

## 2.5 Simulations Results

In order to determine the feasibility of the proposed controller, the MT-PMSG system whose parameters are listed in Table 2.2 and topology given in Fig. 2.2 was implemented in Matlab/Simulink™. For this case, IGBTs are ideal switches,  $m_r$  is set to 1 to provide the maximum IMC voltage transfer ratio, and the PMSG output voltage is set to 640 Vrms to overcome a 10% voltage drop in the IMC filters and the 86% IMC voltage ratio limitation. Input and output filters are sized in order to get a THD lower than 5% in the input current and the output voltage [23], and have cut-off frequencies of 4 kHz and 1 kHz, respectively. The gains  $\tau$  and  $C$ , are selected to make the denominator of (2.15) stable.

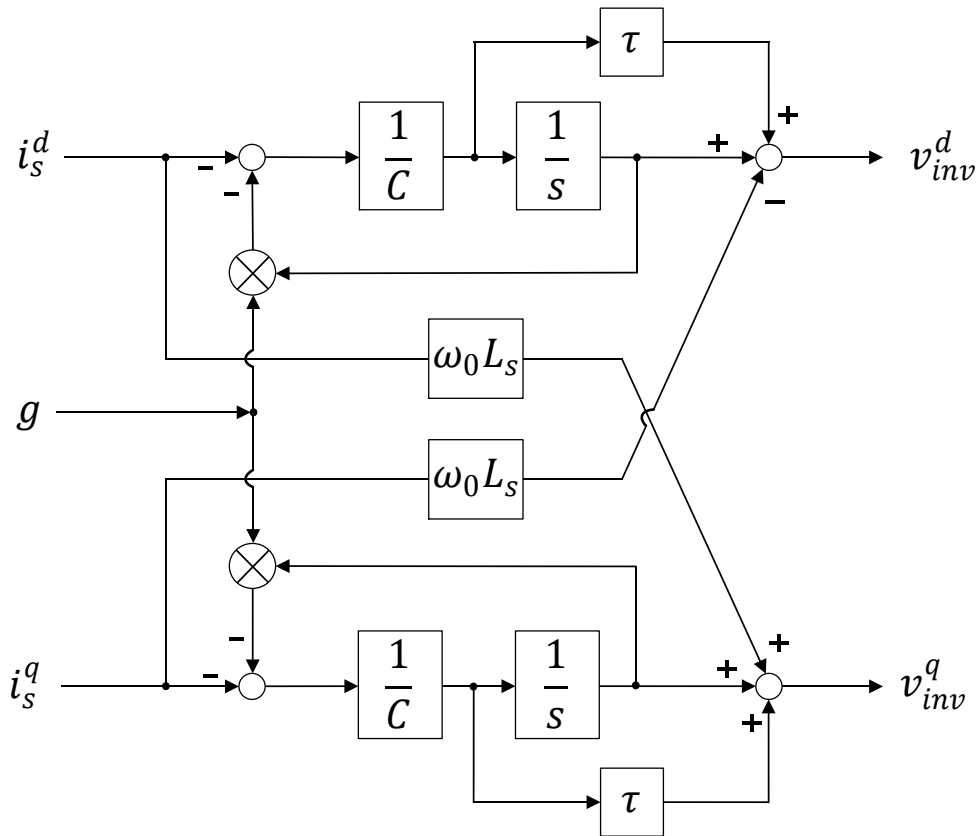


Fig. 2.5. Proposed control block diagram for the IMC inverter

Table 2.2. Parameters of the MT-PMSG System

Parameter	Nominal value
IMC rated power	15 kVA
Generator line-to-line voltage	640 Vrms
Generator frequency	400 Hz
Grid line-to-line voltage	480±5% Vrms
Grid equivalent impedance	$L_s=3$ mH
Grid frequency	60 Hz
$LC$ input filter	$L_{fi}=50$ $\mu$ H, $C_{fi}=50$ $\mu$ F
$LC$ output filter	$L_{fo}=3$ mH, $C_{fo}=5$ $\mu$ F
Switching frequency	30 kHz
$C$	0.0003 $s\Omega^{-1}$
$\tau$	0.002 s

Fig. 2.6 shows the  $i_d$  current variation (red) when the reference current (black) changes while  $i_q$  (blue) remains relatively unchanged since unity power factor is commanded. It is desired to inject 8 Arms at  $t = 20$  ms ( $g = \frac{8}{277} = 0.028$  U), and 13 Arms at  $t = 50$  ms ( $g = \frac{13}{277} = 0.047$  U). The  $d$ -axis current follows the reference which is a (negative) replica of the conductance  $g$ . The settling time is under 10 ms with a 23% overshoot for the worst case. By changing the forward direct and indirect gains in the stable region, it is possible to decrease the settling time. However, this causes larger overshoots in the current. As shown in Fig. 2.7, the inverter output line-to line voltages are nearly sinusoidal with a  $THD_v$  of 3.54%. The 20% overshoot in only the voltage between phases a and b at  $t = 20$  ms is a transient caused as the controller commands new switching states for the inverter in response to a change in the commanded currents; however, this transient does not affect the system stability or semiconductor devices. Lastly, Fig. 2.8 shows the three-phase currents injected into the grid with a 3.1%  $THD_i$ .

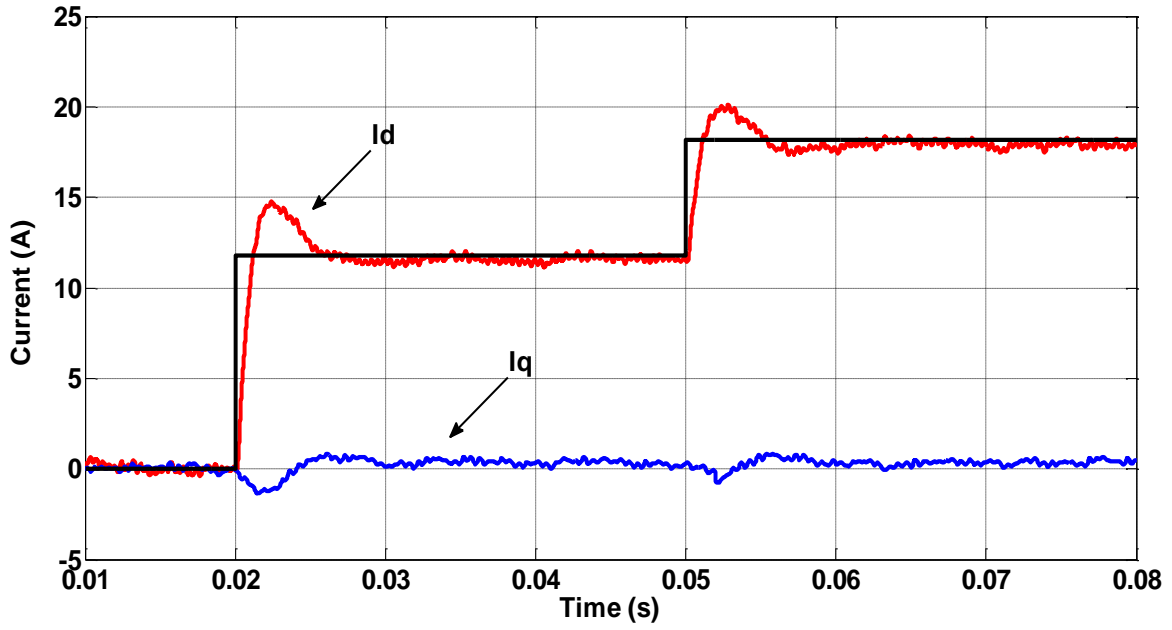


Fig. 2.6.  $d$  and  $q$  current variations for changes of the reference current

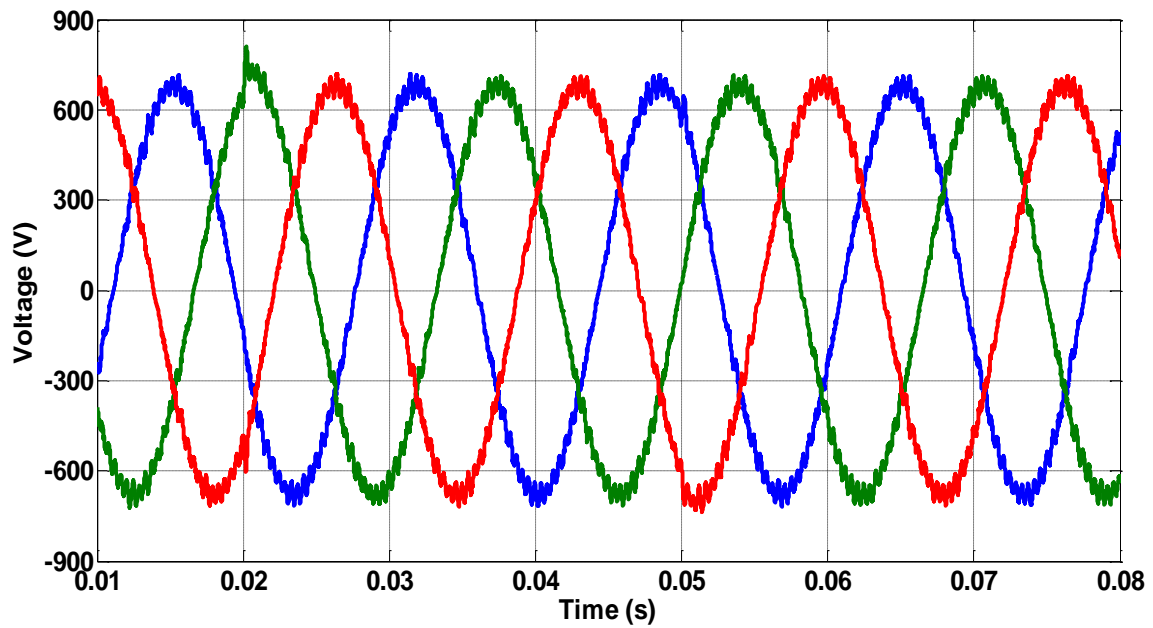


Fig. 2.7. Inverter output line voltage

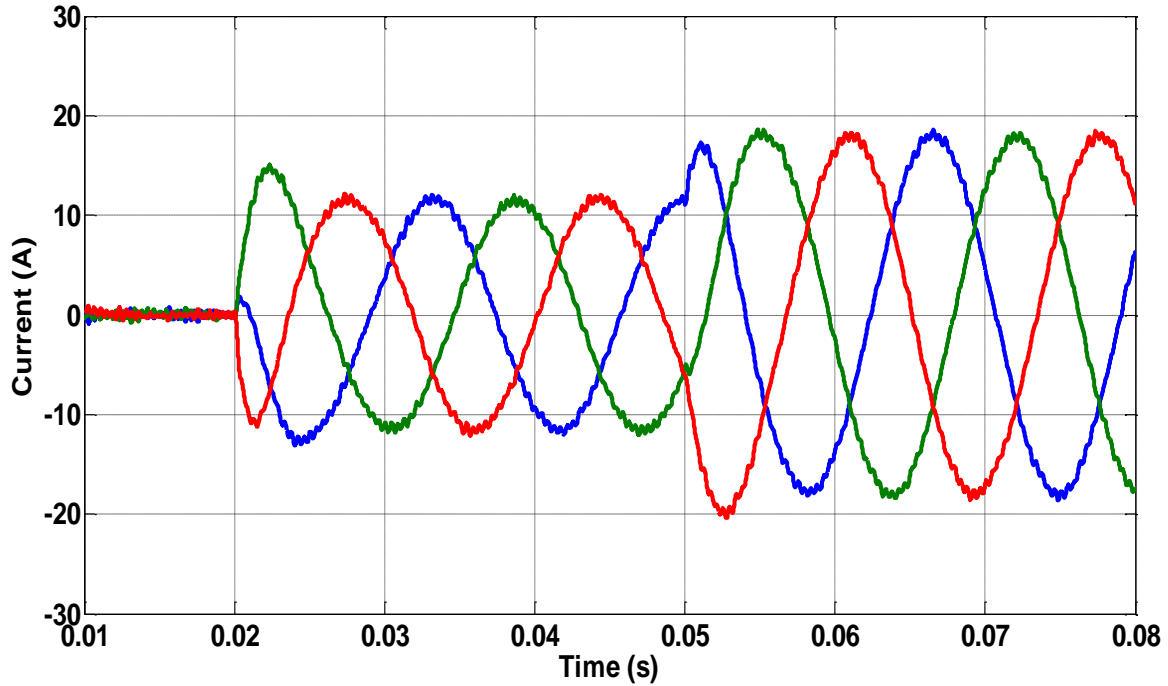


Fig. 2.8. Output currents of the IMC

## 2.6 Conclusions

This paper extended the body of knowledge related to using an IMC to connect a high-frequency MT-PMSG set to the power distribution system of a data center. An analysis of the semiconductor device losses showed that the IMC becomes more efficient than the BBC for switching frequencies above 10 kHz. This was mainly due to the capability of reducing rectifier switching losses by switching the IMC rectifier when the null voltage vector was applied to the inverter stage. The IMC high-frequency operation should allow for size reductions of the filter components, and thus, size reductions of the PEI required for the MT.

A new control strategy in the  $d - q$  frame was presented to control the current injected by the IMC into the grid without sensing the grid voltages. Simulation results illustrated the feasibility

of the control technique to inject the commanded currents without causing any significant or adverse overvoltages or overcurrents.

## Acknowledgments

The authors are grateful for the financial support from GRid-connected Advanced Power Electronics Systems (GRAPES), a National Science Foundation Industry/University Cooperative Research Center. Mr. Andrés Escobar Mejía is grateful for the financial support from the Fulbright Program and the Universidad Tecnológica de Pereira (Colombia).

## References

- [1] S. Satish Rajagopalan, B. Fortenbery, D. Symanski, "Power quality disturbances within DC data centers," in *IEEE 32nd International Telecommunications Energy Conference*, pp. 1–7, June 2010.
- [2] K.E. Herold, R. Radermacher, "Integrated power and cooling systems for data centers," in *Proceedings of the International Society on Thermal Phenomena*, pp. 808–811, August 2002.
- [3] M. Seymour, C. Aldham, M. Warner, H. Moezzy, "The increasing challenge of data center design and management: Is CFD a must?," in *Electronics Cooling Magazine*, pp. 28–33, December 2011.
- [4] U.S. Environmental Protection Agency ENERGY STAR Program, "Report to Congress on Server and Data Center Energy Efficiency Public Law 109-431, August 2007. [Online]. Available: [http://www.energystar.gov/ia/partners/prod\\_development/downloads/EPA\\_Datacenter\\_Report\\_Congress\\_Final1.pdf](http://www.energystar.gov/ia/partners/prod_development/downloads/EPA_Datacenter_Report_Congress_Final1.pdf)
- [5] National Renewable Energy Laboratory (NREL), Best practices guide for energy-efficient data center design," U.S. Department of Energy, March 2011. [Online]. Available: <http://www1.eere.energy.gov/femp/pdfs/eedatacenterbestpractices.pdf>

- [6] K. Darrow, B. Hedman, “Opportunities for combined heat and power in data centers, ICF International, March 2009. [Online]. Available: [http://www1.eere.energy.gov/manufacturing/datacenters/pdfs/chp\\_data\\_centers.pdf](http://www1.eere.energy.gov/manufacturing/datacenters/pdfs/chp_data_centers.pdf)
- [7] S. Grillo, S. Massucco, A. Morini, A. Pitto, F. Silvestro, “Microturbine control modeling to investigate the effects of distributed generation in electric energy networks,” *IEEE Systems Journal*, vol. 4, no. 3, pp. 303–312, September 2010.
- [8] EPA CHP Partnership, “Combined Heat and Power,” [Online]. Available: [http://www.epa.gov/chp/documents/datacenter\\_fs.pdf](http://www.epa.gov/chp/documents/datacenter_fs.pdf)
- [9] U.S. Environmental Protection Agency Combined Heat and Power Partnership, “The role of distributed generation and combined heat and power (CHP) systems in data centers,” August 2007. [Online]. Available: [http://www.epa.gov/chp/documents/datactr\\_whitepaper.pdf](http://www.epa.gov/chp/documents/datactr_whitepaper.pdf)
- [10] S. K. Maddula, J. C. Balda, “Lifetime of electrolytic capacitors in regenerative induction motor drives,” in *Proceedings of the IEEE 36th Power Electronics Specialists Conference*, pp. 153–159, June 2005.
- [11] R. Lai, F. Wang, R. Burgos, Y. Pei, D. Boroyevich, B. Wang, T.A. Lipo, V.D. Immanuel, K.J. Karimi, “A systematic topology evaluation methodology for high-density three-phase PWM AC-AC converters,” *IEEE Transactions on Power Electronics*, vol. 23, no. 6, pp. 2665–2680, November 2008.
- [12] S.-K. Chung, “Phase-locked loop for grid-connected three-phase power conversion systems,” in *Proceedings of the IEE Electric Power Applications*, vol. 147, no. 3, vol. 147, pp. 213–219, May 2000.
- [13] P. Rodríguez, A. Luna, I. Candela, R. Mujal, R. Teodorescu, F. Blaabjerg, “Multiresonant frequency-locked loop for grid synchronization of power converters under distorted grid conditions,” *IEEE Transactions on Industrial Electronics*, vol. 58, no. 1, pp. 127–138, January 2011.
- [14] N. Mahendran, G. Gurusamy, “Replacement of two step power conversion system using matrix converter,” *European Journal of Scientific Research*, vol. 48, no. 2, pp. 238–248, 2010.



- [15] P. W. Wheeler, J. Rodríguez, J. C. Clare, L. Empringham, A. Weinstein “Matrix Converters: A Technology Review,” *IEEE Transactions on Industrial Electronics*, vol. 49, no. 2, pp. 276–288, April 2002.
- [16] J.W. Kolar, T. Friedli, F. Krismer, S. D. Round, “The essence of three-phase AC/AC converter systems,” in *Proceedings of EPE-PEMC*, pp. 27-42, September 2008.
- [17] S. Bernet, S. Ponnaluri, R. Teichmann, “Design and loss comparison of matrix converters and voltage-source converters for modern AC drives,” *IEEE Transactions on Industrial Electronics*, vol. 49, no. 2, pp. 304–314, April 2002.
- [18] J.W. Kolar, F. Schafmeister, S. D. Round, H. Ertl, “Novel three-phase ac-ac sparse matrix converters,” *IEEE Transaction on Power Electronics*, vol. 22, no. 5, pp. 1649–1661, September 2007.
- [19] T. Friedli, J.W. Kolar, “Comprehensive comparison of three-phase ac-ac matrix converter and voltage dc-link back-to-back converter systems,” in *Proceedings of IEEE/IEEE International Power Electronics Conference, IPEC 2010*, Sapporo, Japan, pp. 2789-2798, June 21–24, 2010.
- [20] J.A. Andrade-Romero, J.F. Romero, M. Rafikov, “Optimal control of indirect matrix converter based microturbine generation system,” in *proceedings of the 9<sup>th</sup> International Conference in Control and Automation (ICCA)*, pp. 1085–1090, December 2011.
- [21] M. Hamouda, K. All-Haddad, H. Blanchette, “Input-state feedback linearization control of two-stage matrix converters interfaced with high-speed microturbine generators,” in *proceedings of the IEEE Canada Electrical power Conference*, pp. 302–307, October 2007.
- [22] Wenlang, C. Zhiyoung, Y. Lingzhi, Y. Ning, “Modeling and control on grid-connected inverter stage of two-stage matrix converter for direct-drive wind power system,” in *Proceedings of the 29<sup>th</sup> Chinese Control Conference*, pp. 4928–4932, July 2010.
- [23] *IEEE Recommended practices and requirements for harmonic control in electrical power system*, IEEE Standard 519, June, 1992.
- [24] M. Apap, J.C. Clare, P.W. Wheeler, M. Bland, K. Bradley, “Comparison of losses in matrix converters and voltage source inverters,” in *Proceedings of the IEE Seminar on Matrix Converters*, London, U.K., pp. 4/1–4/6, April 2003.

- [25] B. Wang, G. Venkataramanan, "Analytical modeling of semiconductor losses in matrix converters," in *Proceedings of the CES/IEEE 5<sup>th</sup> International Power and Motion Control Conference, IPEMC 2006*, August 2006.
- [26] S. Round, F. Schafmeister, M. Heldwein, E. Pereira, L. Serpa, J. Kolar, "Comparison of performance and realization effort of a very sparse matrix converter to a voltage DC link PWM inverter with active front end," *IEEE Transaction*, vol. 126-D, no. 5, pp. 578–588, May 2006.
- [27] D. Graovac, M. Pürschel, "IGBT power losses calculation using date-sheet parameters," Infineon, Application note, version 1.1, January 2009.
- [28] M.L Heldwein, J.W. Kolar, "Impact of EMC filters on the power density of modern three-phase PWM converters," *IEEE Transactions on Power Electronics*, vol. 24, no. 6, pp. 1577–1588, June 2009.
- [29] M.Y Lee, P. Wheeler, Christian Klumpner, "Space-Vector modulated multilevel matrix converter," *IEEE Transactions on Industrial electronics*, vol. 57, no. 10, pp. 3385–3394, October 2010.
- [30] M. Hamouda, F. Fnaiech, K. Al-Haddad, "Space vector modulation scheme for dual-bridge matrix converters using safe-commutation strategy," in *Proceedings of the 31<sup>st</sup> Annual Conference of IEEE Industrial Electronics Society, IECON 2005*, pp. 1060–1065, November 2005.
- [31] L. Huber, D. Borojević, "Space vector modulated three-phase to three-phase matrix converter with input power factor correction," *IEEE Transactions on Industry Applications*, vol. 31, no. 6, pp. 1234–1246, November/December 1995.
- [32] R. Kadri, J.-P. Gaubert, G. Champenois, "An improved maximum power point tracking for photovoltaic grid-connected inverter based on voltage-oriented control," *IEEE Transactions on Industrial Electronics*, vol. 58, no. 1, pp. 66–75, January 2011.
- [33] S.A. Larrinaga, M.A. Rodríguez, E. Oyarbide, J.R. Torrealday, "Predictive control strategy for DC/AC converters based on direct power Control," *IEEE Transactions on Industrial Electronics*, vol. 54, no. 3, pp. 1261–1271, June 2007.
- [34] H. Nikkhajoei, M.R. Iravani, "A matrix converter based micro-turbine distributed generation system," *IEEE Transactions on Power Delivery*, vol. 20, no. 3, pp. 2182–2192, July 2005.

## APPENDIX A.1

### PERMISSIONS



RightsLink®

Home

Create Account

Help



**Title:** An indirect matrix converter for CCHP microturbines in data center power systems

**Conference Proceedings:** Telecommunications Energy Conference (INTELEC), 2012 IEEE 34th International

**Author:** Escobar, A.; Balda, J.C.; Busada, C.A.; Christal, D.

**Publisher:** IEEE

**Date:** Sept. 30 2012-Oct. 4 2012

Copyright © 2012, IEEE

User ID
<input type="text"/>
Password
<input type="text"/>
<input type="checkbox"/> Enable Auto Login
<input type="button" value="LOGIN"/>
<a href="#">Forgot Password/User ID?</a>

If you're a [copyright.com](#) user, you can login to RightsLink using your [copyright.com](#) credentials. Already a RightsLink user or want to [learn more?](#)

#### Thesis / Dissertation Reuse

**The IEEE does not require individuals working on a thesis to obtain a formal reuse license, however, you may print out this statement to be used as a permission grant:**

*Requirements to be followed when using any portion (e.g., figure, graph, table, or textual material) of an IEEE copyrighted paper in a thesis:*

- 1) In the case of textual material (e.g., using short quotes or referring to the work within these papers) users must give full credit to the original source (author, paper, publication) followed by the IEEE copyright line © 2011 IEEE.
- 2) In the case of illustrations or tabular material, we require that the copyright line © [Year of original publication] IEEE appear prominently with each reprinted figure and/or table.
- 3) If a substantial portion of the original paper is to be used, and if you are not the senior author, also obtain the senior author's approval.

*Requirements to be followed when using an entire IEEE copyrighted paper in a thesis:*

- 1) The following IEEE copyright/ credit notice should be placed prominently in the references: © [year of original publication] IEEE. Reprinted, with permission, from [author names, paper title, IEEE publication title, and month/year of publication]
- 2) Only the accepted version of an IEEE copyrighted paper can be used when posting the paper or your thesis on-line.
- 3) In placing the thesis on the author's university website, please display the following message in a prominent place on the website: In reference to IEEE copyrighted material which is used with permission in this thesis, the IEEE does not endorse any of [university/educational entity's name goes here]'s products or services. Internal or personal use of this material is permitted. If interested in reprinting/republishing IEEE copyrighted material for advertising or promotional purposes or for creating new collective works for resale or redistribution, please go to [http://www.ieee.org/publications\\_standards/publications/rights/rights\\_link.html](http://www.ieee.org/publications_standards/publications/rights/rights_link.html) to learn how to obtain a License from RightsLink.

If applicable, University Microfilms and/or ProQuest Library, or the Archives of Canada may supply single copies of the dissertation.

BACK

CLOSE WINDOW

Copyright © 2014 [Copyright Clearance Center, Inc.](#) All Rights Reserved. [Privacy statement.](#)  
Comments? We would like to hear from you. E-mail us at [customercare@copyright.com](mailto:customercare@copyright.com)

© 2014 IEEE. Reprinted with permission from A. Escobar, J.C. Balda, C.A. Busada and D. Chirstal, “*An Indirect Matrix Converter for CCHP Microturbines in Data Center Power Systems,*” September/October, 2013.

In reference to IEEE copyrighted material which is used with permission in this thesis, the IEEE does not endorse any of University of Arkansas products or services. Internal or personal use of this material is permitted. If interested in reprinting/republishing IEEE copyrighted material for advertising or promotional purposes or for creating new collective works for resale or redistribution, please go to:

[http://www.ieee.org/publications\\_standards/publications/rights/rights\\_link.html](http://www.ieee.org/publications_standards/publications/rights/rights_link.html) to learn how to obtain a License from RightsLink.



**Department of Electrical Engineering**

1 University Avenue, 3217 Bell Engineering Center, Fayetteville, AR 72701, (479) 575-3005, (479) 575-7967 (fax)

August 3, 2014

To whom it may concern,

This letter is to verify that Mr. Andrés Escobar Mejía, ID number: 010533274, is the first author and did at least 51% of the work for the paper titled "AN INDIRECT MATRIX CONVERTER FOR CCHP MICROTURBINES IN DATA CENTER POWER SYSTEMS".

Kind Regards,

Dr. Juan Carlos Balda

University Professor and Major Advisor to Mr. Escobar Mejía

Department Head

## CHAPTER THREE

### NEW CONTROL STRATEGY FOR INDIRECT MATRIX CONVERTERS OPERATING IN BOOST MODE

A. Escobar, J.K. Hayes, J.C. Balda, C.A. Busada, “New control strategy for indirect matrix converters operating in boost mode,” in *Proceedings of the IEEE Energy Conversion Congress and Exposition*, ECCE 2013, pp. 2715–2720, September, 2013.

#### **Abstract**

Distributed generation (DG) units will become more common not only in microgrids but also conventional power grids due to advantages such as demand-side management capability, the potential for electricity generation at low costs, reduced congestion of transmission lines, and power quality improvements. Matrix converters (MCs) have been proposed as a power electronic interface (PEI) for interconnecting DG units based on microturbines that require efficient and reliable ac-ac converters. A novel current control strategy for indirect matrix converters (IMCs) used as the PEI for DG units operating at variable frequency is introduced. The proposed controller does not require sensing the DG unit output voltages and has the capability of regulating the IMC voltage in order to accommodate the commanded active power. The effectiveness of the proposed control approach is validated using a 5-kVA SiC-based IMC prototype to interface a variable-frequency voltage source with the grid.

#### **3.1 Introduction**

Typically, DG units are connected to the electric grid using voltage source converters (VSCs) which must fulfill the requirements set at the point of common coupling by [1]. The conventional back-to-back converter (BBC), which has a controlled or uncontrolled rectifier and a VSC-based

inverter stage, is the preferred PEI for microturbines, wind turbines or other resources requiring ac-ac conversion.

Over the last few years, MCs have attracted much attention due to their multiple advantages as an ac-ac converter when compared with the traditional BBC. Features such as unity input and output power factors, bidirectional power flow, sinusoidal input currents and output voltages, and lack of bulky and lifetime-limited electrolytic capacitors in the dc link make MCs an appealing solution for niche applications [2], [3], especially those requiring volume and weight reductions. However, limitations such as a low input-to-output voltage ratio (i.e., limited to 86%), a complex commutation sequence, the lack of ride-through capability due to no energy storage components in the dc link, and the lack of commercially available bidirectional power semiconductor devices have prevented MCs from becoming a standard product in industry (e.g., adjustable-speed drive).

There are two types of MCs: conventional matrix converters (CMCs) and IMCs [4]. The CMC uses nine bidirectional switching positions, realized as two unidirectional switching devices in a common-source or common-emitter configuration, to allow a direct connection between the input and the output. The IMC, also called the dual-bridge topology [5], called here the dual-stage topology, separates the ac-ac conversion into rectifier and inverter power stages. This allows independent modulation of each stage, overcoming some of the disadvantages of the CMC, such as the complex commutation algorithm [2]–[4]. The IMC rectifier stage is composed of six bidirectional switching positions, realized using twelve unidirectional devices, for applications that require bidirectional power flow capability, such as motor drives or certain distributed generators (e.g., microturbines). The inverter stage is a conventional two-level, three-phase voltage source inverter (VSI) requiring six unidirectional switches.

As the input-to-output voltage ratio is a limiting factor for certain applications, several methods to increase this ratio have been proposed. Some methods proposed new over-modulation strategies that, although did not require more semiconductor devices, increased input filter requirements due to higher input current THD [6]. Other approaches presented new topologies that added more components either to the input stage of the CMC and IMC [7], or to the virtual dc link [8]–[10], increasing overall system losses and making MCs no longer seen as an “all-silicon” solution.

Another method is given in reference [11], where a motor drive based on the IMC operating under boost mode is proposed. Here, the traditional two-level VSC stage is connected to the input three-phase source and the current source converter (CSC) stage is connected to the load. Boost mode was also applied to grid-connected DG units [12] and wind turbine systems [13], [14]. Under boost operation, the VSC is controlled as an active front-end rectifier where the zero voltage vector (ZVV) is applied to the VSC to boost the input voltage (or DG output voltage). The CSC is modulated in such a way that the virtual dc-link voltage corresponds to the maximum grid line-to-line voltages for the corresponding sector as explained in [15]. Sensors are required at the VSC side to synchronize the IMC input voltages with the DG output voltages.

IMCs have been previously considered as an alternative PEI for grid-connected DG units [13]–[19]. The voltage ratio limitation may not be viewed as a disadvantage since it is normally possible to increase the DG output voltage to match the grid voltage; for instance, by increasing the microturbine speed, though it is not always cost free. Furthermore, electrolytic capacitors, which provide ride-through capabilities for motor drives under system perturbations like voltage sags, may not be required at this level since the IMC is directly connected to the DG unit. However, any change in the power (current) references must be compensated by the energy



stored in shaft of the DG unit. In the case of the BBC, the electrolytic capacitor provides short-time energy required during changes in the power references and decouples the rectifier and inverter stages allowing for the implementation of independent controllers.

Taking into account the above, a new control strategy that does not require sensing the DG output voltages for synchronizing an IMC operating in boost mode with the grid is proposed. This paper is organized as follows: The system under study is described in section 3.2, the pulse-width modulation (PWM) techniques used for the IMC rectifier and inverter stages and the proposed controller to regulate the grid injected currents is given in section 3.3, the experimental results are presented in section 3.4, and lastly, the conclusions of this research are addressed in section 3.5.

### **3.2 IMC-Based DG System Description**

The topology of the system under study is given in Fig. 3.1, where the IMC is used to interface a DG unit with the electrical grid. The DG-side converter operates as a bidirectional voltage source rectifier (VSR), and the grid-side converter as a bidirectional current source inverter (CSI) [12] when bidirectional power flow is required for some applications like starting a microturbine. The bidirectional switch in the CSI stage is realized as two unidirectional switching devices in a common-emitter or common-collector configuration or other possible arrangements [20]. Filters are placed at the input and output of the IMC to adequately remove high-order harmonics that otherwise affect the DG unit and the quality of the power delivered to the grid. The total harmonic distortions (THD) for input voltages and output currents are kept below 5% (see [1]). The voltage source  $v_s$  and the inductor  $L_s$  represent the DG unit back-emf and synchronous reactance, respectively.

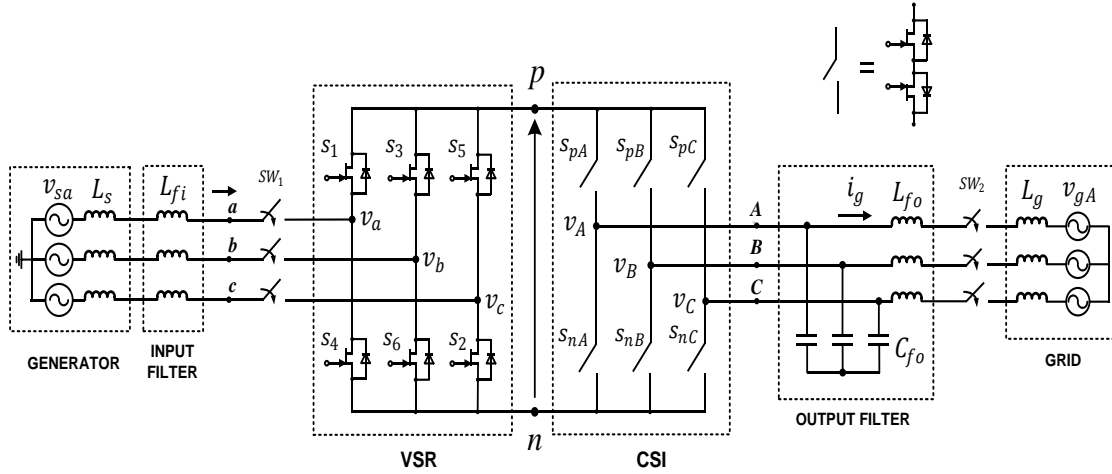


Fig. 3.1. Configuration of the IMC in boost mode as the PEI for a DG unit

The filter inductor  $L_{fi}$  serves two purposes: to interconnect the sinusoidal voltage source to the VSR, and to perform the function of the boost inductor to match the source voltage with the grid voltage. For the output filter, a parallel capacitor bank and series inductors,  $C_{fo}$  and  $L_{fo}$ , respectively, are used to filter the current high-frequency components. The grid is represented by an inductor  $L_g$ , which represents the equivalent series impedance of the isolation (distribution) transformer, in series with an ideal voltage source  $v_g$ .

### 3.3 Indirect Matrix Converter Control Strategy

#### 3.3.1 VSR and CSI Modulation

The control of the IMC rectifier and inverter stages has been extensively investigated [21]. In general, space vector modulation (SVM) is implemented in both power stages to produce the desired input current and output voltage sinusoidal waveforms at unity power factor [22]–[24].

The VSR switching sequence must have ZVVs to boost the input voltage (i.e., using the input inductance). These vectors are produced in the VSR by turning ON either  $S_1, S_3$  and  $S_5$  or  $S_2, S_4$  and  $S_6$ . Fig. 3.2(a) shows the six active nonzero voltage vectors  $V_1 \sim V_6$  and two ZVVs,  $V_0, V_7$  in

the VSR. The reference voltage vector  $V_{in}^*$  is synthesized by making use of the two adjacent active vectors  $V_\alpha$  and  $V_\beta$  defining a particular sector. The duty cycles are determined by the controller proposed in section 3.4.

The grid-connected converter consists of a CSI that can typically assume nine allowed combinations divided into six active nonzero current vectors  $I_1 \sim I_6$  and three null current vectors. The CSI modulation keeps the dc-link voltage commutating between the largest and the second largest positive line-to-line grid voltages [2]. For this case, none of the ZVVs are used to avoid causing a short circuit between the grid phases, which in turn will make the virtual dc-link voltage zero [12]. For the active stages, one of the upper (bottom) switches remains ON whereas two of the bottom (upper) switches of different phases modulate to achieve the maximum voltage in the dc link. All other switches remain OFF.

As shown in Fig. 3.2(b), the reference IMC output current can be synthesized by making use of the two adjacent active vectors,  $I_\alpha$  and  $I_\beta$ , defining any of the six SVM sectors to realize the commanded current vector  $I_{out}^*$ . The CSI commutates when a ZVV is present in the VSR, hence zero dc-link current, reducing switching losses.

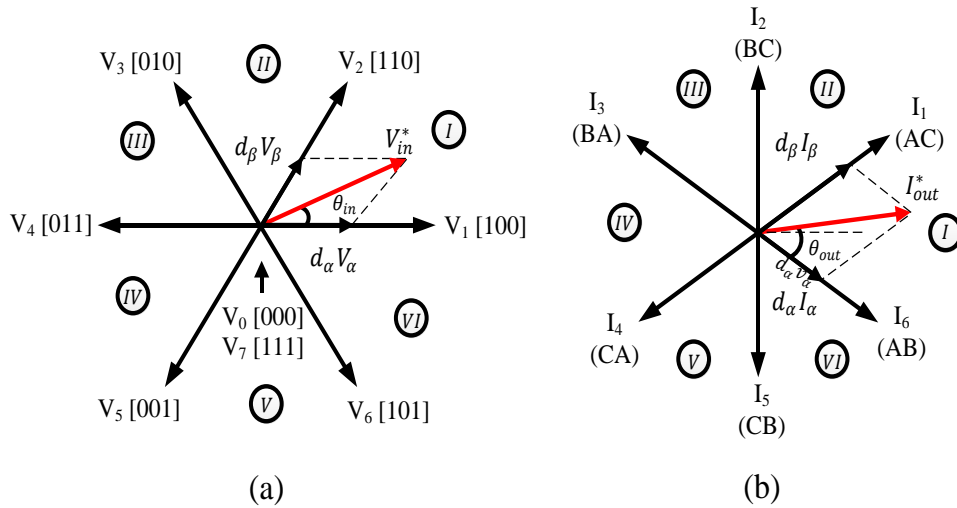


Fig. 3.2. VSR (a) and CSI (b) space vector diagrams [12], [25]

### 3.3.2 Proposed Sensorless Controller

Assuming a very high switching frequency ( $f_{sw}$ ) for control purposes, the VSR can be considered as an ideal three-phase voltage source  $v_{VSR}$  at the source fundamental frequency. Then, a per-phase equivalent circuit having  $v_s$  and  $v_{VSR}$  connected by an inductor  $L = L_s + L_{fi}$  could be used to develop the proposed controller. Applying Kirchhoff's voltage law to this circuit, the voltage in the  $d - q$  frame is written in the Laplace domain as follows:

$$\begin{bmatrix} s i_s^d \\ s i_s^q \end{bmatrix} = \frac{1}{L} \begin{bmatrix} v_s^d - v_{VSR}^d \\ v_s^q - v_{VSR}^q \end{bmatrix} + \begin{bmatrix} \omega_i i_s^q \\ -\omega_i i_s^d \end{bmatrix}, \quad (3.1)$$

where  $\omega_i$  is the DG unit frequency, and  $i_s^{dq}$ ,  $v_s^{dq}$  and  $v_{VSR}^{dq}$  represent the DG unit output current and internal or back emf voltage, and the VSR input voltage. The dynamic responses of the axes are related through the cross-coupling terms  $\omega_i i_s^d$  and  $\omega_i i_s^q$ . Eliminating these terms through the control algorithm will improve the dynamic response of the system. Several techniques have been proposed to regulate the active and reactive powers injected by the DG unit [17], [26]. In all of the cases, it is required to sense the generated voltages to determine the required VSR input voltages. To avoid sensing the DG unit output voltages and decouple the dynamics of the  $d - q$  axes, the control technique whose schematic is depicted in Fig. 3.3 is proposed to calculate the control signals for the VSR [19]:

$$\begin{bmatrix} v_{VSR}^d \\ v_{VSR}^q \end{bmatrix} = -\frac{As + 1}{Bs + g} \begin{bmatrix} i_s^d \\ i_s^q \end{bmatrix} + \omega_i L \begin{bmatrix} i_s^q \\ -i_s^d \end{bmatrix}, \quad (3.2)$$

where  $A$  and  $B$  represent the forward direct gain and the forward indirect gain, respectively, and  $g$  is the conductance gain to determine the desired current injected into the grid at unity displacement power factor. The feed-forward terms  $\omega_i L i_s^d$  and  $\omega_i L i_s^q$  are introduced to decouple the effect of the cross-coupling terms in (3.1). The terms  $v_{VSR}^d$  and  $v_{VSR}^q$  are then used to determine the VSR PWM signals. Substituting (3.2) into (3.1) yields:

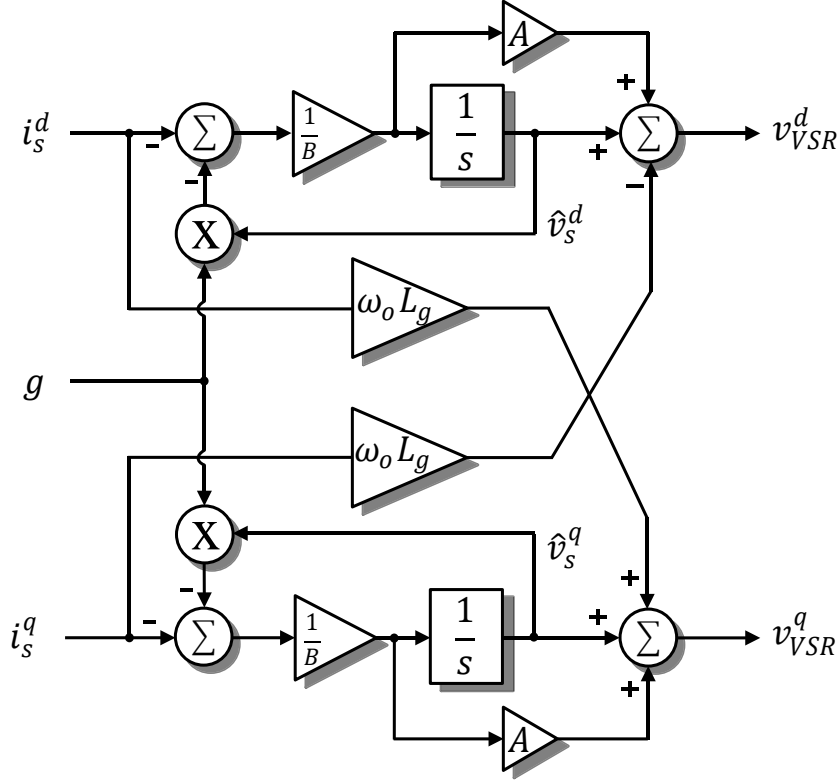


Fig. 3.3. Proposed control block diagram for the IMC

$$\begin{bmatrix} i_s^d \\ i_s^q \end{bmatrix} = \frac{Bs + g}{BLs^2 + (Lg + A)s + 1} \begin{bmatrix} v_s^d \\ v_s^q \end{bmatrix}. \quad (3.3)$$

Under steady-state conditions,  $s \rightarrow 0$ , and (3.3) becomes:

$$\begin{bmatrix} i_s^d \\ i_s^q \end{bmatrix} = g \begin{bmatrix} v_s^d \\ v_s^q \end{bmatrix}. \quad (3.4)$$

This indicates that the currents are in phase with the DG unit output voltages. Hence, if the conductance  $g$  is positive, the DG unit injects active power into the grid; and if negative, it draws power from the grid.

The estimated DG unit voltages  $\hat{v}_s^d$  and  $\hat{v}_s^q$  are determined as the output of the integrators shown in Fig. 3.3. These estimated voltages and the measured current are used to calculate the injected active power.

The analysis of the characteristic equation in (3.3) determines the performance of the proposed controller. For this second order equation, the stability is guaranteed when  $(Lg + A) > 0$  and  $B > 0$ . The gain  $A$  is selected in such a way that (3.3) remains stable when  $g$  changes between the maximum and minimum values, which are functions of the converter rated values. From (3.4), the conductance  $g$  is equal to the ratio between the maximum current provided by the DG unit and the DG unit line-to-line voltage in the steady state. For positive values of  $g$ , power flows from the DG unit to the grid, thus  $A$  is determined as  $-Lg < A$ . If negative then  $Lg < A$ . The gain  $B$  is chosen in such a way that  $B > (Lg + A)^2 / 4L$ .

### 3.4 Experimental Results

The proposed controller is experimentally validated with a 5-kVA SiC-based IMC prototype composed of eighteen discrete SiC-JFETs (1200V/30A,  $T_j = 125^\circ C$ ) from SemiSouth; twelve for the CSI and six for the VSR. Discrete SiC Schottky diodes (1200V/17A,  $T_j = 125^\circ C$ ) from CREE are used in both converter stages. One bidirectional position (e.g.,  $S_{pA}$ ) consists of two JFETs and two diodes in a common-source configuration. The prototype schematic and overall test setup is presented in Fig. 3.4. The VSR is connected through the  $L_{fi}$  inductor to a three-phase 5-kVA Si-based inverter used to mimic the behavior of a microturbine operating at a fundamental output frequency of 100 Hz. The CSI is connected to the 60-Hz grid through the LC filter,  $L_{fo}$  and  $C_{fo}$ . Both input and output filters are designed to achieve a THD of lower than 5% in the input voltage and the output current, and have cut-off frequencies of 1 kHz and 4 kHz, respectively. A step-up transformer with equivalent series impedance  $L_g$  is used to provide galvanic isolation between the IMC and the grid.

The closed-loop control of the IMC system is implemented using a TMS320F28335 DSP from Texas Instruments that has a 150-MHz system clock, ADC inputs and PWM outputs for the IMC control. In accordance with the proposed control algorithm, the input current  $i_s$  is sensed using LEM current transducers and signal-conditioned via a DSP-based control board to interface with the DSP to generate the appropriate PWM signals at  $f_{sw}$ . The parameters of the system are listed in Table 3.1.

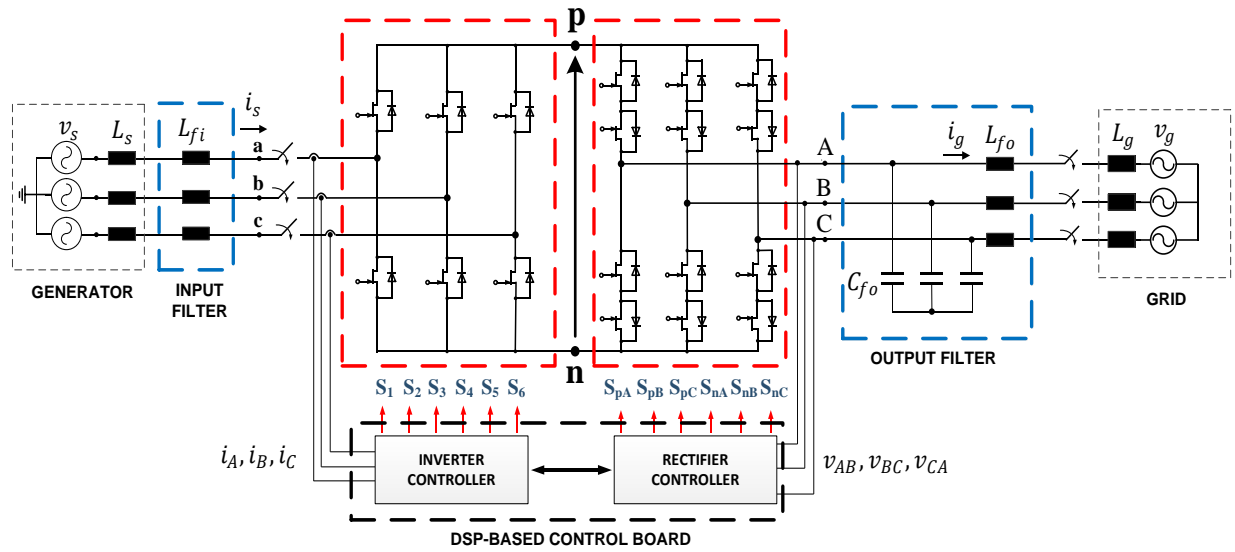


Fig. 3.4. Overall control scheme

Table 3.1. System parameters

Parameter	Nominal Value
$L = L_s + L_{fi}$	1.5 mH
$C_{fo}$	10 $\mu$ F
$L_{fo}$	70 $\mu$ H
$L_g$	0.9 mH
$f_{sw}$	30 kHz
$i_{s,max}$	20 A <sub>rms</sub>
$v_s$	50 V <sub>rms</sub>
$A$	-0.1 mH $\bar{U}$
$B$	9.6 $\mu$ H $\bar{U}^2$

The gain  $A$  is calculated with the rated values of the DG unit, whereas the gain  $B$  is determined by the step response of (3.3) illustrated in Fig. 3.5. The gain  $B$  is selected in such a way that the current does not exceed 20% of the rated current of the system when the DG unit output voltage  $v_s$  is equal to its peak value. This assures the safety of the power semiconductors when the converter locks onto the grid.

The voltage across the  $L_{fi}$  inductor is the difference between the DG unit output voltage and the VSR voltage. In addition, the  $L_{fi}$  inductor has the same function as the inductor in a conventional boost converter; therefore, it plays an important role in the performance of the IMC. The maximum inductor size required to boost the voltage is [27]:

$$L < \frac{\sqrt{\frac{V_{dc}^2}{3} - (|v_s|)^2}}{\omega_i i_s^d} \quad (3.5)$$

where  $V_{dc}$  is the average value of the dc-link voltage, which is equal to  $3V_m/2$  [15],  $V_m$  is the peak of the desired IMC output voltage, and  $|v_s|$  is the peak output voltage of the DG unit. The maximum inductor size for the selected test conditions is 2.2 mH.

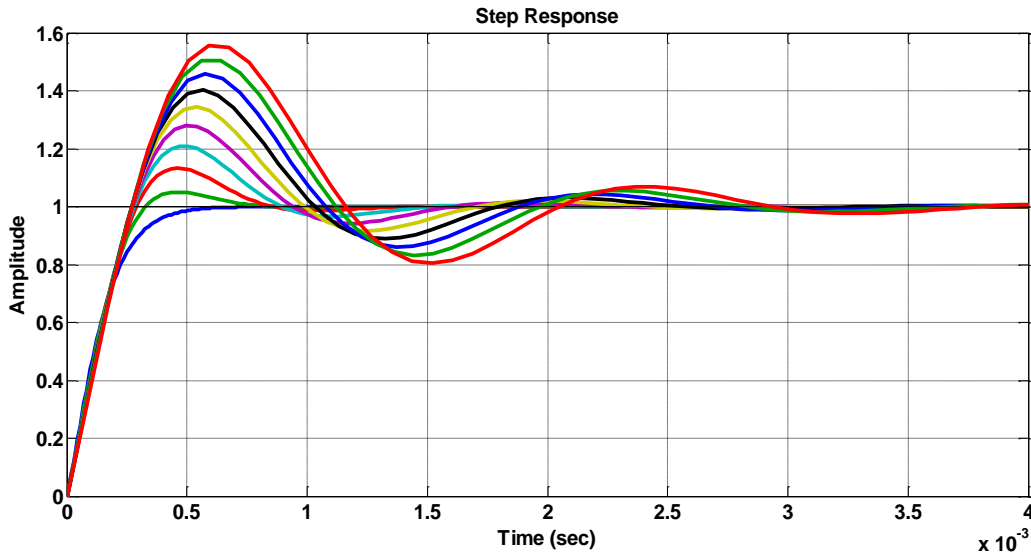


Fig. 3.5. Step response of (3.3) used to determine  $B$



A high inductor value causes a small ripple in the current; whereas a low inductor value makes the IMC more controllable, increasing the dynamic response of the system. This ripple current causes the inductor to charge and discharge energy periodically. Thus, the ZVV is used in the VSR in the same manner as in a boost controlled rectifier. The  $L_{fi}$  inductor stores energy during the ZVV states (current increases), and releases energy during the active switching states. However, there are tradeoffs between the ripple current and inductor value as illustrated in Fig. 3.6, which presents the relationship between the input current THD and the inductance for switching frequencies from 10 kHz to 40 kHz, calculated through simulations. Thus, a  $L = 1.5$  mH value below the calculated maximum inductance is chosen to maintain the current THD under 5%.

The experimental results are presented in Fig. 3.7 and Fig. 3.8. As illustrated in Fig. 3.7, the output line-to-line voltage of the generator is set to 50 Vrms at a frequency of 100 Hz. It is desired to boost the generator voltage by 50% and to inject 2 Arms into the grid, which corresponds to a generator current  $i_s$  of 3 Arms ( $g = \frac{3}{28.875} = 0.1\text{U}$ ).

The variable-frequency DG unit is synchronized to the grid as follows. First, the grid-side breaker is closed. If the voltage drop across the output filter inductor is negligible, the voltage across the capacitor corresponds to the primary side of the step-up transformer. The voltage sensors at the output of the CSI sense the grid voltage for control purposes to obtain the virtual dc-link voltage.

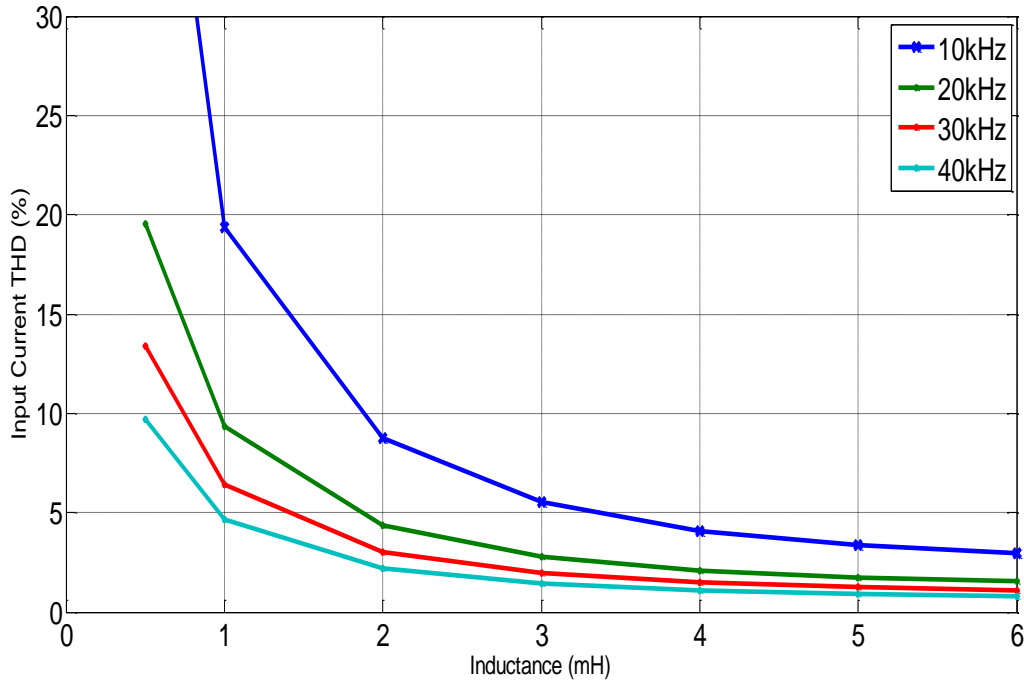


Fig. 3.6. Input current THD as a function of  $L_{fi}$

From Fig. 3.7, the grid voltage is set, through the transformer, to 75 Vrms. The virtual dc-link voltage waveform has six envelopes per fundamental cycle of the grid voltage, corresponding to the control of the CSI, and has a peak magnitude equal to that of the grid voltage. The generator-side breaker is then closed. The transient of the generator current when the breaker is initially closed allows the proposed controller to lock on to the generator voltage. Since  $g = 0$ , no current will flow, and the generator voltage and VSR input voltage will be equal. When  $g$  is set to  $0.1\bar{U}$  as explained above, the VSR input voltage is boosted to the grid level as shown in Fig. 3.7. The generator current is 3 Arms and the injected grid current is 2 Arms; refer to Fig. 3.8.

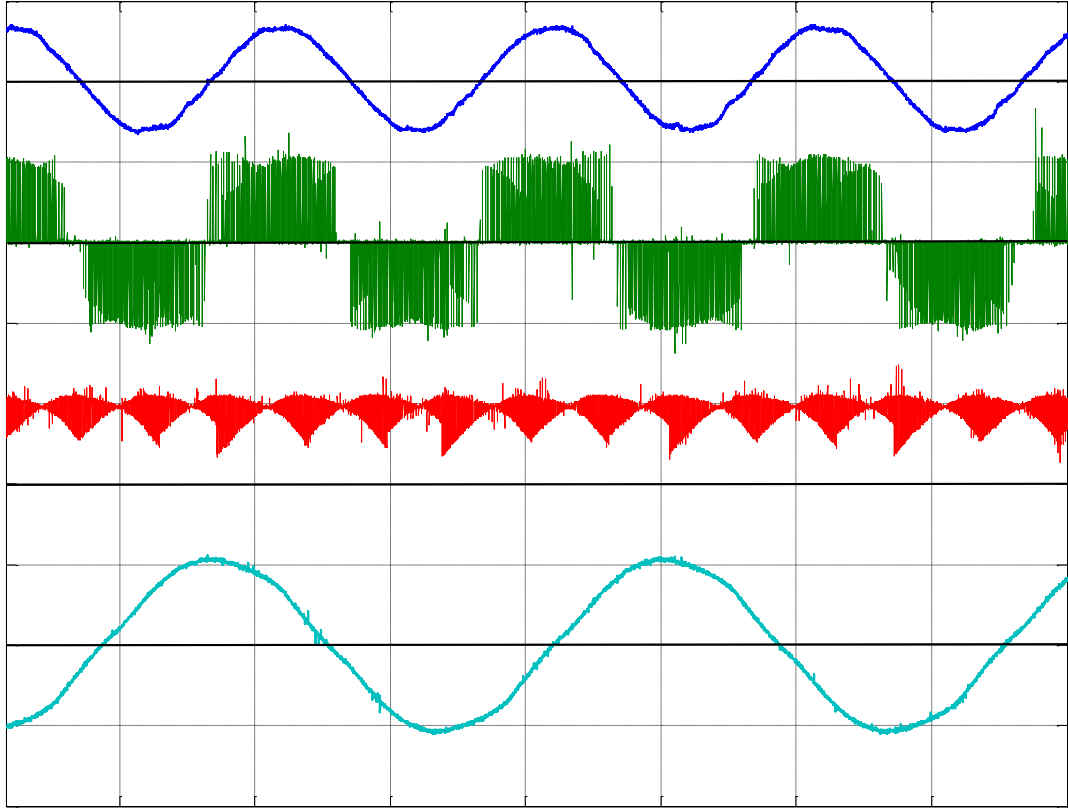


Fig. 3.7. Generator output voltage (top), VSR input voltage and virtual dc-link voltage (middle), grid voltage (bottom) - Voltage scale is 100 V per division with a time scale of 5 ms per division

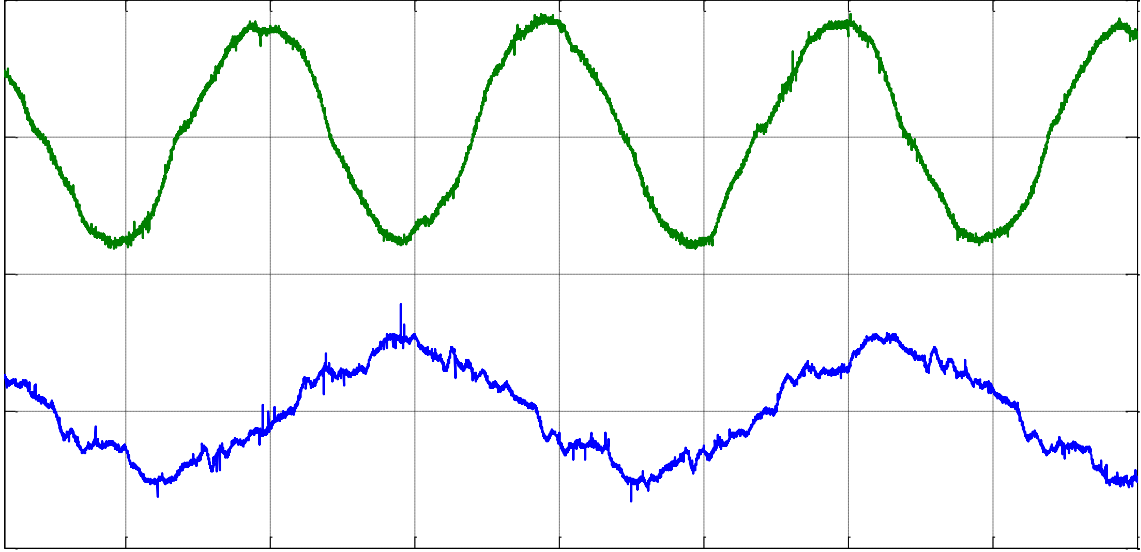


Fig. 3.8. Generator output current (top), injected grid current (bottom). The current scale is 5 A per division with a time scale of 5 ms per division

### **3.5 Conclusions**

Indirect matrix converters have several merits that warrant consideration as the power electronic interface for variable-frequency distributed generation units. A novel current control strategy for IMCs operating under the boost mode was proposed. This strategy did not require sensing the DG output voltage to synchronize with the power grid. Under steady-state conditions, the currents of the DG unit are in phase with the grid voltages, thus injecting (or drawing) the commanded active power. A method was illustrated to properly select the controller gains and thus guarantee the system stability. Experimental results were presented to validate the proposed current control strategy. One advantage for this sensorless controller is that it can be used as a back-up control strategy in the case of DG unit output voltage sensor failure. In future works, the proposed controller will be tested under different grid conditions such as voltage variations and voltage harmonic content.

### **Acknowledgments**

The authors are grateful to the National Science Foundation Industry/University Cooperative Research Center on GRid-connected Advanced Power Electronics Systems (GRAPES). Mr. Andrés Escobar-Mejía is grateful for the financial support as assistant professor of the Universidad Tecnológica de Pereira (Colombia) through the studies commission grant for full-time professors and the Fulbright-LASPAU program.

## References

- [1] IEEE Standard for Interconnecting Distributed Resources with Electric Power Systems, IEEE Standard 1547, July 2003.
- [2] T. Friedli, J.W. Kolar, “Comprehensive comparison of three-phase ac-ac matrix converter and voltage dc-link back-to-back converter systems,” in *Proceedings of IEEE/IEEE International Power Electronics Conference*, IPEC 2010, Sapporo, Japan, pp. 2789–2798, June 2010.
- [3] T. Friedli, J.W. Kolar, J. Rodriguez, P.W. Wheeler, “Comparative evaluation of three-phase ac-ac matrix converter and voltage dc-link back-to-back converter systems,” *IEEE Transactions on Industrial Electronics*, vol. 59, no. 12, pp. 4487–4510, December 2012.
- [4] J.W. Kolar, T. Friedli, F. Krismer, S.D. Round, “The essence of three-phase AC/AC converter systems,” in *Proceedings of the 13<sup>th</sup> International Power Electronics and Motion Control Conference*, EPE-PEMC 2008, pp. 27–42, 2008.
- [5] L. Wei, T.A. Lipo, H. Chan, “Matrix converter topologies with reduced number of switches,” in *Proceedings of the IEEE 33<sup>rd</sup> Annual Power Electronics Specialists Conference*, PESC02, pp. 57–63, November 2002.
- [6] G.T. Chiang, J. Itoh, “Comparison of two overmodulation strategies in an indirect matrix converter,” in *IEEE Transactions on Industrial Electronics*, vol. 60, no. 1, pp. 43–53, January 2013.
- [7] J. Itoh, K. Koiwa, and K. Kato, “Input current stabilization control of a matrix converter with boost-up functionality,” in *Proceedings of the International Power Electronics Conference*, IPEC 2010, pp. 2708–2714, June 2010.
- [8] B. Ge, Q. Lei, W. Qian, F.Z. Peng, “A family of Z-source matrix converters,” *IEEE Transactions on Industrial Electronics*, vol. 59, no. 1, pp. 35–46, January 2012.
- [9] T. Wijekoon, C. Klumpner, P. Zanchetta, P.W. Wheeler, “Implementation of a Hybrid AC–AC direct power converter with unity voltage transfer,” *IEEE Transactions on Power Electronics*, vol. 23, no. 4, pp. 1918–1926, July 2008.
- [10] S. Zhang, K.J. Tseng, T.D. Nguyen, “Novel three-phase AC-AC Z-Source converters using matrix converter theory,” in *Proceedings of the Energy Conversion Congress and Exposition*, ECCE 2009, pp. 3063–3070, September 2009.

- [11] L. Wei, T.A. Lipo, “Investigation of the dual bridge matrix converter operating under boost mode,” Research Repor 2004-12. [Online]. Available: [http://lipo.ece.wisc.edu/2004pubs/2004\\_12.pdf](http://lipo.ece.wisc.edu/2004pubs/2004_12.pdf). [Accessed July 2014].
- [12] X. Liu, P. C. Loh, P. Wang, F. Blaabjerg, Y. Tang, E.A. Al-Ammar, “Distributed generation using indirect matrix converter in reverse power mode,” *IEEE Transactions on Power Electronics*, vol. 28, no. 3, pp. 1072–1082, March 2013.
- [13] M. Aner, E. Nowicki, D. Wood, “Employing a very sparse matrix converter for improved dynamics of grid-connected variable speed small wind turbines,” in *Proceedings of the IEEE Power and Energy Conference at Illinois, PEI*, February 2012.
- [14] M. Aner, E. Nowicki, “Two-level backward operation of a VSMC for PMSG grid-connected variable speed wind turbine systems,” in *Proceedings of the IEEE International Electric Machines & Drives Conference, IEMDC 2011*, pp. 1100–1106, May 2011.
- [15] L. Wei, T.A. Lipo, “A novel matrix converter topology with simple commutation,” in *Proceedings of the 36<sup>th</sup> IEEE Industry Applications Conference*, vol. 3, pp. 1749–1754, October 2001.
- [16] J.A. Andrade-Romero, J.F. Romero, M. Rafikov, “Optimal control of indirect matrix converter based microturbine generation system,” in *Proceedings of the 9<sup>th</sup> International Conference in Control and Automation (ICCA)*, pp. 1085–1090, December 2011.
- [17] M. Hamouda, K. All-Haddad, H. Blanchette, “Input-state feedback linearization control of two-stage matrix converters interfaced with high-speed microturbine generators,” in *Proceedings of the IEEE Canada Electrical Power Conference*, pp. 302–307, October 2007.
- [18] Wenlang, C. Zhiyoung, Y. Lingzhi, Y. Ning, “Modeling and control on grid-connected inverter stage of two-stage matrix converter for direct-drive wind power system,” in *Proceedings of the 29<sup>th</sup> Chinese Control Conference*, pp. 4928–4932, July 2010.
- [19] A. Escobar, J.C. Balda, C.A. Busada, D. Christal, “An indirect matrix converter for CCHP microturbines in data center power systems,” in *Proceedings of the 34<sup>th</sup> International Telecommunications Conference, INTELEC 2012*, October 2012.
- [20] L. Empringham, J.W. Kolar, J. Rodriguez, P.W. Wheeler, J. Clare, “Technological issues and industrial application of matrix converters: A review,” *IEEE Transactions on Industrial Electronics*, vol. 60, no. 10, pp. 4260–4271, October 2013.

- [21] J. Rodriguez, M. Rivera, J.W. Kolar, P.W. Wheeler, “A Review of control and modulation methods for matrix converters,” *IEEE Transactions on Industrial Electronics*, vol. 59, no. 1, pp. 58–70, January 2012.
- [22] M.Y. Lee, P. Wheeler, C. Klumpner, “Space-vector modulated multilevel matrix converter,” *IEEE Transactions on Industrial Electronics*, vol. 57, no. 10, pp. 3385–3394, October 2010.
- [23] S.M., Dabour, E.M. Rashad, “Analysis and implementation of space-vector-modulated three-phase matrix converter,” in *Proceedings of the IET Power Electronics*, vol. 5, no. 8, pp. 1374–1378, September 2012.
- [24] R. Pena , R. Cardenas , E. Reyes , J. Clare, P. Wheeler “A topology for multiple generation system with doubly fed induction machines and indirect matrix converter,” *IEEE Transactions on Industrial Electronics*, vol. 56, no. 10, pp. 4181–4193, October 2009.
- [25] P. C. Loh, R. J. Rong, F. Blaabjerg, P. Wang, “Digital carrier modulation and sampling issues of matrix converters,” *IEEE Transactions on Power Electronics*, vol. 24, no. 7, pp. 1690–1700, July 2009.
- [26] H. Nikkhajoei, M.R. Iravani, “A matrix converter based micro-turbine distributed generation system,” *IEEE Transactions on Power Delivery*, vol. 20, no. 3, pp. 2182–2192, July 2005.
- [27] S.L. Sanjuan, “Voltage oriented control of three-phase boost PWM converter,” M.S. Thesis, Department of Energy and Environment Division of Electric Power Engineering, Chalmers University of technology, Göteborg, Sweden, 2010.

## APPENDIX B.1

### PERMISSIONS

Home Create Account Help



Requesting permission to reuse content from an IEEE publication

**Title:** New control strategy for indirect matrix converters operating in boost mode  
**Conference Proceedings:** Energy Conversion Congress and Exposition (ECCE), 2013 IEEE  
**Author:** Escobar-Mejia, A.; Hayes, J.K.; Balda, J.C.; Busada, C.A.  
**Publisher:** IEEE  
**Date:** 15-19 Sept. 2013  
Copyright © 2013, IEEE

User ID

Password

Enable Auto Login

LOGIN

[Forgot Password/User ID?](#)

If you're a [copyright.com](#) user, you can login to RightsLink using your [copyright.com](#) credentials. Already a [RightsLink](#) user or want to [learn more?](#)

#### Thesis / Dissertation Reuse

**The IEEE does not require individuals working on a thesis to obtain a formal reuse license, however, you may print out this statement to be used as a permission grant:**

*Requirements to be followed when using any portion (e.g., figure, graph, table, or textual material) of an IEEE copyrighted paper in a thesis:*

- 1) In the case of textual material (e.g., using short quotes or referring to the work within these papers) users must give full credit to the original source (author, paper, publication) followed by the IEEE copyright line © 2011 IEEE.
- 2) In the case of illustrations or tabular material, we require that the copyright line © [Year of original publication] IEEE appear prominently with each reprinted figure and/or table.
- 3) If a substantial portion of the original paper is to be used, and if you are not the senior author, also obtain the senior author's approval.

*Requirements to be followed when using an entire IEEE copyrighted paper in a thesis:*

- 1) The following IEEE copyright/ credit notice should be placed prominently in the references: © [year of original publication] IEEE. Reprinted, with permission, from [author names, paper title, IEEE publication title, and month/year of publication]
- 2) Only the accepted version of an IEEE copyrighted paper can be used when posting the paper or your thesis on-line.
- 3) In placing the thesis on the author's university website, please display the following message in a prominent place on the website: In reference to IEEE copyrighted material which is used with permission in this thesis, the IEEE does not endorse any of [university/educational entity's name goes here]'s products or services. Internal or personal use of this material is permitted. If interested in reprinting/republishing IEEE copyrighted material for advertising or promotional purposes or for creating new collective works for resale or redistribution, please go to [http://www.ieee.org/publications\\_standards/publications/rights/rights\\_link.html](http://www.ieee.org/publications_standards/publications/rights/rights_link.html) to learn how to obtain a License from RightsLink.

If applicable, University Microfilms and/or ProQuest Library, or the Archives of Canada may supply single copies of the dissertation.

BACK

CLOSE WINDOW

Copyright © 2014 [Copyright Clearance Center, Inc.](#) All Rights Reserved. [Privacy statement.](#)  
Comments? We would like to hear from you. E-mail us at [customer@copyright.com](mailto:customer@copyright.com)



© 2013 IEEE. **Reprinted with permission from A. Escobar, J.K. Hayes, J.C. Balda, and C.A. Busada, “*New Control Strategy for Indirect Matrix Converters Operating in Boost Mode,*” September, 2013.**

In reference to IEEE copyrighted material which is used with permission in this thesis, the IEEE does not endorse any of University of Arkansas products or services. Internal or personal use of this material is permitted. If interested in reprinting/republishing IEEE copyrighted material for advertising or promotional purposes or for creating new collective works for resale or redistribution, please go to:

[http://www.ieee.org/publications\\_standards/publications/rights/rights\\_link.html](http://www.ieee.org/publications_standards/publications/rights/rights_link.html) to learn how to obtain a License from RightsLink.



**Department of Electrical Engineering**

1 University Avenue, 3217 Bell Engineering Center, Fayetteville, AR 72701, (479) 575-3005, (479) 575-7967 (fax)

August 3, 2014

To whom it may concern,

This letter is to verify that Mr. Andrés Escobar Mejía, ID number: 010533274, is the first author and did at least 51% of the work for the paper titled "NEW CONTROL STRATEGY FOR INDIRECT MATRIX CONVERTERS OPERATING IN BOOST MODE".

Kind Regards,

Dr. Juan Carlos Balda

University Professor and Major Advisor to Mr. Escobar Mejía

Department Head

## CHAPTER FOUR

### NEW POWER ELECTRONIC INTERFACE COMBINING DC TRANSMISSION, A MEDIUM-FREQUENCY BUS AND AN AC-AC CONVERTER TO INTEGRATE DEEP- SEA FACILITIES WITH THE AC GRID

A. Escobar, Yusi Liu, J.C. Balda, K. George, “New power electronic interface combining dc transmission, a medium-frequency bus and an ac-ac converter to integrate deep-sea facilities with the ac grid,” in *Proceedings of the IEEE Energy Conversion Congress and Exposition, ECCE 2014*, pp. 4335–4344, September, 2014.

#### **Abstract**

A new bidirectional dc-ac power electronic interface (PEI) consisting of a dc link, an HVdc terminal based on modular multilevel converters (MMCs), medium-frequency transformers (MF-XFMRs) – higher frequencies are also possible – and ac-ac converters is proposed for interconnecting two ac systems, or dc and ac systems. The advantages of each component make the proposed topology convenient for applications that require compactness, flexibility, and reliability. For example, integration of offshore and onshore wind farms with the power grid, ac and/or dc grids interconnections, and supplying power to conventional and future deep-sea oil and gas facilities. The PEI main overall topology, operating principles and design equations are described. Size and efficiency are evaluated for the proposed topology for different operating frequencies and compared with the conventional approach. A case study of a deep-sea electric power system (DEPS) is illustrated through time-domain simulations for different operating conditions to demonstrate the feasibility of the proposed ideas.

## 4.1 Introduction

The concept of direct-current electric power transmission at any voltage but particularly at high and medium voltages (HVdc and MVdc) has become standard for transmitting power between two points across distances above 600 km without technical limitations [1]. Advantages, such as a reduced number of conductors, lack of series/parallel capacitors for reactive compensation, lower capital cost due to simpler tower structure for overhead lines, less right-of-way requirements, and flexibility make the two-terminal HVdc transmission approach more attractive than conventional ac transmission, especially to integrate remote renewable energy resources with the grid [2], [3]. Conventionally, there are two widely used HVdc terminal topologies: thyristor-based line commutated converters (LCCs) and IGBT-based voltage source converters (VSCs). The LCC topology has a higher degree of maturity and has been operating for decades with high efficiency and reliability. However, due to its nature, operation requires reactive power support, a strong ac grid for current commutation and harmonic filters which in turn represent a large footprint area when compared with the VSC topology [4]. These limitations plus the dependency on an ac grid for its correct operation (lack of black-start operation) make VSC topology preferable for offshore facilities. Within the VSC HVdc, the MMC generally using a half-bridge in each sub-module (SM), is the preferable solution due to its multiple advantages when compared to the other VSC topologies [5]. Regardless of the type of VSC-HVdc terminal, a fundamental-frequency transformer matches the grid voltage to the MMC's ac port keeping a large modulation index, provides galvanic isolation [6], [7], prevents the dc voltage from passing to the ac side, and avoids the flow of zero-sequence current components into the MMC-based terminal under unbalanced grid conditions [8], [9].

In the past few decades, the use of high-frequency transformers (HF-XFMRs) and MF-XFMRs in the so-called power electronic transformer (PET) or solid-state transformer (SST) topology have been reported to replace bulky fundamental-frequency transformers for traction [10] and utility-scale [11] applications. Advantages such as volume and weight reduction make the MF- and HF-XFMR more attractive for particular applications [12], [13]. However, the PET or SST reliability, due to the higher number of components and costs, are still open concerns that need to be evaluated.

Matrix converters are ac-ac converters which do not involve energy storage components in the dc link. This characteristic is considered advantageous in applications where space, reliability and weight are major concerns. They have been successfully implemented in low-power applications such as aircrafts [14] and motor drives; and in high-power applications such as wind power generation [15] and large motor drives [16].

Considering the benefits of the three above mentioned power converters, a new dc-ac PEI suitable for interfacing two ac systems through an HVdc link, or dc and ac systems, is proposed as illustrated in Fig. 4.1. The proposed topology contemplates the use of two HVdc terminals (based on the VSC-MMC), two ac-ac converters and two MF- or HF-XFMRs.

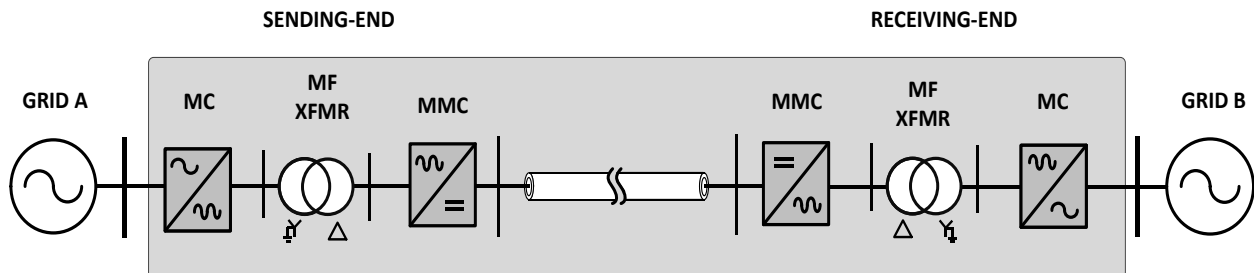


Fig. 4.1. Proposed dc-ac PEI connecting two ac systems with fundamental frequency of 50/60 Hz

The indirect matrix converter (IMC) is selected for implementing the functions of the ac-ac converter but other ac-ac converter topologies can be used (e.g., back-to-back converter or conventional matrix converter). At the sending-end, the IMC is used to increase the “ac grid A” fundamental frequency to medium frequencies (e.g., < 1 kHz). The IMC output supplies the primary side of a MF-XFMR which steps-up the voltage to the required transmission levels. Then, the MMC-based terminal is used as an ac-dc converter. At the receiving-end, this topology is used in reverse in order to connect with the “ac grid B”. The transformer (with  $\Delta$  connection at the MMC side) helps to provide galvanic insulation and to eliminate zero-sequence components that could flow to the MMC terminal under unbalanced grid conditions.

The potential advantages of the proposed PEI are:

- Fewer passive components: The MMC current and voltage ac-side waveforms are nearly sinusoidal, which means that filters at the MF-XFMR side are not required. The IMC eliminates the use of the bulky electrolytic capacitor and produces nearly sinusoidal currents.
- Volume and weight reductions: The increase of the transformer fundamental frequency ( $f_1$ ) allows for the reduction of passive components leading to compact and lightweight designs. Components such as the MF-XFMR and the capacitor in each SM of the MMC, are potentially reduced in volume since their size is inversely proportional to the frequency of the connected ac system [17].
- Fault current blocking capabilities: For half-bridge based MMCs, the IMC in the sending-end and the receiving-end may operate as a solid-state circuit breaker controlling and/or interrupting the flow of fault currents. The PEI controller shuts down the converter to block the fault currents and thus avoids failure of the power semiconductor devices. In the case of a Si IGBT-based IMC, 3.3kV devices can withstand 2~4 times the nominal current for 5-10  $\mu$ s

[18]–[21], whereas lower voltage IGBTs can withstand 4~10 times the nominal current during the same time [22].

- Bidirectional power-flow capability: Both, the IMC and the MMC topologies allow for currents flowing in either direction.

The remainder of the paper is organized as follows: Each stage (IMC, MF-XMFR and MMC) of the PEI is described in detail in section 4.2. The application for the proposed topology is illustrated in section 4.3. A complete analysis in terms of size and losses is presented in sections 4.4 and 4.5, respectively. Time-domain simulations of a DEPS case study are presented in section 4.6. Lastly, conclusions are addressed in section 4.7.

## 4.2 Proposed Topology Overview

The proposed dc-ac topology is illustrated in Fig. 4.2 where it is assumed that the current flows from the dc side to the ac side. The main components are described below.

### 4.2.1 Modular Multilevel Converter Stage

The use of MMCs for HVdc transmission interconnections is gaining popularity due to the features it possesses when compared with traditional VSC topologies [23], [24]. First, the arm currents are never interrupted avoiding undesirable overvoltages that may cause SM power semiconductors failure. Second, the inductance of each arm can be increased limiting the ac current rise rate in case of faults. Third, a nearly sinusoidal output waveform with low harmonic content is possible by stacking modules. Lastly, the semiconductors in each module can be switched at low frequency ( $f_{sw\_MMC} \cong 5f_1$ ) which in turn represents less stress and switching loss when compared with other similar converters [25].

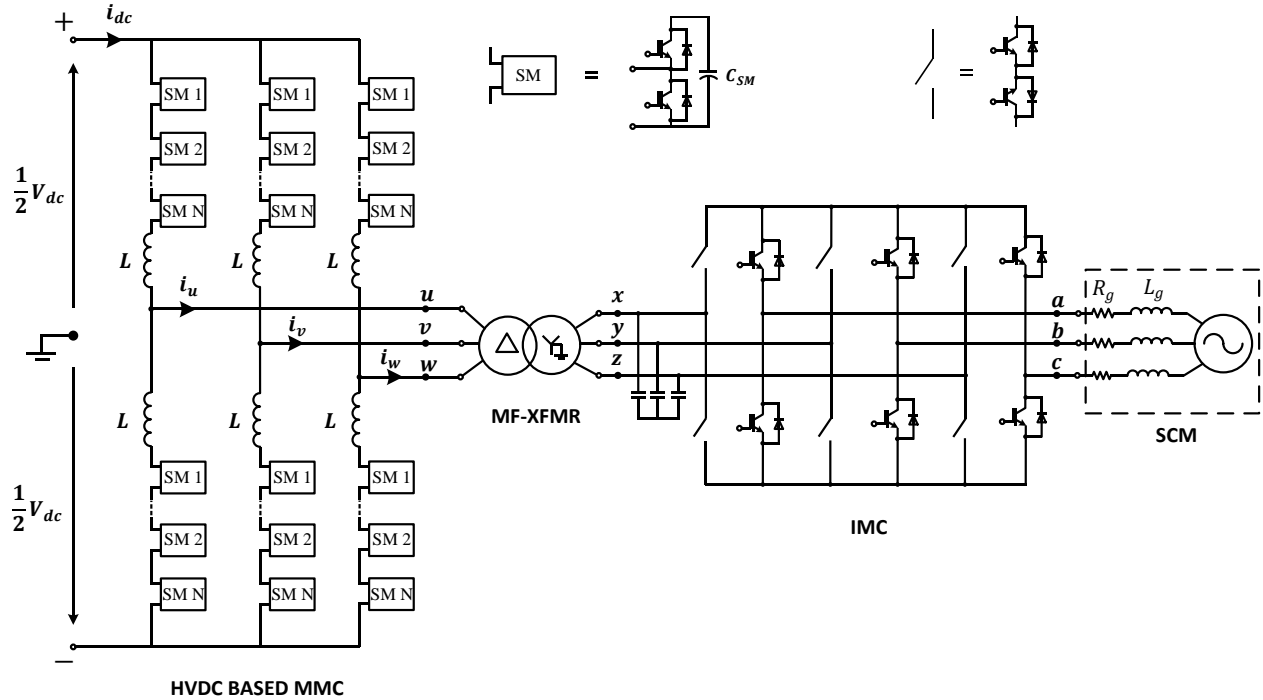


Fig. 4.2. Proposed PEI components (IMC rectifier and inverter stages are interleaved to reduce parasitics, and the IMC input and output filters are not shown)

#### 4.2.2 Medium-Frequency Transformer Stage

The fundamental-frequency transformer is usually considered one of the most efficient, reliable and employed components for different stages of power systems. It is also considered one of the heaviest and bulkiest components requiring large areas in power substations and extra structure in the case offshore platforms. Variables like the selection of the core magnetic material, type of conductor and winding arrangement, thermal management to evacuate the heat associated with copper and core losses, and insulation requirements, need to be evaluated when designing power transformers. It is desired to operate the transformer at high flux density  $B_{max}$  without exceeding the material saturation flux density  $B_{sat}$ . However, an inappropriate  $B_{max}$  could lead into large transformer core loss  $P_{fe}$ .



Several hard-magnetic materials like silicon-steel are considered the preferable solution for the low-frequency range (<1 kHz) and power ratings from a few Watts to thousands of Megawatts because it provides high saturation flux density and relatively low core loss. The attention paid to soft-magnetic materials such as amorphous, ferrite and nanocrystalline for high-, medium- and low-power applications has increased with the development of fast semiconductor devices, new manufacturing process and the interest in new applications demanding small footprints and high efficiencies. A comparison between soft and hard magnetic material in terms of flux density, core loss among others properties is listed in Table 4.1. As indicated, silicon-steel presents a high saturation flux density but has high core loss at high frequencies, whereas nanocrystalline soft-magnetic material presents superior performance to ferrite materials for high-frequency applications, which means that it is promising for applications demanding low volume and high efficiency. Yet, cost and the lack of standard off-the-shelf cores suitable for large transformers are limitations that delay nanocrystalline as a commercial product for medium- and high-power applications [11]. Ferrite cores present the lowest saturation flux density among different materials, however it is not suggested for high-power applications (more than 50 kVA) because the material is brittle. Among materials, amorphous has the potential for applications demanding small footprints and relatively high efficiencies since it exhibits good flux densities and low core losses. Also, its price is nearly comparable to silicon and it is commercially available in different shapes that are commonly used in the realization of medium- and high-power transformers. Despite advantages and disadvantages of each magnetic material, the core selection is not a simple task and demands the knowledge of variables such as cost, efficiency and transformer ratings.

Table 4.1. Comparison between different magnetic materials [26], [27]

Parameter	Silicon-steel	Nanocrystalline		Ferrite	Amorphous
$B_{sat}$ [T]	<2	<1.4		<0.6	<1.5
Core loss [W/kg] @20 kHz/0.2T	>100	<8.0		<18	≈35
Permeability [Gs/Oe] @ 20kHz	16,000	20,000		2,000	10,000- 150,000
Resistivity [ $\mu\Omega\cdot\text{cm}$ ]	Ribbon	80		-	-
	Cut	130		106	130
	Core	-			
Density [ $\text{g}/\text{cm}^3$ ]	≈7.7	≈7.2		≈5	≈7.18
Curie Temperature [°C]	745	600		210	399
Cost [\$/kg]	41	Namglass	210	91	51
		Vitroperm	218		
		500F			
		Nanoperm	288		
		Finemet (FT-3m)	310		

#### 4.2.3 AC-AC Converter Stage

Matrix converters have been extensively investigated as ac-ac power converter for different applications [28]. The main advantage is that the bulky and life-time limited electronic capacitor commonly used as energy storage component in, for instance, back-to-back converters is not required for the ac-ac conversion process. The electrolytic capacitor serves mainly two purposes: decouples the input and output stages for controlling purposes, and provides short-term energy storage in case either side demands it, for instance, during a voltage sag or transient. Despite these advantages, capacitors are considered one the weakest components in power converters because their lifetime gets reduced with operation hours, particularly at high temperatures. There are two types of MCs: Conventional matrix converters (CMCs) and indirect matrix converters (IMCs). The CMC facilitates the direct connection between the input and output by using nine bidirectional switches, whereas the IMC uses two stages for the ac-ac conversion which reduces

the clamp circuit required for overvoltage protection of the semiconductor devices and facilitates independent modulation of the inverter and rectifier stages. The proposed dc-ac PEI uses the IMC since it has more advantages over CMCs, however, the operating principle of the proposed PEI topology can be extended to the CMC case or any other ac-ac converter.

### **4.3 Proposed Topology for Subsea Power Systems**

This section considers a subsea power system as an application of the proposed PEI. Offshore facilities, such as oil and gas platforms (also known as rigs), are increasing in production as the industry continues to explore for new deep-sea fields. These facilities operating at water depths of 300 meters to 3,000 meters are responsible for the extraction of 40% of the world's oil and gas [29], and require large amounts of power to drive on-site equipment such as pumps and compressors that are used to extract (from subsea wellheads and reservoirs) and export the hydrocarbons to oil tankers or nearby floating production, storage, and offloading (FPSO) vessels [30]. The pumps and compressors are driven by electric motors that are equipped with adjustable-speed drives (ASDs) capable of regulating motors' speed and torque [31]. To satisfy the energy demand, on-board power generation (e.g., gas turbines and internal combustion engine machines running in parallel reaching efficiencies from 20 to 40 %) is typically used as the main source of electricity to power equipment on the platform. In other cases, HVac and HVdc transmission lines from offshore wind farms and onshore power grids are proposed to provide power to these facilities [32], [33]. Unfortunately, the converter size and weight increase the platform area and complexity.

In recent years, the oil and gas industry has shown interest in developing production facilities on the seabed [34] due to its multiple advantages compared to conventional exploration floating

platforms that bring power for equipment located on the seabed close to subsea production centers. Remote wellheads will be collected together to a main station and then to the shore through subsea power cables and umbilicals designed to withstand high pressures and last the lifetime of the subsea facility [29]. Lower operating costs and risks, due to a reduction of harsh weather conditions commonly present in platforms and FPSOs [35], are some of the main advantages of these production facilities that will be located hundreds of miles from the shore and will require a deep-sea electric power system for its operation. Performance, redundancy and reliability will be essential to ensure continuous operation at all times since repair and preventive maintenance for subsea facilities will be costly and challenging. Typical inland substation schemes such as double bus-double breaker, breaker-and-a-half and others [36] will be desirable in future deep-sea substations (DSS) to increase flexibility and reliability indices. Furthermore, special housings and heavy-seals will be required to keep power equipment such as step-up/down transformers, protective devices (e.g., circuit breakers, reclosers, switchgears, etc.), and power converters safe from corrosion, high pressure, and humidity.

Different topologies have been proposed to supply electric power to these deep-sea production facilities. Reference [37] proposed a MF ac link, [38] used a fundamental-frequency HVac link, and [39] presented a topology using an MVdc transmission link to bring power to the deep-sea substation.

Considering the requirements for future DSSs and the need to power them up from either inland power substations or offshore wind farms [40], one possible scenario for the novel PEI presented in Fig. 4.1, is to deliver power from either inland power substations or offshore wind farms [40] to DSSs for future offshore oil and gas subsea facilities as illustrated in Fig. 4.3.

At the inland power substation, the IMC is selected to increase the ac grid fundamental frequency to medium frequencies (e.g., < 1 kHz). The IMC output supplies the primary side of a MF-XFMR which steps-up the voltage to the required transmission levels (for low-power applications, a high-frequency transformer could be used). Then, the MMC-based HVdc terminal is used as the ac-dc converter. At the receiving-end, this topology is used in reverse order to provide power to the deep-sea equipment.

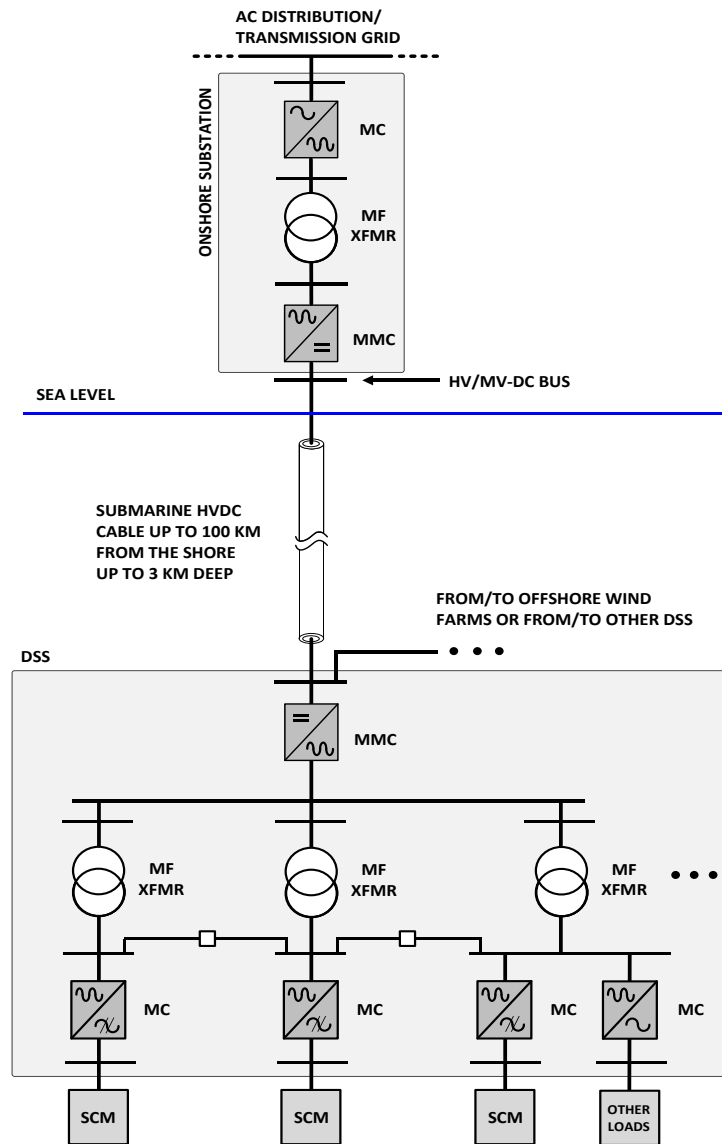


Fig. 4.3. Proposed PEI applicable to subsea facilities

As illustrated, the proposed DEPS is based on an HVdc link having terminals based on a voltage source converter (VSC), MF-XFMRs and MCs. The power from a land base power substation is transmitted to the DSS via a high-voltage or medium-voltage dc-link depending on the power rating levels. At the DSS, a VSC based on the MMC concept is used to convert the dc voltage into ac medium-frequency sinusoidal voltages. Then, MF-XFMRs are used to step-down the voltage to distribution levels required by the facility equipment. The nominal rating and number of MF-XFMRs depends on the power requirements of the DSS which is associated with the number of subsea compression modules (SCM) and other loads working at fixed frequency. The MF-XFMRs can be connected in parallel to increase the reliability of the system without affecting the short-current rating at the DSS location. At the MF-XFMR low-voltage side, a MC is used to reduce the fundamental medium-frequency to variable frequencies or a fixed frequency according to the requirements of the extraction equipment in the subsea well. Each SCM normally comprises a high-speed electric motor driven by a centrifugal compressor [41] which is used to enhance the well production by boosting the reservoir pressure.

## **4.4 Passive Components Size Evaluation**

### *4.4.1 MMC Capacitor and Arm Inductor Ratings*

As illustrated in Fig. 4.2, each MMC terminal has one leg per-phase (two arms per-leg) and a series connection of SMs to satisfy dc-link voltage level. The number of SMs ( $N$ ) per-arm is function of the voltage across the dc link and the voltage rating of the power semiconductor devices in each SM. The SM capacitor serves two purposes: maintain the voltage across each SM constant and provide ride-through capabilities in case of transient events from either side. A voltage balancing technique is required to ensure that the voltage across each capacitor is

maintained close to  $+\frac{1}{N}V_{dc}$ . Each SM comprises of capacitors as energy storage component, two power semiconductor devices (e.g., Si IGBTs) and other auxiliary components.

The required capacitor in each SM is given by [42]:

$$C_{SM} = \frac{\Delta W_{SM}}{2\varepsilon\bar{V}_{SM}^2} \quad [F] \quad (4.1)$$

where  $\varepsilon$  is the capacitor maximum allowable voltage ripple, and  $\bar{V}_{SM}$  is the average voltage across each SM. The energy variation per SM,  $\Delta W_{SM}$ , is expressed as [42]–[44]:

$$\Delta W_{SM} = \frac{2}{3k\omega_o \cos \varphi} \left( \frac{P_{dc}}{N} \right) \left[ 1 - \left( \frac{k \cos \varphi}{2} \right)^2 \right]^{\frac{3}{2}} \quad (4.2.a)$$

$$k = 2 \frac{\hat{V}_{u1}}{V_{dc}}, \quad (4.2.b)$$

where  $P_{dc}$  is the converter total power transfer from the dc-ac MMC ( $V_{dc}I_{dc}$ ),  $\omega_o$  is the angular frequency of the fundamental component of the ac output voltages,  $\varphi$  is the phase shift between voltage and line current, and  $k$  is defined as the amplitude modulation index which is twice the ratio between each arm fundamental peak line-to-neutral ac output voltage ( $\hat{V}_{u1}$ ) and the voltage in the dc link ( $V_{dc}$ ) [45]. From (4.2.a) and (4.1), it is possible to establish that the capacitor nominal value is inversely proportional to the fundamental frequency of the ac output voltages; thus, the increase of the MMC fundamental frequency leads to its size reduction.

The required SM capacitance when the frequency varies between 60 Hz and 1 kHz is shown in Fig. 4.4. As illustrated, there is a drastic change in the capacitor size by increasing the fundamental frequency and changing the rated voltage of the semiconductor devices. In the case of a 3.3 kV SM, the capacitance is reduced by a factor of four when the fundamental frequency of the output voltages varies from 60 Hz to 250 Hz. This indicates that there is an advantage in terms of the MMC terminal as the fundamental frequency increases.

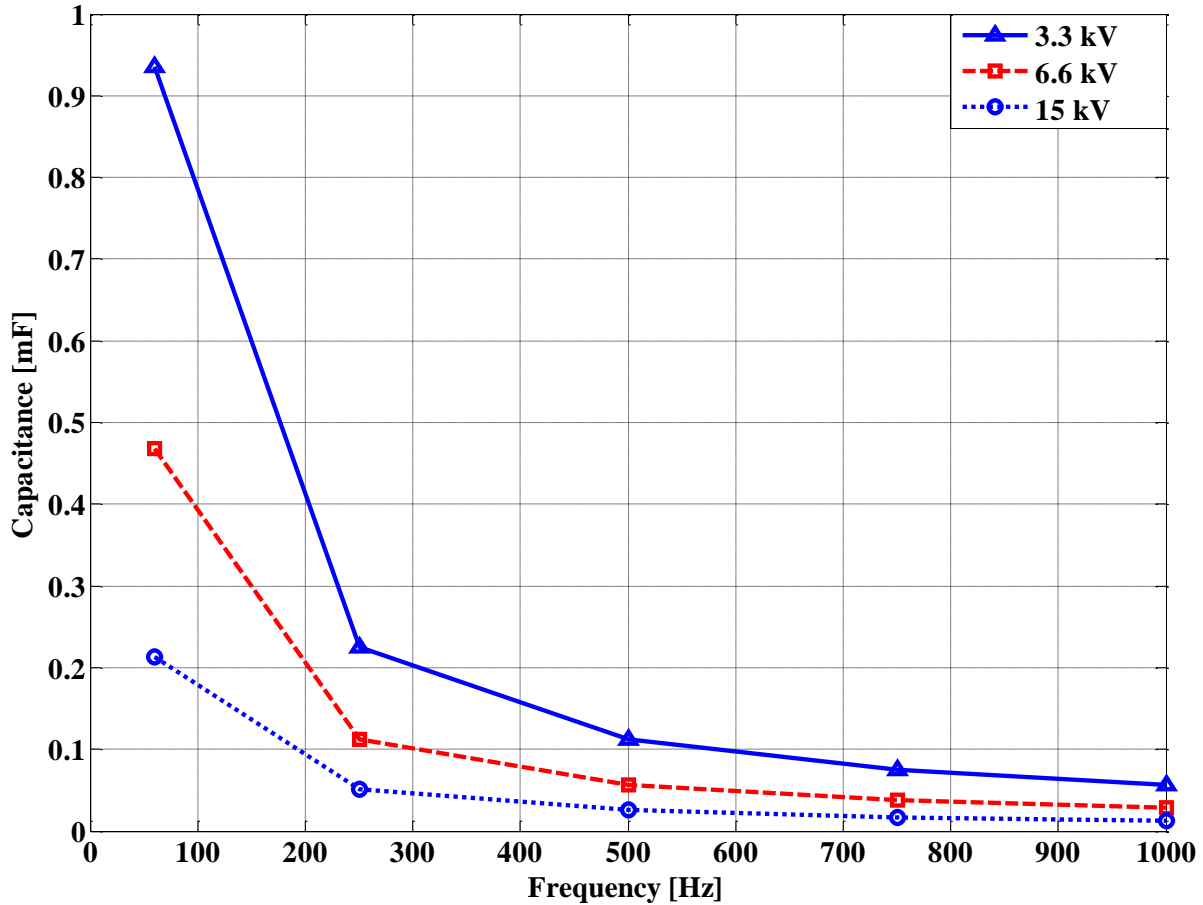


Fig. 4.4. Capacitor size comparison as function of the fundamental frequency

The nominal value of the MMC arm inductor can also be reduced when the fundamental frequency increases. Keeping the same inductor causes a large voltage drop across it for different operating frequencies. This may be an inconvenient since it is required to increase the MMC modulation index beyond its nominal value [46].

#### 4.4.2 MF Transformer Core and Winding Size

The transformer core and winding selections are critical since they have a large influence on the transformer efficiency, volume and weight. Its optimal design is an iterative process that requires a good knowledge of the variables involved and the application in order to get a practical



model. The complexity in the design increases when the excitation waveform is not sinusoidal as in the case of dc-dc converters. This is not the case for a MMC terminal since the output voltage waveform is nearly sinusoidal. Furthermore, losses due to parasitic and winding capacitances are not a problem since the frequency is too low to contemplate these effects.

Increasing the transformer fundamental frequency leads to a reduction in the core size which in turn will potentially reduce transformer cost when the same material for the core is considered for different frequencies. However, other considerations must be evaluated since transformer's design is not a straightforward task, mainly due to the number of variables involved and their non-linear dependency. The volume of the core  $V_c$  and the windings  $V_w$  for a power transformer can be calculated as function of the area product  $A_p$  as indicated in [47]:

$$V_c = k_c A_p^{3/4} \quad (4.3.a)$$

$$V_w = k_w A_p^{3/4}, \quad (4.3.b)$$

where  $k_c$  and  $k_w$  are constants that depend on the transformer characteristics [47] and  $A_p$  is calculated as function of the transformer total power rating  $\sum VA$  as:

$$A_p = \left( \frac{\sqrt{2} \sum VA}{K_v f_1 B_o k_f K_t \sqrt{k_u \Delta T}} \right)^{8/7}, \quad (4.4)$$

where  $K_v$  is the waveform factor (i.e., 4 for sinusoidal excitation),  $k_f$  is the core stacking factor,  $k_u$  the window utilization factor and  $\Delta T$  the temperature rise. The optimum flux density for a particular frequency is given by [47]:

$$B_o = \frac{(h_c k_a \Delta T)^{2/3}}{\sqrt[3]{4} (\rho_w k_w k_u)^{1/12} (k_c K_c f_1^\alpha)^{7/12}} \left( \frac{K_v f_1 k_f k_u}{\sum VA} \right)^{1/6} \quad (4.5)$$

where  $h_c$  is the coefficient of heat transfer,  $\rho_w$  the resistivity of the conductor and the coefficients  $K_c$ , and  $\alpha$  are obtained by full-fitting the core loss curve in the material datasheet

provided by manufacturers. As indicated in (4.4), the  $A_p$  is reduced by increasing the transformer fundamental frequency  $f_1$ , however, this can lead into a reduction of  $B_o$  as shown in (4.5). The potential transformer size reduction for different operating conditions is illustrated in Fig. 4.5. For the comparison, each transformer is carefully sized to not exceed both the maximum magnetic flux density and the Curie temperature for each core material. Other components such as tanks, fans, and insulators are not included in the analysis, but they can potentially increase the size of the transformer by a factor of three [48].

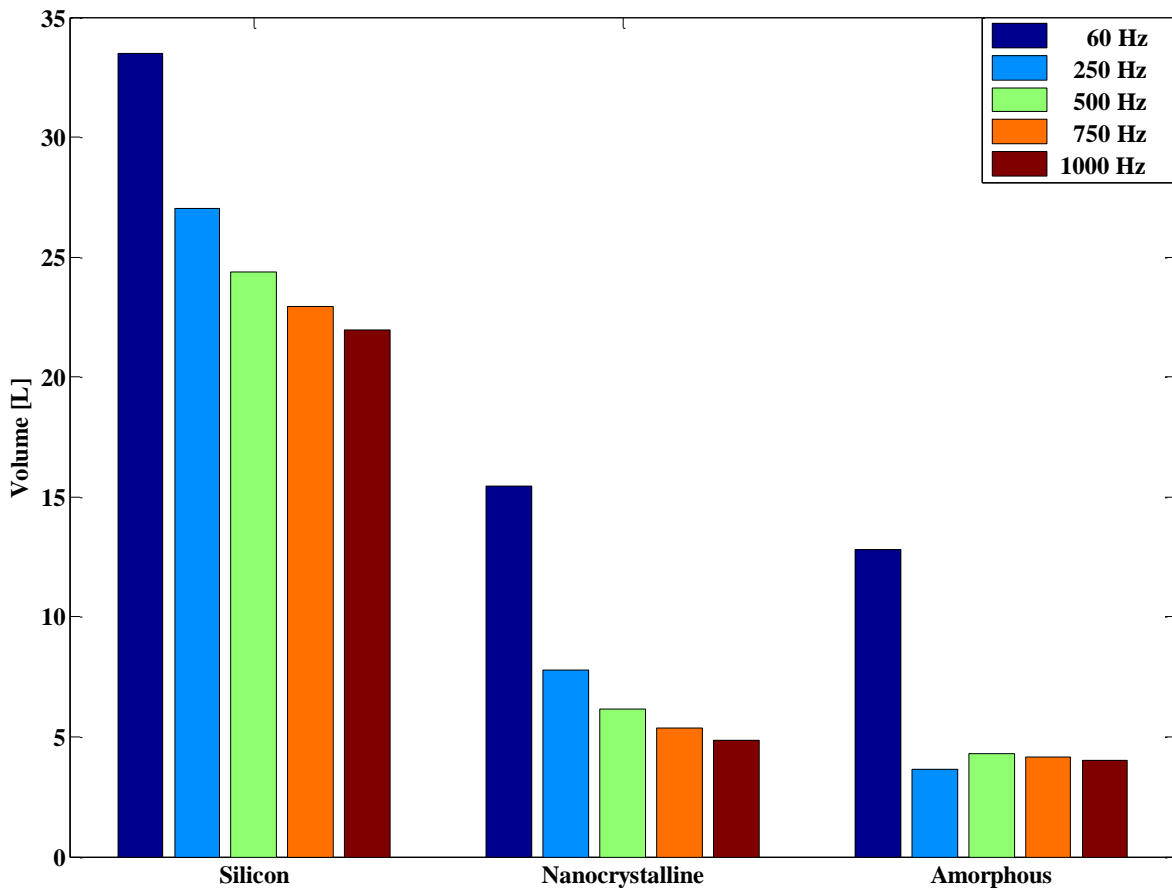


Fig. 4.5. Transformer volume for different fundamental frequencies

## 4.5 Topology Loss Analysis

### 4.5.1 MF Transformer Losses

In order to evaluate the transformer core loss per unit of volume or weight (i.e., depending on the information provided by manufacturers), the Steinmetz equation (4.6) is commonly used:

$$P_{fe} = K_c f_1^\alpha B_{max}^\beta, \quad (4.6)$$

where  $f_1$  is the excitation fundamental frequency, and the coefficient  $\beta$  is obtained by full-fitting the core loss curve in the material datasheet provided by manufacturers. Equation (4.6) assumes pure sinusoidal voltage excitation at the transformer input. For other waveforms, like the square waveform in the SST case, the use of the modified Steinmetz equation becomes necessary to get an approximation of the core loss [49]. Such a case is not considered here since the excitation of the transformer is a sinusoidal with a fundamental frequency lower than 1 kHz.

### 4.5.2 IMC Conduction and Switching Losses

The IMC conduction losses in the rectifier stage are calculated as [50]:

$$P_{c\_CSB} = \frac{9}{2\pi} (V_{CEo} + V_{Do}) m_r I_o \cos \varphi_o + \frac{3\sqrt{3}}{2\pi^2} (r_{CE} + r_D) m_r I_o^2 (1 + 4\cos^2 \varphi_o) \quad (4.7)$$

where  $m_r$  is the rectifier modulation index,  $I_o$  the peak of the output current and  $\varphi_o$  the output angular displacement. The switching losses are not considered in this stage since the rectifier commutates when a zero-voltage state vector is applied to the inverter stage [51].

The conduction and switching losses of the inverter stage are calculated as [50]:

$$P_{c\_VSB} = 6 \left[ \frac{(V_{CEo} + V_{Do}) I_o}{2\pi} + \frac{(V_{CEo} - V_{Do}) I_o}{8} m_i \cos \varphi_o + \frac{(r_{CE} + r_D) I_o^2}{8} + \frac{(r_{CE} - r_D) I_o^2}{3\pi} m_i \cos \varphi_o \right] \quad (4.8.a)$$

$$P_{sw\_VSB} = \frac{27}{\pi^2} f_{sw\_IMC} (E_{on} + E_{off} + E_{rr}) \frac{V_i}{V_{dcnom}} \frac{I_o}{I_{cnom}} \cos \varphi_i \quad (4.8.b)$$

where  $m_i$  is the inverter modulation index,  $V_i$  the peak input phase voltage,  $\varphi_i$  the input angular displacement and  $f_{sw\_IMC}$  the IMC switching frequency.

#### 4.5.3 MMC Switching Losses

One of the advantages of MMCs is their low switching loss when compared with 2-level and 3-level VSC HVdc topologies. Their modular characteristic allows low harmonic content at low switching frequency; however, there is a trade-off between harmonic content, number of SM and switching frequency. The method suggested in [46] is applied to calculate the MMC conduction and switching losses. The switching frequency is set to be five times the fundamental frequency for each case (e.g.,  $f_{swMMC} = 300$  Hz for  $f_1 = 60$  Hz). If the equivalent MMC arm inductor is kept as 0.15 pu, then the MMC modulation index remains constant for all different fundamental case calculations. Therefore, each IGBT's turn-on and turn-off intervals with regards to its fundamental period are the same for different fundamental frequencies. With this consideration, the switching losses are proportional to the fundamental frequency whereas the conduction losses are the same.

#### 4.6 Proposed PEI Topology Case Study

Many factors influence the power rating and the voltage level of the HVdc link used to bring power to the DSS. In general, there is not a standard dc voltage level to transmit power using an HVdc link, however, issues like type of conductors, insulation requirements, and the application, are considered for their selection.

For offshore platforms, sensitive equipment like circuit breakers, dc-ac converters, switch gears and transformers, are usually located on a platform where they are kept dry. The cable to

connect the offshore substation with the one on the shore is the only component located under the water. Its manufacturing process is very mature and uses materials with polymeric insulation designed to withstand high pressures and mechanical stress allowing the submarine transmission to reach up to  $\pm 450$  kVdc to deliver power up to 1 GW [52], [53].

Nowadays, transformers for subsea applications (<20 MVA, 132/22.5 kV) have been deployed in waters reaching 3 km deep for oil and gas production applications [54]. They have the same characteristics as conventional oil-filled transformers with the only difference of especial enclosures designed to operate under high-pressure, keeping internal component insulated from the external conditions.

In order to present the feasibility of the proposed topology, the three-phase system illustrated in Fig. 4.2 is extensively simulated in the time-domain environment using Matlab/Simulink™. The parameters for the whole system are listed in Table 4.2. Four different fundamental frequencies for the converter are evaluated for the loss and volume analysis. Due to the voltage and power ratings requirements for motor drives in the oil and gas industry [55], the system is designed to bring power to a 5 MW 4.16 kV IMC-based motor drive operating at 50% full-load. The transmission dc-link voltage is assumed as  $\pm 20$  kVdc, thus the output line-to-line voltage of the MMC (with  $N = 8$ ) is 22 kVac.

The MMC SM capacitor and arm inductor and the global efficiency for the proposed PEI when the fundamental frequency at the output of the MMC changes from 60 Hz to 1000 HZ are listed in Tables 4.3 and 4.4, respectively. The conduction and switching losses for the IMC and the MMC are evaluated using a third generation 6.5 kV IGBT. As presented the total losses in the

MMC terminal at 250 Hz is almost 3.3 times the losses at 60 Hz, and the system efficiency is reduced from 93.52% to 90.42%.

Table 4.2. General parameters for the case study	
<b>MODULAR MULTILEVEL CONVERTER</b>	
Power rating (S)	5 MVA
DC link voltage ( $V_{dc}$ )	$\pm 20$ kV
Number of SM per-arm	8
Arm reactance ( $L_a = L_b = L_c$ )	0.2 pu
Amplitude modulation index	0.91
Power Semiconductor Device	5SNA 0600G650100 ABB $V_{CE}=6.5$ kV, $I_C=600$ A @ $T_c=85^\circ\text{C}$ $E_{on}=3.8$ J, $E_{off}=1.95$ J @ $V_{CC}=3600$ V, $I_C=600$ A
<b>STEP-DOWN TRANSFORMER</b>	
Power Rating	3x2 MVA
Voltage ratio ( $a$ )	25/5 kV
Total leakage inductance	0.05 pu
Core material	Amorphous
<b>INDIRECT MATRIX CONVERTER</b>	
Power Semiconductor Device (two per-switching position)	5SNA 0600G650100 ABB

Table 4.3. MMC Capacitor and inductor size reduction

Parameter	@ 60 Hz	@ 250 Hz	@ 500 Hz	@ 750 Hz	@ 1000 Hz
SM Capacitor [mF]	0.1954	0.0469	0.0234	0.0156	0.0117
Arm Inductor [mH]	28	6.72	3.36	2.24	1.68

Table 4.1. Estimated global efficiency for the PEI

Stage loss [kW]	@ 60 Hz	@ 250 Hz	@ 500 Hz	@ 750 Hz	@ 1000 Hz
MMC (@ $f_{sw\_MMC} = 3f_1$ )	29.63	100	192.87	285.74	378.37
MF-XMFR	217.20	330	405	441	474
IMC (@ $f_{sw\_IMC} = 4$ kHz)	99.70	99.70	99.70	99.70	99.70
<b>Total</b>	<b>346.53</b>	<b>529.70</b>	<b>697.57</b>	<b>826.44</b>	<b>952.07</b>
<b>System Efficiency (%)</b>	<b>93.52</b>	<b>90.42</b>	<b>87.76</b>	<b>85.82</b>	<b>84.00</b>

The system's steady-state operation when the MMC operates at a fundamental frequency of 250 Hz is depicted in Fig. 4.6. As shown, the MMC output voltage is stepped down to  $4.16 \pm 10\%$  kV to feed the IMC as shown in Fig. 4.6 (bottom left). The IMC's switching frequency is set to 4 kHz and the time step for the simulations is 1  $\mu$ s. For the IMC operating as an ASD at the above mentioned power conditions, the currents at the input and the output of the MF-XFMR are shown in Fig. 4.6 (top right) and (bottom right), respectively.

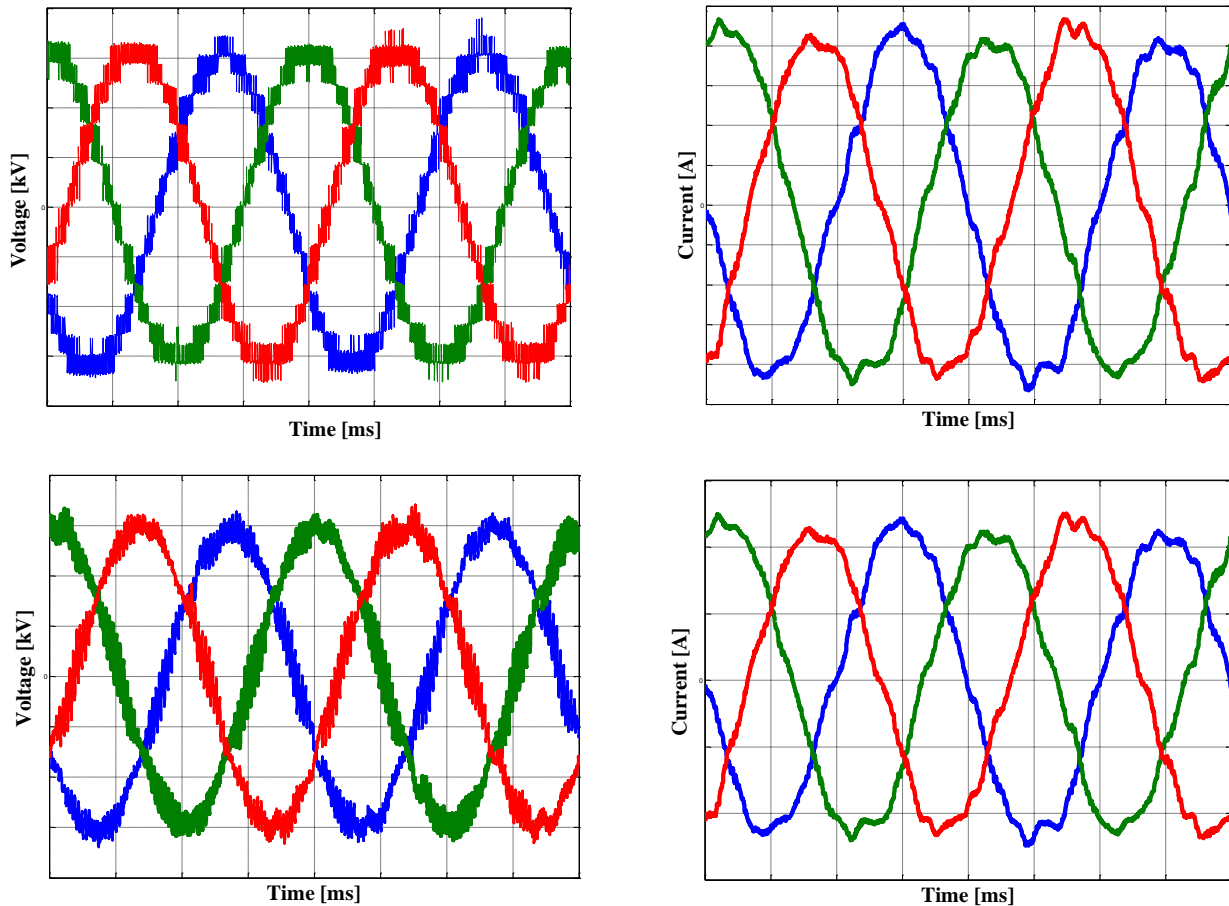


Fig. 4.6. MMC output line-to-line voltages (a) at 10 kV/div and output currents (b) at 20 A/div. MF-XFMR output voltages (c) at 2 kV/div and output currents (d) at 200 A/div. All figures with a time scale of 1ms per division

## **4.7 Conclusions**

A new PEI suitable for the interconnection of two ac systems or dc and ac systems was introduced. The topology combined a MMC, a MF-XMFR and an IMC. The fundamental frequency of MMC ac output can be increased to allow for reductions of the passive component sizes; however, semiconductor devices losses in this stage set the upper limit of the operating fundamental frequency. A case study of a deep-sea facility for an oil or gas field demonstrated the proposed ideas.

The analysis of the case study showed that operating the MMC at a fundamental frequency of 250 Hz enabled a 75% reduction in the required capacitance per module, which in turns, it should allow for a significant reduction in the total system footprint. The penalty was a 3% reduction in the efficiency at the system level.

The main challenges for deep-sea facilities are the cost and design of the enclosures that can withstand the high pressures and keep sensitive equipment isolated from the water. The cost associated with maintenance due to the limited availability of components will be high, thus the proposed PEI brings the possibility of keeping down the initial cost since allows for volume savings and reduction in passive components.

## **Acknowledgments**

The authors are grateful for the financial support from the National Science Foundation Industry/University Cooperative Research Center on Grid-connected Advanced Power Electronics Systems (GRAPES). Mr. Andrés Escobar-Mejía is grateful for the financial support as assistant professor of the Universidad Tecnológica de Pereira (Colombia) through the studies commission grant for full-time professors and the Fulbright-LASPAU program.



## References

- [1] K. Meah, S. Ula, “Comparative evaluation of HVDC and HVAC transmission systems,” in *Proceedings of the IEEE Power Engineering Society General Meeting*, pp. 1–5, June, 2007.
- [2] R. Adapa, “High-wire act: HVdc technology: The state of the art,” in *IEEE Power and Energy Magazine*, vol. 10, no. 6, pp. 18–29, November, 2012.
- [3] H. Wang, M.A. Redfern, “The advantages and disadvantages of using HVDC to interconnect AC networks,” in *Proceedings of the 45<sup>th</sup> IEEE Universities Power Engineering Conference*, UPEC 2010, pp. 1–5, September, 2010.
- [4] C. Zhan, C. Smith, A. Crane, A. Bullock, D. Grieve, “DC transmission and distribution system for a large offshore Wind Farm,” in *Proceedings of the 9<sup>th</sup> IET International Conference on AC and DC Power Transmission*, ACDC 2010, pp. 1–5, October, 2010.
- [5] J.A. Ferreira, “The multilevel modular dc converter,” in *IEEE Transactions on Power Electronics*, vol. 28, no. 10, pp. 4460–4465, October, 2013.
- [6] D.S. Sanchez, T.C. Green, “Control of a modular multilevel converter-based HVDC transmission system,” in *Proceedings of the 14<sup>th</sup> IEEE European Conference on Power Electronics and Applications*, EPE 2011, pp. 1–10, August-September, 2011.
- [7] G.P. Adam, K.H. Ahmed, S.J. Finney, B.W. Williams, “Modular multilevel converter for medium-voltage applications,” in *Proceedings of the IEEE International Electric Machines and Drives Conference*, IEMDC 2011, pp. 1013–1018, May, 2011.
- [8] M. Guan, Z. Xu, “Modeling and control of a modular multilevel converter-based HVDC system under unbalances grid conditions,” *IEEE Transactions on Power Electronics*, vol. 27, no. 12, pp. 4858–4867, December, 2012.
- [9] T. Lüth, M.M.C. Merlin, T.C. Green, F. Hassan, C.D. Barker, “High-frequency operation of a dc/ac/dc system for HVdc applications,” *IEEE Transactions on Power Electronics*, vol. 29, no. 8, pp. 4107–4115, August, 2014.
- [10] P. Drábek, Z. Peroutka, M. Pittermann, M. Cédli, “New configuration of traction converter with medium-frequency transformer using matrix converters,” in *IEEE Transactions on Industrial Electronics*, vol. 58, no. 11, pp. 5041–5048, November, 2011.

- [11] X. She, R. Burgos, G. Wang, F. Wang, A.Q. Huang, "Review of solid state transformer in the distribution system: from components to field application," in *Proceedings of the IEEE Energy Conversion Congress and Exposition, ECCE 2012*, pp. 4077–4084, September, 2012.
- [12] G. Brando, A. Dannier, R. Rizzo, "Power electronic transformer application to grid connected photovoltaic systems," in *Proceedings of IEEE International Conference on Clean Electrical Power, ICCEP 2009*, pp. 685–690, June, 2009.
- [13] R.K Gupta, G.F. Castelino, K.K. Mohapatra, N. Mohan, "A novel integrated three-phase, switched multi-winding power electronic transformer converter for wind power generation system," in *Proceedings of the 35<sup>th</sup> IEEE Annual Conference on Industrial Electronics, IECON 2009*, pp. 4481–4486, November, 2009.
- [14] S. Lopez, P. Zanchetta, P.W. Wheeler, A. Trentin, L. Empringham, "Control and implementation of a matrix-converter-based ac ground power supply unit for aircraft servicing," *IEEE Transactions on Industrial Electronics*, vol. 57, no. 6, pp. 2076–2084, June, 2010.
- [15] R. Cárdenas, R. Peña, J. Clare, P. Wheeler, "Analytical and experimental evaluation of a WECS based on a cage induction generator fed by a matrix converter," *IEEE Transactions on Energy Conversion*, vol. 26, no.1, pp. 204–215, March, 2011.
- [16] J. Kang, E. Yamamoto, M. Ikeda, E. Watanabe, "Medium-voltage matrix converter design using cascaded single-phase power cell modules," *IEEE Transactions on Industrial Electronics*, vol. 58, no.11, pp. 5007–5013, November, 2011.
- [17] Q. Tu, Z. Xu, L. Xu, "Reduced switching-frequency modulation and circulating current suppression for modular multilevel converters," *IEEE Transactions on Power Delivery*, vol. 26, no. 3, pp. 2009–2017, July, 2011.
- [18] S. Dieckerhoff, S. Bernet, D. Krug, "Evaluation of IGBT multilevel converters for transformerless traction applications," in *Proceedings of the 34<sup>th</sup> IEEE Annual Power Electronics Specialist Conference, PESC 2003*, vol. 4, pp. 1757–1763, June, 2003.
- [19] X. Gong, "A 3.3kV IGBT module and application in modular multilevel converter for HVDC," in *Proceedings of the IEEE International Symposium on Industrial Electronics, ISIE 2012*, pp. 1944–1949, May, 2012.

- [20] MITSUBISHI ELECTRIC, “HV IGBT Modules CM1000E4C-66R,” [Online]. Available: [http://www.mitsubishielectric.com/semiconductors/content/product/powermod/powmod/hv\\_igbtmod/hvigtbt/cm1000e4c-66r-e.pdf](http://www.mitsubishielectric.com/semiconductors/content/product/powermod/powmod/hv_igbtmod/hvigtbt/cm1000e4c-66r-e.pdf). [Accessed July 2014].
- [21] ABB, “IGBT Module 5SNA 1200E330100,” [Online]. Available: [http://www05.abb.com/global/scot/scot256.nsf/veritydisplay/558860a7860de104c12579fa0048de68/\\$file/5SNA%201200E330100\\_5SYA1556-04%2004-2012.pdf](http://www05.abb.com/global/scot/scot256.nsf/veritydisplay/558860a7860de104c12579fa0048de68/$file/5SNA%201200E330100_5SYA1556-04%2004-2012.pdf). [Accessed July 2014].
- [22] N. Mohan, T.M. Undeland, W.P Robbins, “Insulated gate bipolar transistors,” in *Power Electronics. Converters, Applications and Design*, 3<sup>rd</sup> Edition, Wiley, 2003, chapter 25, section 25–7, pp. 637.
- [23] S. Allebrod, R. Hamerski, R. Marquardt, “New transformerless, scalable modular multilevel converters for HVDC-transmission,” in *Proceedings of the IEEE Power Electronics Specialists Conference, PESC 2008*, pp. 174–179, June, 2008.
- [24] S. Chuangpishit, A. Tabesh, Z. Moradi-Shahrbabak, M. Saeedifard, “Topology design for collector systems of offshore wind farms with pure DC power systems,” *IEEE Transactions on Industrial Electronics*, vol. 61, no. 1, pp. 320–328, January, 2014.
- [25] M. Glinka, R. Marquardt, “A new AC/AC multilevel converter family,” *IEEE Transactions on Industrial Electronics*, vol. 52, no. 3, pp. 662–669, June, 2005.
- [26] X. She, R. Burgos, G. Wang, F. Wang, A.Q. Huang, “Review of solid state transformers in the distribution system: From components to field applications,” in *Proceedings of the IEEE Energy Conversion Congress and Exposition, ECCE 2012*, pp. 4077–4084, September, 2012.
- [27] J.A. Ferreira, S.W.H de Haan, Y. Wang, “Design of low-profile nanocrystalline transformer in high-current phase-shifted DC-DC converter,” in *Proceedings of the IEEE Energy Conversion Congress and Exposition, ECCE*, pp. 2177–2181, September, 2010.
- [28] T. Friedli, J.W. Kolar, “Milestones in Matrix Converter Research,” in *Proceedings of the IEEJ Journal of Industry Applications*, vol. 1, no.1 pp. 2–14, July, 2012.
- [29] ABB, “Oil and gas the energy we love to hate,” [Online]. Available: [http://www05.abb.com/global/scot/scot271.nsf/veritydisplay/b63708df92b90becc12579250051e616/\\$file/abb%20review%202-11\\_72dpi.pdf](http://www05.abb.com/global/scot/scot271.nsf/veritydisplay/b63708df92b90becc12579250051e616/$file/abb%20review%202-11_72dpi.pdf). [Accessed July 2014].

- [30] R.R. Brown, “FPSO: lessons learned,” in *IEEE Industry Applications Magazine*, vol. 10, no. 2, pp.18–23, March/April, 2004.
- [31] ABB, “Testing large ASDSs,” [Online]. Available: [http://www05.abb.com/global/scot/scot271.nsf/veritydisplay/b63708df92b90becc12579250051e616/\\$file/abb%20review%202-11\\_72dpi.pdf](http://www05.abb.com/global/scot/scot271.nsf/veritydisplay/b63708df92b90becc12579250051e616/$file/abb%20review%202-11_72dpi.pdf). [Accessed July 2014].
- [32] H.G. Svendsen, M. Hadiya, E.V. Øyslebø, K. Uhlen, “Integration of offshore wind farm with multiple oil and gas platforms,” in *Proceedings of the IEEE Trondheim PowerTech*, pp. 1–6, June, 2011.
- [33] J. Song-Manguelle, R. Datta, M.H. Todorovic, R. Gupta, D. Zhang, S. Chi, L. Garces, R. Lai, “A modular stacked DC transmission and distribution system for long distance subsea applications,” in *Proceedings of the IEEE Energy Conversion Congress and Exposition, ECCE 2012*, pp. 4437–4444, September, 2012.
- [34] Siemens, “Energy for everyone – oil & gas systems,” [Online]. Available: [https://www.siemens.com/innovation/en/publikationen/publications\\_pof/pof\\_spring\\_2008/energy/tiefsee.htm](https://www.siemens.com/innovation/en/publikationen/publications_pof/pof_spring_2008/energy/tiefsee.htm). [Accessed July 2014].
- [35] H. Brazil, R. Conachey, G. Savage, P. Baen, “Electrical heat tracing for surface heating on arctic vessels and structures to prevent snow and ice accumulation,” *IEEE Transactions on Industry Applications*, vol. 49, no. 6, pp. 2466–2470, November-December, 2013.
- [36] T. Gönen, “Design of subtransmission lines and distribution substations,” in *Electric Power Distribution Systems Engineering*, 2<sup>nd</sup> Edition, CRC Press, 2008, chapter 4, section 4.4, pp. 178–180.
- [37] V. Karstad, A.E. Skjellnes, “Electrical power system for a subsea system,” U.S. Patent 8251614 B2, August 28, 2012.
- [38] General Electric, “GE oil and gas drilling and production,” [Online]. Available: [http://www.ge-energy.com/content/multimedia/\\_files/downloads/VetcoGray%20Subsea%20Power%20Systems.pdf](http://www.ge-energy.com/content/multimedia/_files/downloads/VetcoGray%20Subsea%20Power%20Systems.pdf). [Accessed July 2014].
- [39] C.M. Sihler, R. Roesner, R. Datta, “MVDC power transmission system for sub-sea loads,” U.S. patent 7880419 B2, June 11, 2009.

- [40] P. Lundberg, M. Callavik, M. Bahrman, P. Sandeberg, "Platforms for change," in *IEEE Power and Energy Magazine*, vol. 10, no. 6, pp. 30–38, November, 2012.
- [41] General Electric, "The new look of offshore production," [Online]. Available: [http://site.ge-energy.com/businesses/ge\\_oilandgas/en/literature/en/downloads/offshore\\_production.pdf](http://site.ge-energy.com/businesses/ge_oilandgas/en/literature/en/downloads/offshore_production.pdf). [Accessed July 2014].
- [42] D. Guzman, "High voltage direct current energy transmission using modular multilevel converters," M.S. thesis, University of Arkansas, 2012.
- [43] Y. Zhang, G.P. Adam, T.C. Lim, S.J. Finney, B.W. Williams, "Analysis and experiment validation of a three-level modular multilevel converters," in *Proceedings of the 8<sup>th</sup> IEEE International Conference on Power Electronics and ECCE Asia, ICPE & ECCE 2011*, pp. 983–990, May, 2011.
- [44] J. Kolb, F. Kammerer, M. Braun, "Dimensioning and design of a modular multilevel converter for drive applications," in *Proceedings of the 15<sup>th</sup> IEEE International Conference on Power Electronics and Motion Control, EPE/PEMC 2012*, pp. 1–8, September, 2012.
- [45] Q. Tu, Z. Xu, H. Huang, J. Zhang, "Parameter design principle of the arm inductor in modular multilevel converter based HVDC," in *Proceedings of the IEEE International Conference Power System Technology, POWERCON 2010*, pp. 1–6, October, 2010.
- [46] J. Li, X. Zhao, Q. Song, H. Rao, S. Xu, M. Chen, "Loss calculation method and loss characteristic analysis of MMC based VSC-HVDC systems," in *Proceedings of the IEEE International Symposium on Industrial Electronics, ISIE 2013*, pp. 1–6, May, 2013.
- [47] W.G. Hurley, W.H. Wölfle, J.G. Breslin, "Optimized transformer design: Inclusive of high-frequency effects," *IEEE Transactions on Power Electronics*, vol 13, no. 4, pp. 651–659, July, 1998.
- [48] Mitsubishi Electric, "Large power transformers," [Online]. Available: <http://www.meppi.com/Products/Transformers/GSU%20Documents/Mitsubishi%20LargePowerTx.pdf>. [Accessed July 2014].
- [49] R. Garcia, A. Escobar, K. George, J.C. Balda, "Loss comparison of selected core magnetic materials operating at medium and high frequencies and different excitation voltages," in *Proceedings of the 5<sup>th</sup> International Symposium on Power Electronics for Distribution Generation Systems, PEDG 2014*, in Press.

- [50] A. Escobar, J.C. Balda, C.A. Busada, and D. Christal, “An indirect matrix converter for CCHP microturbines in data center power systems,” in *Proceedings of the 34<sup>th</sup> IEEE International Telecommunications Energy Conference*, pp. 1–6, October, 2012.
- [51] S. Round, F. Schafmeister, M. Heldwein, E. Pereira, L. Serpa, J.W. Kolar, “Comparison of performance and realization effort of a very sparse matrix converter to a voltage DC link PWM inverter with active front end,” *IEEEJ Transaction*, vol. 126-D, no. 5, pp. 578–588, May, 2006.
- [52] ABB, “Recent advances in high-voltage direct-current power transmission systems,” [Online]. Available: [http://www05.abb.com/global/scot/scot221.nsf/veritydisplay/cd7e0a6506f37d10c1257211002a42ac/\\$file/12.pdf](http://www05.abb.com/global/scot/scot221.nsf/veritydisplay/cd7e0a6506f37d10c1257211002a42ac/$file/12.pdf). [Accessed July 2014].
- [53] Siemens, “HVdc – High voltage direct current transmission: Unrivaled practical experiences,” [Online]. Available: [http://www.energy.siemens.com/us/pool/hq/power-transmission/HVDC/HVDC-Classic/HVDC\\_Transmission\\_EN.pdf](http://www.energy.siemens.com/us/pool/hq/power-transmission/HVDC/HVDC-Classic/HVDC_Transmission_EN.pdf). [Accessed July 2014].
- [54] ABB, “Power below the waves: Transformers at depths of 3 km,” [Online]. Available: [http://www05.abb.com/global/scot/scot271.nsf/veritydisplay/e7f894cf5abcc3dbc1257ab8003a7bdf/\\$file/33-36%20sr107\\_72dpi.pdf](http://www05.abb.com/global/scot/scot271.nsf/veritydisplay/e7f894cf5abcc3dbc1257ab8003a7bdf/$file/33-36%20sr107_72dpi.pdf). [Accessed July 2014].
- [55] ABB, “ABB drives in chemical, oil and gas medium voltage drives for greater profitability and performance,” [Online]. Available: [http://www05.abb.com/global/scot/scot216.nsf/veritydisplay/7afdc73aa9256670c12578b5004a2ae5/\\$file/cog%20brochure%20revc\\_lowres.pdf](http://www05.abb.com/global/scot/scot216.nsf/veritydisplay/7afdc73aa9256670c12578b5004a2ae5/$file/cog%20brochure%20revc_lowres.pdf). [Accessed July 2014].

## APPENDIX C.1

### PERMISSIONS



RightsLink®

Home

Create Account

Help



**Title:** New power electronic interface combining DC transmission, a medium-frequency bus and an AC-AC converter to integrate deep-sea facilities with the AC grid

**Conference Proceedings:** Energy Conversion Congress and Exposition (ECCE), 2014 IEEE

**Author:** Escobar-Mejia, Andres; Liu, Yusi; Balda, Juan Carlos; George, Kenny

**Publisher:** IEEE

**Date:** 14-18 Sept. 2014

Copyright © 2014, IEEE

User ID
<input type="text"/>
Password
<input type="text"/>
<input type="checkbox"/> Enable Auto Login
<input type="button" value="LOGIN"/>
<a href="#">Forgot Password/User ID?</a>
If you're a <a href="#">copyright.com</a> user, you can login to RightsLink using your copyright.com credentials. Already a RightsLink user or want to <a href="#">learn more?</a>

#### Thesis / Dissertation Reuse

**The IEEE does not require individuals working on a thesis to obtain a formal reuse license, however, you may print out this statement to be used as a permission grant:**

*Requirements to be followed when using any portion (e.g., figure, graph, table, or textual material) of an IEEE copyrighted paper in a thesis:*

- 1) In the case of textual material (e.g., using short quotes or referring to the work within these papers) users must give full credit to the original source (author, paper, publication) followed by the IEEE copyright line © 2011 IEEE.
- 2) In the case of illustrations or tabular material, we require that the copyright line © [Year of original publication] IEEE appear prominently with each reprinted figure and/or table.
- 3) If a substantial portion of the original paper is to be used, and if you are not the senior author, also obtain the senior author's approval.

*Requirements to be followed when using an entire IEEE copyrighted paper in a thesis:*

- 1) The following IEEE copyright/ credit notice should be placed prominently in the references: © [year of original publication] IEEE. Reprinted, with permission, from [author names, paper title, IEEE publication title, and month/year of publication]
- 2) Only the accepted version of an IEEE copyrighted paper can be used when posting the paper or your thesis on-line.
- 3) In placing the thesis on the author's university website, please display the following message in a prominent place on the website: In reference to IEEE copyrighted material which is used with permission in this thesis, the IEEE does not endorse any of [university/educational entity's name goes here]'s products or services. Internal or personal use of this material is permitted. If interested in reprinting/republishing IEEE copyrighted material for advertising or promotional purposes or for creating new collective works for resale or redistribution, please go to [http://www.ieee.org/publications\\_standards/publications/rights/rights\\_link.html](http://www.ieee.org/publications_standards/publications/rights/rights_link.html) to learn how to obtain a License from RightsLink.

If applicable, University Microfilms and/or ProQuest Library, or the Archives of Canada may supply single copies of the dissertation.

BACK

CLOSE WINDOW

© 2013 IEEE. **Reprinted with permission from A. Escobar, Y. Liu, J.C. Balda, and K. George, “*New Power Electronic Interface Combining dc transmission, a Medium-Frequency Bus and ac-ac Converter to Integrate Deep-Sea Facilities with the ac Grid,*” September, 2013.**

In reference to IEEE copyrighted material which is used with permission in this thesis, the IEEE does not endorse any of University of Arkansas products or services. Internal or personal use of this material is permitted. If interested in reprinting/republishing IEEE copyrighted material for advertising or promotional purposes or for creating new collective works for resale or redistribution, please go to:

[http://www.ieee.org/publications\\_standards/publications/rights/rights\\_link.html](http://www.ieee.org/publications_standards/publications/rights/rights_link.html) to learn how to obtain a License from RightsLink.





**Department of Electrical Engineering**

1 University Avenue, 3217 Bell Engineering Center, Fayetteville, AR 72701, (479) 575-3005, (479) 575-7967 (fax)

August 3, 2014

To whom it may concern,

This letter is to verify that Mr. Andrés Escobar Mejía, ID number: 010533274, is the first author and did at least 51% of the work for the paper titled "NEW POWER ELECTRONIC INTERFACE COMBINING DC TRANSMISSION, A MEDIUM-FREQUENCY BUS AND AN AC-AC CONVERTER TO INTEGRATE DEEP-SEA FACILITIES WITH THE AC GRID".

Kind Regards,

Dr. Juan Carlos Balda

University Professor and Major Advisor to Mr. Escobar Mejía

Department Head

## CHAPTER FIVE

### A SENSORLESS GRID SYNCHRONIZATION METHOD FOR MODULAR MULTILEVEL CONVERTERS IN HVDC SYSTEMS

A. Escobar, J.K. Hayes, J.C. Balda, C.A. Busada, “A sensorless grid synchronization method for modular multilevel converters in HVdc systems,” submitted to *IEEE Transaction on Industry Applications*, in review.

#### **Abstract**

The modular multilevel converter (MMC) topology is currently preferred for high-voltage direct current (HVdc) power applications since it has many advantages over other comparable multilevel topologies for power ratings under 1 GW. A new control technique not requiring grid sensors for synchronizing a MMC-based HVdc terminal with the grid is proposed in this paper. The sensorless technique is implemented in the rotating  $d - q$  synchronous frame to independently regulate the active and reactive power flow exchange. Resonant controllers are used to ensure proper performance of the current controller under abnormal grid conditions such as small fundamental frequency variations and temporary voltage unbalances caused by ac faults. Results from extensive time-domain simulations using an 8-level, 400-MW,  $\pm 200$ -kV MMC terminal demonstrate the operation of the proposed controller under balanced and unbalanced situations.

#### **5.1 Introduction**

High- and medium-voltage direct current (HVdc and MVdc) electric power transmission have become more common for transmitting power over long distances [1]. Advantages such as lower conduction losses, lower capital costs, flexibility, smaller right of way requirements, and smaller

footprint area, among others [2], [3], make HVdc more attractive than conventional ac transmission systems, especially to integrate renewable energy resources (e.g., off-shore wind farms) [4], [5] with the transmission grid or to interconnect two ac grids [6]–[8].

Among the many types of voltage source converters (VSCs), modular multilevel converter (MMC), using a half-bridge in each sub-module (SM), presents multiple advantages when compared to the other VSC topologies [9]. The concept of MMCs, first introduced in [10] and [11], is becoming more attractive in different HVdc projects based on VSC-HVdc [12]–[14]. Features such as modularity, simple structure, low switching losses and less harmonic content in the output voltages (i.e., minimum filter size to meet IEEE standard 519-1992 total harmonic distortion requirements) [15]–[17] make MMCs suitable for high- and medium-voltage applications rated less than 1 GW [18]. The general topology of a MMC-based terminal connected to the grid through a  $\Delta/Y$  step-down transformer is illustrated in Fig. 5.1. The half-bridge configuration is implemented here because it is widely used due to its increased efficiency and simplicity when compared with other SM topologies [12].

The control methods and modulation techniques proposed to connect VSCs with the grid [19], accomplishing zero steady-state error at the fundamental frequency, can be extended to regulate the power flow in ac-dc and dc-ac MMCs [20], [21] as in the case of the well-known vector control approach in the  $d - q$  synchronous frame [22], [23]. This controller requires a minimum of five sensors (four on the ac side for voltages and currents and one for the dc link) and a synchronization algorithm or phase-locked loop (PLL), which extracts the amplitude, phase angle and/or the frequency of the grid voltage fundamental component in order to accomplish the  $d - q$  transformation. The ac-side sensors are usually placed at the output of the converter filter, which is located at a distance that depends on the physical characteristics of the MMC terminal.

Avoiding the use of these sensors will potentially contribute to the improvement of the reliability of the MMC terminal by reducing the amount of components that can potentially fail [24].

Different sensorless schemes have been proposed for VSC to estimate the grid voltages under grid balanced operation [25], [26], however, during unbalanced conditions, the performance of a sensorless controller will deteriorate and the proportional-integral (PI) controller commonly implemented to track the current reference is unable to achieve zero steady-state error.

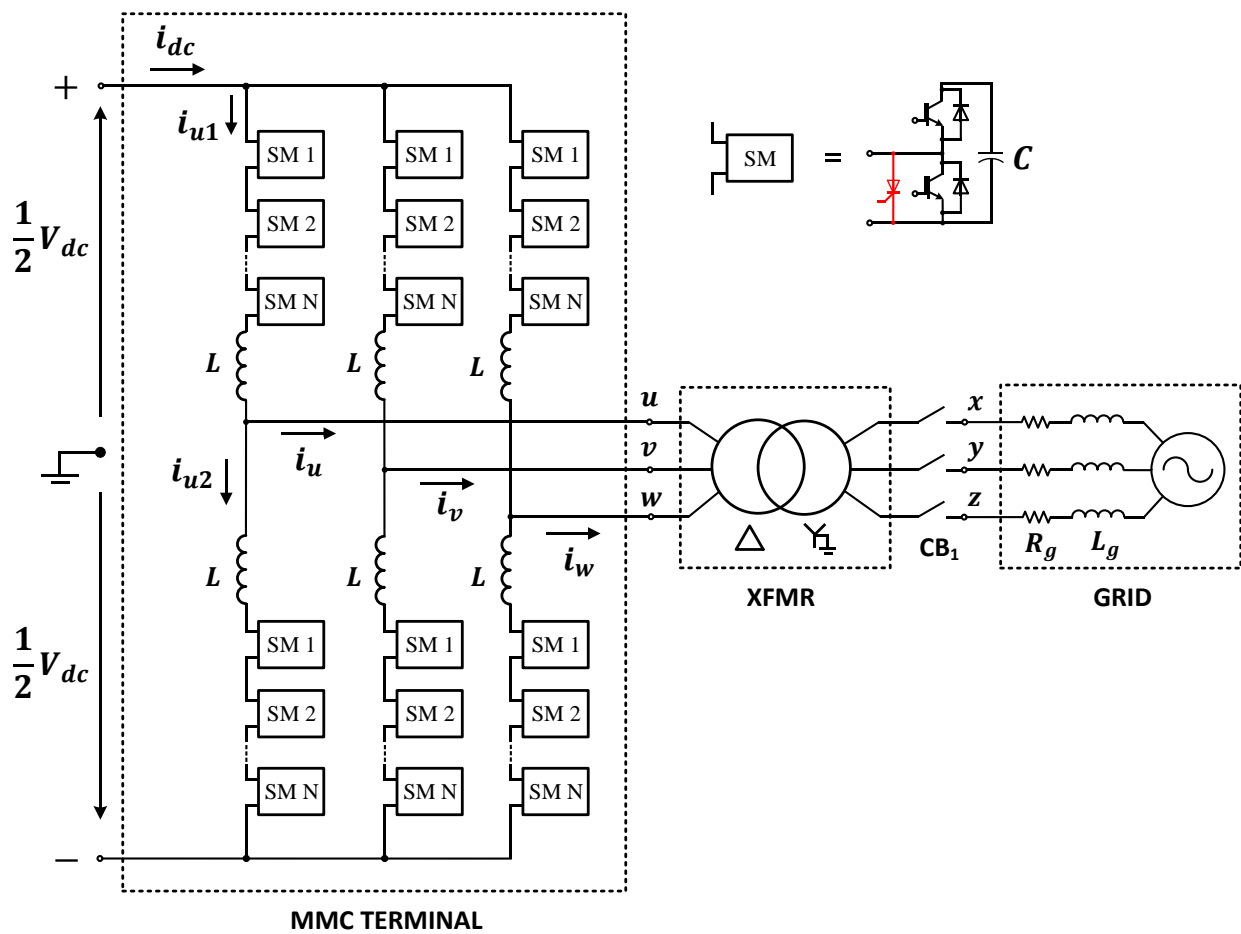


Fig. 5.1. HVdc terminal based on the MMC concept. Thyristors within the SM are used for bypassing the SM in case switch failure

Several publications have evaluated the performance of MMC-based HVdc terminals under balanced and unbalanced grid conditions. In [27], a mathematical model for the back-to-back (ac-dc and dc-ac) MMC-based HVdc system is presented along with the proposed control strategy for balanced and unbalanced grid operating conditions. In [28] a proportional-resonant controller is proposed in the stationary frame to limit the impact of grid unbalances into the MMC. Reference [29] tackles the second-order harmonic issue in the dc current and voltage by implementing a voltage ripple controller. In all cases, it is required to sense the grid currents and voltages in order to fully control the MMC terminal as well as a dedicated controller to reduce circulating currents due to the distorted nature of the arm voltages [20], [30].

In the case of three-phase VSCs, reduced order generalized integrators (ROGIs)-based current controllers have been proposed to control the power transfer during normal and abnormal grid conditions [31], [32]. This ROGI eliminates only a particular frequency of positive or negative sequence in the rotating  $d - q$  frame with better performance and less computational effort than the second order generalized integrator (SOGI) [33]. The use of resonant controllers in the rotating  $d - q$  frame allows for the injection of harmonic-free currents into the grid, improving the performance of the converter during unbalanced grid conditions.

A current control scheme for MMC-based transmission systems that eliminates the need for voltage sensors on the grid side is proposed in this paper. The proposed controller allows for independent control of the active and reactive powers injected into the grid by properly controlling the output voltages of the VSC-based MMC terminal. In conjunction with the proposed controller, standard integrators in a rotating frame and resonant controllers in a stationary frame facilitate the elimination of unwanted components that are caused by unbalanced voltages.

The remainder of the paper is organized as follows: the traditional current control technique for the inverter terminal of an HVdc link, including the equations modeling the controller, is briefly described in Section 5.2. The proposed sensorless controller for controlling the active and reactive powers injected into the grid during balanced and unbalanced conditions is presented in Section 5.3. The functionality of the proposed control technique is demonstrated under different conditions in Section 5.4 using Matlab/Simulink™ simulations. Finally, conclusions are given in Section 5.5.

## 5.2 MMC AC-Side Current Control Conventional Approach

Traditionally voltage oriented control (VOC) in the rotating  $d - q$  reference frame has been used as a current controller for grid-connected converters [22], [23], [27]–[35]. For MMC-based HVdc systems, this control technique can also be applied to regulate the active and reactive power flows [27], [36]. To this end, a MMC terminal with an infinite number of levels is assumed, leading to sinusoidal current and sinusoidal voltage waveforms at the ac side. As a result, the MMC terminal presented in Fig. 5.1 can be replaced by an ideal three-phase voltage source whose amplitude and phase can be determined by an appropriate controller. Then, an equivalent per-phase circuit having two voltage sources connected by the transformer equivalent impedance ( $R_t$  and  $\omega_o L_t$  referred to the MMC side) can be used for control purposes. Applying Kirchhoff's voltage law to this equivalent circuit of the HVdc terminal and grid combination at the MMC side, the voltages in the  $dq$  frame are written in the Laplace domain with zero initial conditions as follows:

$$s i_u^{dq} = \frac{1}{L_t} (v_{MMC}^{dq} - v_g^{dq} - R_t i_u^{dq} - j\omega_o L_t i_u^{dq}), \quad (5.1)$$

where  $s$  is the Laplace operator,  $\omega_o$  is the grid fundamental frequency and vectors like  $v_{MMC}^{dq} = v_{MMC}^d + jv_{MMC}^q$  are constant and rotate at the MMC synchronous speed under steady-state conditions (i.e., 50/60 Hz). The inductance  $L_t$  represents the nominal value of the transformer leakage inductance. The cross-coupling term  $\omega_o L_t i_u^{dq}$  shows the dependency between axes and thus it is desirable to remove it in order to improve the system dynamic response. The term  $v_g^{dq}$  represents the equivalent grid voltages referred to the MMC side. To this end, and assuming that  $R_t \approx 0$ , the control law for the MMC is written as [23]:

$$v_{MMC}^{dq} = \left( K_p + \frac{K_i}{s} \right) (i_u^{*dq} - i_u^{dq}) + v_g^{dq} + j\omega_o L_t i_g^{dq}. \quad (5.2)$$

The analysis of the MMC terminal operation during unbalanced conditions requires the decomposition of (5.1) into positive, negative and zero sequences  $(i_u^{+dq}, i_u^{-dq}, i_u^0)$ . In the case of asymmetric faults on the grid side, the current controller (5.2) is not fully effective in a transformerless configuration since the zero-sequence component can circulate into the dc side causing power fluctuations [28] and only the positive and negative components can be effectively controlled [36]. For a three-wire system (i.e., Y/ $\Delta$  transformer connection with the  $\Delta$ -connection on the MMC side), the zero-sequence circuit is excluded from the analysis due to the absence of a fourth wire. As shown in (5.2), the control action requires sensing the grid currents, frequency and voltages, as well as having good knowledge of the transformer equivalent inductance  $L_t$ .

Once  $v_{MMC}^d$  and  $v_{MMC}^q$  are calculated, they are transformed into the  $abc$  natural reference frame using the inverse Park's transformation to determine the appropriate gate signals for each SM. From Fig. 5.1, the grid current for phase  $u$  is calculated as:

$$i_u(t) = i_{u1}(t) - i_{u2}(t), \quad (5.3)$$

where  $i_{u1}$  and  $i_{u2}$  are the MMC upper- and lower-arm currents, respectively, which are sensed as part of the capacitor balancing technique [23]. Since current sensors are part of the converter in each leg, there is no need to implement extra current sensors to measure the grid current.

### 5.3 Proposed Sensorless Control Technique

#### 5.3.1 Balanced Operating Conditions

From (5.2), the desired MMC output voltages  $v_{MMC}^{dq}$  are determined by sensing the grid voltages in the  $abc$  natural reference frame and making use of the Park's transformation to obtain the equivalent grid voltages  $v_g^{dq}$  in the rotating  $d - q$  reference frame referred to the MMC side. In a MMC terminal, this signal is usually obtained from voltage sensors located at the transformer secondary side (grid side) [25]. In order to avoid sensing the grid voltages, the control technique, whose schematic is illustrated in Fig. 5.2, is proposed to calculate the control signals for the MMC as [37]:

$$v_{MMC}^{dq} = -\frac{As + 1}{Bs + g^{dq}} i_u^{dq} + j\omega_o L_t i_u^{dq}, \quad (5.4)$$

where  $A$  and  $B$ ,  $\in \mathbb{R}$ , are defined as the forward direct gain and the forward indirect gain, respectively, and  $g^{dq} = g^d + jg^q$ ,  $g \in \mathbb{R}$ , is the conductance vector, whose components are used to determine the active and reactive power exchanges between the grid and the MMC terminal. To decouple the effect of the cross-coupling term in (5.1), and thus, to improve the system dynamic response, the feed-forward term  $\omega_o L_t i_u^{dq}$  is introduced. The vector  $i_u^{dq}$  represents the sensed grid currents (or calculated using  $i_{u1}$  and  $i_{u2}$ ) in the rotating  $d - q$  reference frame. Substituting (5.4) into (5.1) and assuming that the transformer resistance is negligible,  $R_t \approx 0$ , yields:



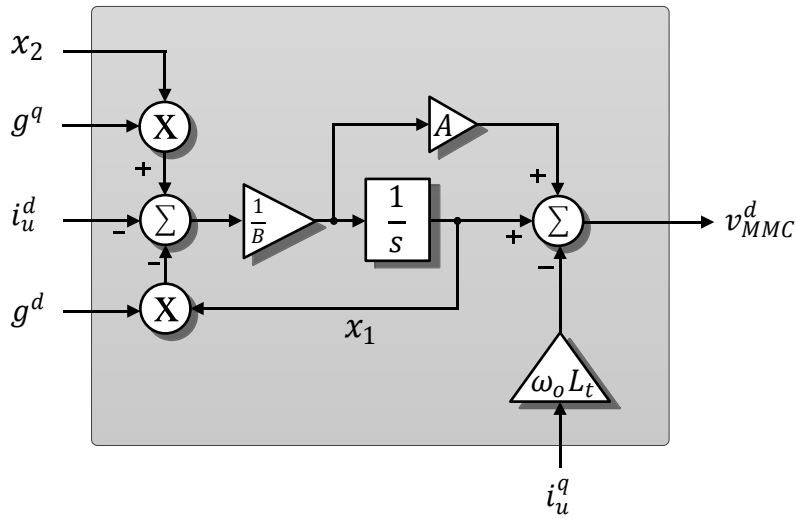
$$i_u^{dq} = -\frac{Bs + g^{dq}}{L_t Bs^2 + s[A + L_t g^{dq}] + 1} v_g^{dq}. \quad (5.5)$$

If the transfer function in (5.5) is stable, then, under steady-state conditions ( $s \rightarrow 0$ ):

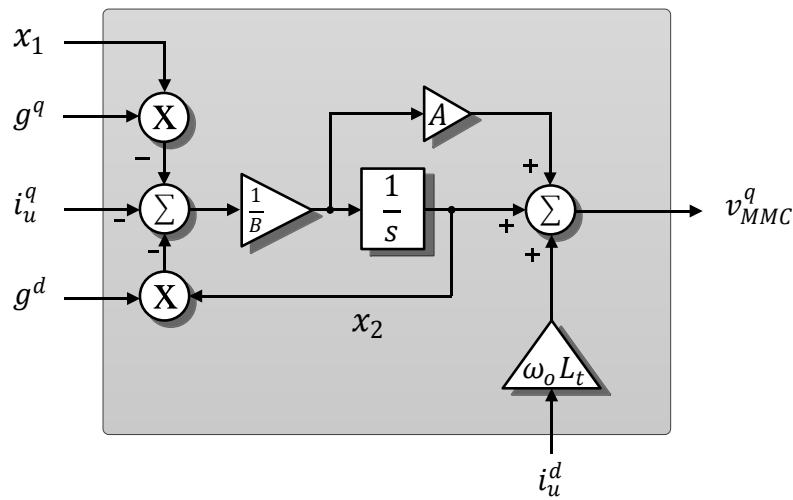
$$i_u^{dq} = -g^{dq} v_g^{dq}, \quad (5.6)$$

which is rewritten as follows:

$$\begin{cases} i_u^d = -g^d v_g^d + g^q v_g^q \\ i_u^q = -g^d v_g^q - g^q v_g^d. \end{cases} \quad (5.7)$$



(a)



(b)

Fig. 5.2. Proposed control block diagram in the  $d$  axis (a) and  $q$  axis (b)

From (5.7), the proposed controller in (5.4) allows the injection of currents that are proportional to the grid voltages in the rotating  $d - q$  reference frame. Different cases can be considered depending on the magnitude and sign of the conductance vector. If  $g^q = 0$ , the injected grid currents are in phase with the grid voltages (unity power factor). If the conductance  $g^d$  is positive, the active power flows from the grid to the MMC terminal; if negative, the active power flow is reversed. When  $g^q \neq 0$ , the MMC output currents are no longer in phase with the grid voltages, allowing for reactive power flow exchange with the sign of  $g^q$  determining whether it is lagging or leading.

From the control schematic illustrated in Fig. 5.2, the output of the integrators in (a) and (b) are calculated as:

$$x_1 = -\frac{i_u^d(Bs + g^d) + i_u^q g^q}{(Bs + g^d)^2 + (g^q)^2} \quad \text{and} \quad x_2 = -\frac{i_u^q(Bs + g^d) - i_u^d g^q}{(Bs + g^d)^2 + (g^q)^2} \quad (5.8)$$

which can be written in steady-state ( $s \rightarrow 0$ ) as:

$$x_1 = -\frac{i_u^d g^d + i_u^q g^q}{(g^d)^2 + (g^q)^2} \quad \text{and} \quad x_2 = -\frac{i_u^q g^d - i_u^d g^q}{(g^d)^2 + (g^q)^2}. \quad (5.9)$$

Solving (5.6) for  $v_g^{dq}$  and comparing its real and imaginary components with (5.9), it is established that  $x_1$  and  $x_2$  correspond to the estimated grid voltage vector  $[\hat{v}_g^d \hat{v}_g^q]^T$ . These estimated voltages and the sensed grid currents are used to calculate the active and reactive powers flowing into/from the grid in accordance with the commanded references. These values are then compared to the active and reactive power references to generate the conductance vector  $[g^d \ g^q]^T$  as shown in Fig. 5.3.

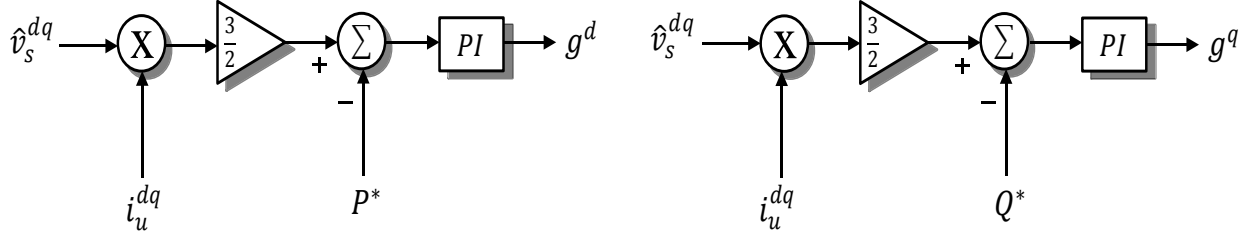


Fig. 5.3. Outer control loop to determine the gains of the conductance vector  $[g^d \ g^q]^T$

### 5.3.2 Distorted and Unbalanced Operating Conditions

As indicated in (5.6), the proposed controller synthesizes the currents such that they track the grid voltage waveform, thus – in a balanced three-phase system –, the grid currents can be seen as constants in the rotating  $d - q$  reference frame. However, in the presence of unbalanced voltages caused by faults or sags on the ac-grid side, the currents  $i_u^d$  and  $i_u^q$  are no longer constant and oscillates at twice the fundamental frequency due to the presence of the negative component in the  $v_g$  voltages. This condition and the presence of harmonic pollution cause unbalances in the injected currents which are considered undesirable. This is because the ac grid requires balanced currents and the dc-link voltage must remain constant to keep the active power flow [28], [38].

In general, the currents  $i_u^d$  and  $i_u^q$  in Fig. 5.2 can be written as:

$$\begin{aligned}
 i_u^d &= \sqrt{\frac{3}{2}} \sum_{h=1}^n (I_{u\_max\_h}) \cos[(\omega_0 - h\omega_0)t] \\
 i_u^q &= \sqrt{\frac{3}{2}} \sum_{h=1}^n (I_{u\_max\_h}) \sin[(\omega_0 - h\omega_0)t],
 \end{aligned} \tag{5.10}$$

where  $n$  represents the maximum considered harmonic component, and  $h$  the harmonic component with  $\{h \in \mathbb{Z} | h \neq 0\}$ . For a pure sinusoidal waveform, both values can be seen as constant. However, the harmonic spectra of the currents  $i_u^d$  and  $i_u^q$  consist of the sum of

harmonics of different sequences, limiting the action of the conventional PI controller presented in (5.2) [39].

Resonant controllers implemented in the rotating  $d - q$  frame and tuned at specific frequencies,  $h\omega_0$ , filter out the undesired harmonic components by having infinite gain at the selected resonant frequency [40]. In a balanced system with voltage harmonic distortion, the  $-5\omega_0$  (negative sequence) and  $+7\omega_0$  (positive sequence) are commonly present. These components cause an oscillation in the  $d - q$  frame which corresponds to the  $\pm 6\omega_0$  harmonic as indicated in (5.10), thus, a SOGI in the  $d - q$  frame is able to compensate for two harmonic components at the same time [33] leading to a significant reduction of the computational effort when compared with similar controllers implemented in the stationary frame. In general, a single resonant controller in  $d - q$  tuned at the frequency  $6k\omega_0$  is required to compensate for each pair of harmonics at  $(6k \pm 1)\omega_0$  with  $\{k \in \mathbb{N} | k \neq 0\}$ . For extremely unbalanced systems, (caused by severe faults) other harmonic components such as the  $+5\omega_0$ ,  $-7\omega_0$  and  $-\omega_0$  become important; therefore, the use of SOGIs and ROGIs in parallel becomes effective to control the MMC terminal during fault conditions while accomplishing the required total harmonic distortion (THD).

In addition to the controller presented in Fig. 5.2, the controller scheme illustrated in Fig. 5.4 is proposed to reduce the effect of voltage harmonics and unbalances in the  $abc$  frame. As illustrated, a ROGI tuned at  $-2\omega_0$  to compensate for  $-\omega_0$  and a SOGI tuned at  $\pm 6\omega_0$  to compensate for the  $-5\omega_0$  and  $+7\omega_0$  are combined. If required, multiple resonant controllers can be paralleled to achieve the required current THD. The combined action of the two resonant controllers is written as:

$$y^{dq} = \left[ \frac{2s}{s^2 + (6\omega_0)^2} + \frac{1}{s + j2\omega_0} \right] u^{dq} \quad (5.11)$$

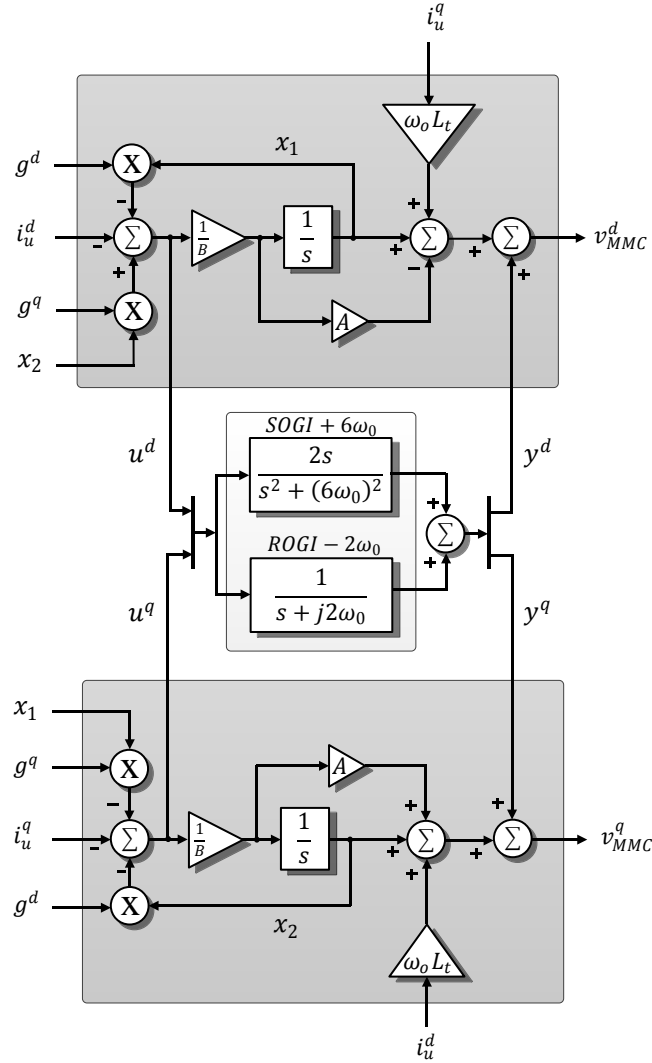


Fig. 5.4. Proposed control block diagram in the  $d$  and  $q$  axes with ROGI and SOGI controllers

### 5.3.3 Controller Parameter Selection

For the balanced and unbalanced cases, the pole location of (5.5) determines the stability and performance of the proposed controller. The gains  $A$  and  $B$  are calculated to accomplish a fast a reliable lock between the MMC terminal and the grid with current transients of minimal duration and magnitude. For the analysis, it is assumed that no reactive power flows between the MMC terminal and the grid, ergo  $g^q = 0$ . The stability of (5.5) is guaranteed when  $(L_t g^d + A) > 0$  and  $B > 0$ . Therefore, the value of  $A$  is calculated as:

$$A > \begin{cases} -L_t g^d & \text{Grid to MMC} \\ L_t g^d & \text{MMC to grid} \end{cases}, \quad \text{with } g^q = 0. \quad (5.12)$$

From (5.12), the gain  $A$  is function of the transformer equivalent inductance, the power flow direction and the magnitude of the injected current. From (5.7) the conductance  $g^d$  is determined as the ratio between the phase current and the grid phase voltage in the steady-state condition. With the operating conditions listed in Table 5.1, the conductance  $g^d$  varies between  $\pm 7.53 \text{ m}\Omega$ . In order to accomplish both conditions present in (5.12), the gain  $A$  is selected to be larger than  $|L_t g^d|$ . In the case of the gain  $B$ , smaller values reduce overcurrents caused by changes in the reference, and make the system's response time very fast since the poles' real component moves far from the origin. The variation of both  $A$  and  $B$  as functions of the maximum current overshoot when the  $\text{CB}_1$  in Fig. 5.1 is closed is illustrated in Fig. 5.5. As indicated, the gain  $A$  is selected to be  $3.16 \times 10^{-3}$  (i.e.,  $15L_t g^d$ ), whereas the gain  $B$  is calculated in such a way that the poles of the characteristic equation (5.5)  $\in \mathbb{R}$  and are located in the left-hand side of the  $s$ -plane, thus:

$$B < 64L_t(g^d)^2 \quad (5.13)$$

Table 5.1. System parameters [41]

Parameter	Nominal value
$P$	400 MW
$V_{dc}$	$\pm 200 \text{ kV}$
$V_g$	230 kV
$C_{SM}$	750 $\mu\text{F}$
$L$	7 mH
$f_{sw}$	1 kHz
$f$	60 Hz
$L_t$	28 mH (8%)
$R_g$	0.8 $\Omega$
$k_p$	$5 \times 10^{-12}$
$k_i$	$1.5 \times 10^{-8}$

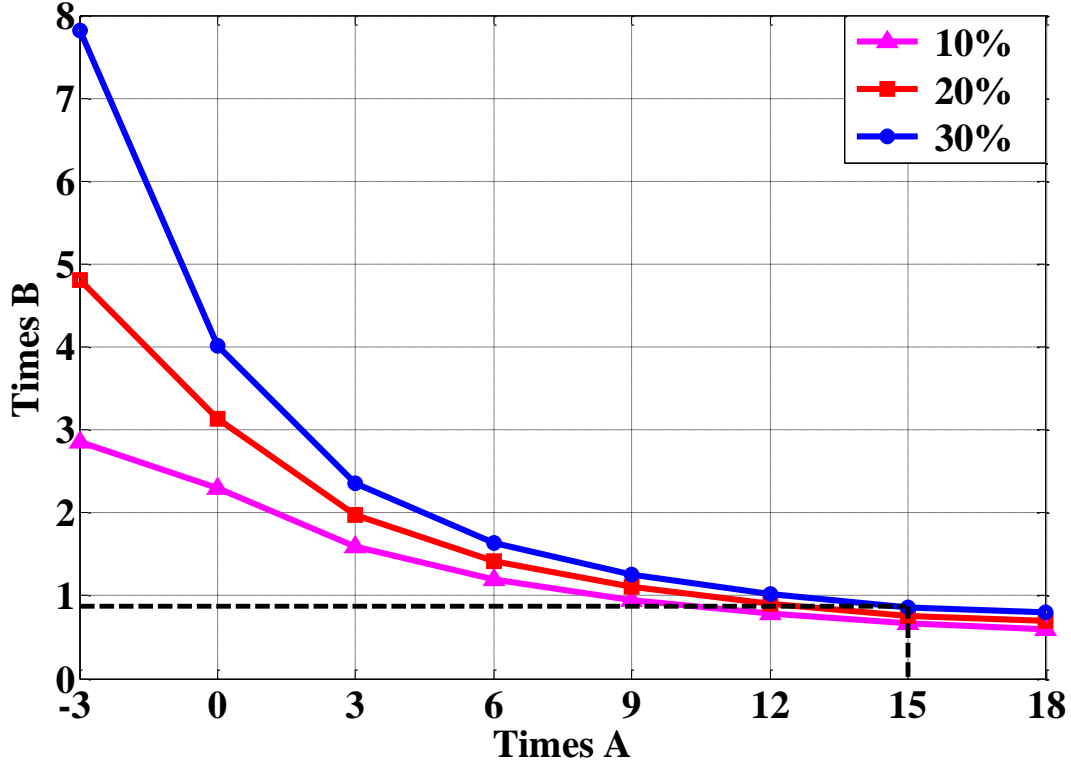


Fig. 5.5. Gains  $A$  and  $B$  variations for 10%, 20% and 30% current overshoots when  $CB_1$  is closed

With these considerations,  $B$  is calculated as  $0.1 \times 10^{-3}$  (i.e., 0.86 times  $64L_t g^d$ ). This assures safe operation when the MMC terminal locks onto the grid, keeping the current response settling time under 2.5 ms (one-quarter cycle) and a magnitude that does not exceed 30% of the MMC rated current when the grid voltage  $v_g$  is equal to its peak value.

#### 5.4 Proposed Controller Validation

To evaluate the performance of the proposed controller presented in Section III, the topology depicted in Fig. 5.1, with parameters listed in Table 5.1, is implemented in Matlab/Simulink™ and extensively evaluated in the time domain under ideal and non-ideal conditions such as voltage variations of the grid voltages, harmonic pollution, frequency changes and unbalanced

grid faults. The number of levels ( $N$ ) of the MMC per arm is eight (accomplishing a THD of 3.45%); MMC terminals in the field have a number of levels which could exceed 200, depending on the ratings of the power semiconductor devices and the rated voltage of the HVdc link [8]. The technique proposed in [23] is implemented for balancing the capacitor voltages. It is assumed that each SM capacitor is pre-charged at the average voltage  $V_{dc}/N$ . The time-step for the simulations is carefully selected as 10 us in order to observe transients during changes in the reference.

The estimated active and reactive powers in the  $dq$  reference frame are calculated as indicated in Fig. 5.3 as follows [34]:

$$\begin{aligned}\hat{P} &= \frac{3}{2}(\hat{v}_g^d i_u^d + \hat{v}_g^q i_u^q) \\ \hat{Q} &= \frac{3}{2}(-\hat{v}_g^d i_u^q + \hat{v}_g^q i_u^d).\end{aligned}\tag{5.14}$$

Each value is then compared with the commanded references,  $P_{ref}$  and  $Q_{ref}$ , respectively, to generate error signals, which are then processed through PI controllers whose outputs are  $g^d$  and  $g^q$ , respectively, as shown in Fig. 5.2. The gains for the PI controllers are listed in Table 5.1.

#### 5.4.1 Grid-Lock and Operation under Ideal Conditions

Normally, during the start-up process, a conventional PLL uses the information from voltage sensors located at the transformer secondary side to lock the MMC terminal onto the grid. In the case of the proposed controller, this information is not needed. Instead, the information is extracted from the current response and used to estimate the grid voltages. Once the circuit breaker  $CB_1$  is closed at  $t = t_0$ , current will flow in either direction due to the initial difference in the phase angle between the MMC output and grid voltages. The current change is used by the controller to extract the information of the grid angle and frequency, and estimate the magnitude



of the grid voltage  $v_g$ . The proper selection of the controller parameters  $A$  and  $B$  helps both the system bandwidth and the stability, as mentioned in Section III, as well as to reduce the time that it takes for the controller to bring the current transient down to zero, avoiding power semiconductor device damage due to overcurrents [25]. The three-phase waveforms for the grid voltages, MMC output voltages and grid currents during initial grid-lock are illustrated in the top, middle, and bottom of Fig. 5.6, respectively. When  $CB_1$  is closed at  $t_0 = 8.33$  ms, the current transient increases, reaching a maximum of 700 A, and is then brought down to zero in less than a quarter cycle. As indicated in Fig. 5.5, the gains  $A$  and  $B$  are selected so that the current never exceeds 130% of the MMC terminal maximum current; however, as the transformer equivalent series inductance opposes the change in current, the transient gets reduced, reaching a maximum of 50% of the peak rated current.

The MMC line-to-line voltages and grid currents during variations in the power references are shown in Fig. 5.7. Initially, the grid power factor (PF) is set to unity. At  $t = 140$  ms the active power flow is reversed from 200 MW (MMC injects power to the grid) to -200 MW (MMC draws power from the grid). Then at  $t = 170$  ms the active power is set to 100 MW. The sudden power flow reversal is performed to demonstrate the stability of the controller when power flows in both directions. As shown, there is no current or voltage overshoot during reference changes. At  $t = 200$  ms the grid PF is changed to 97% (lagging) to evaluate the decoupling between the axes controllers.

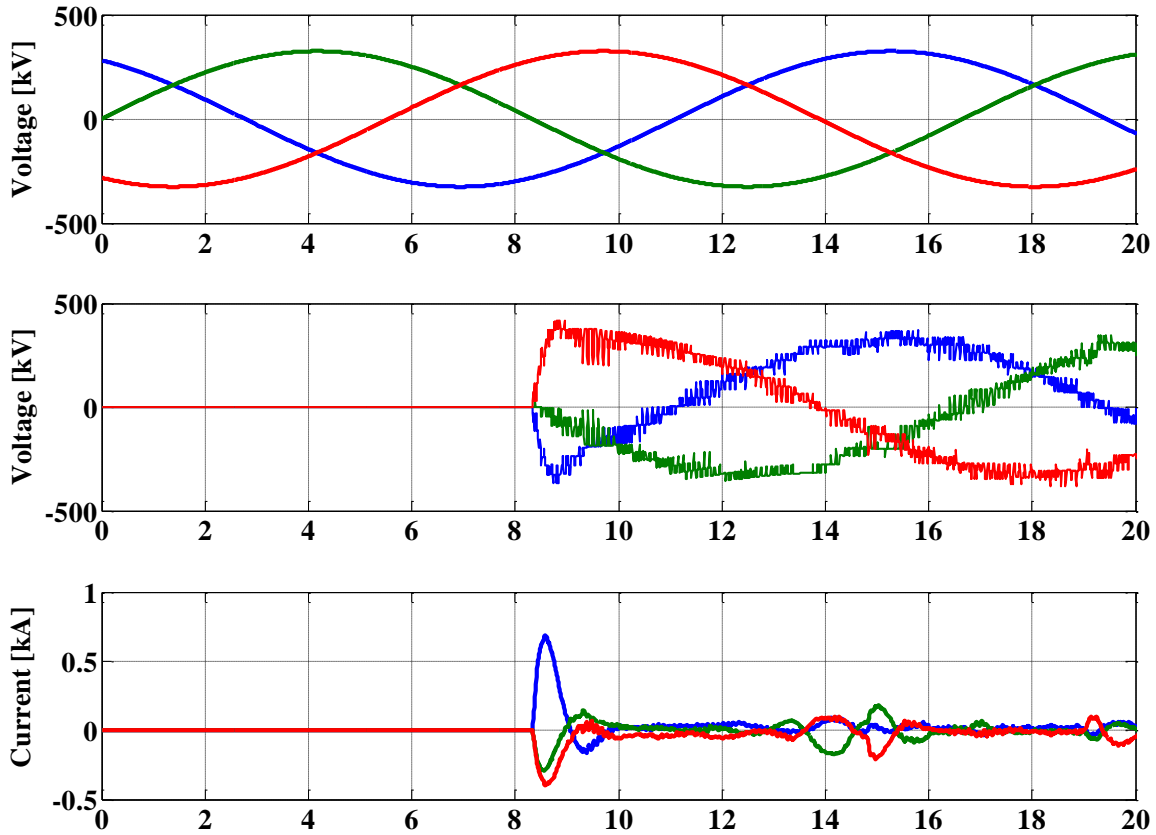


Fig. 5.6. Grid voltage (top), MMC output voltage (middle) and grid current during locking up for a time scale of 2 ms

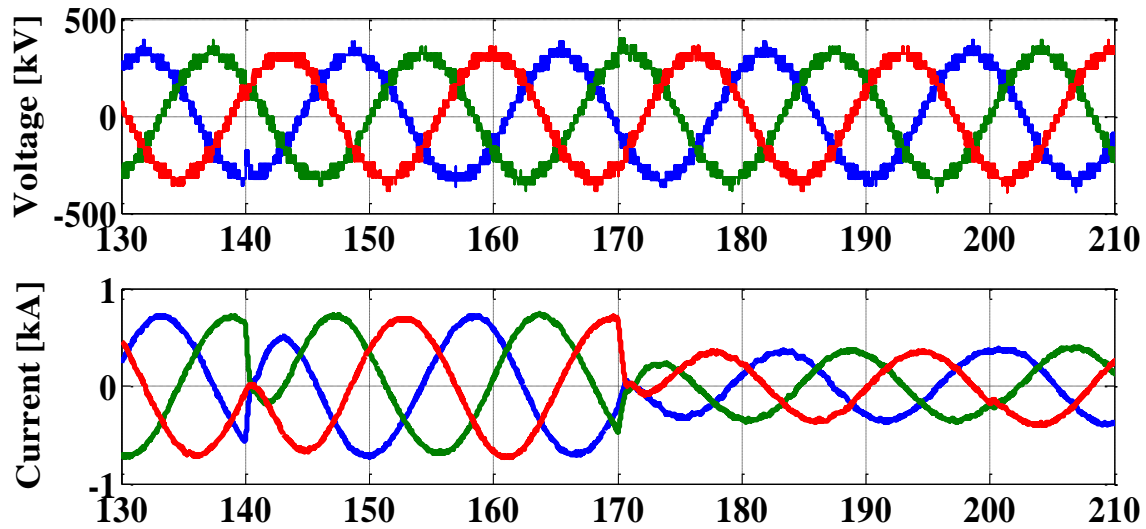


Fig. 5.7. MMC terminal line-to-line voltage (top) with  $2N+1$  number of levels and grid currents (bottom) under variations of the power references for a time scale of 10 ms

For the same condition, the commanded power reference (blue), the estimated active power (green) and the measured active power (red) are shown at the top of Fig. 5.8, whereas the reactive power is displayed at the bottom. The selected PI gains for the controller assure no overshoot and similar settling times; 6.3 ms for the active power and 6 ms for the reactive power. Increasing the PI gains will improve the response of the controller to changes in the reference, reducing the settling time. In return, an overcurrent that could damage the SM semiconductor devices will be present in each phase.

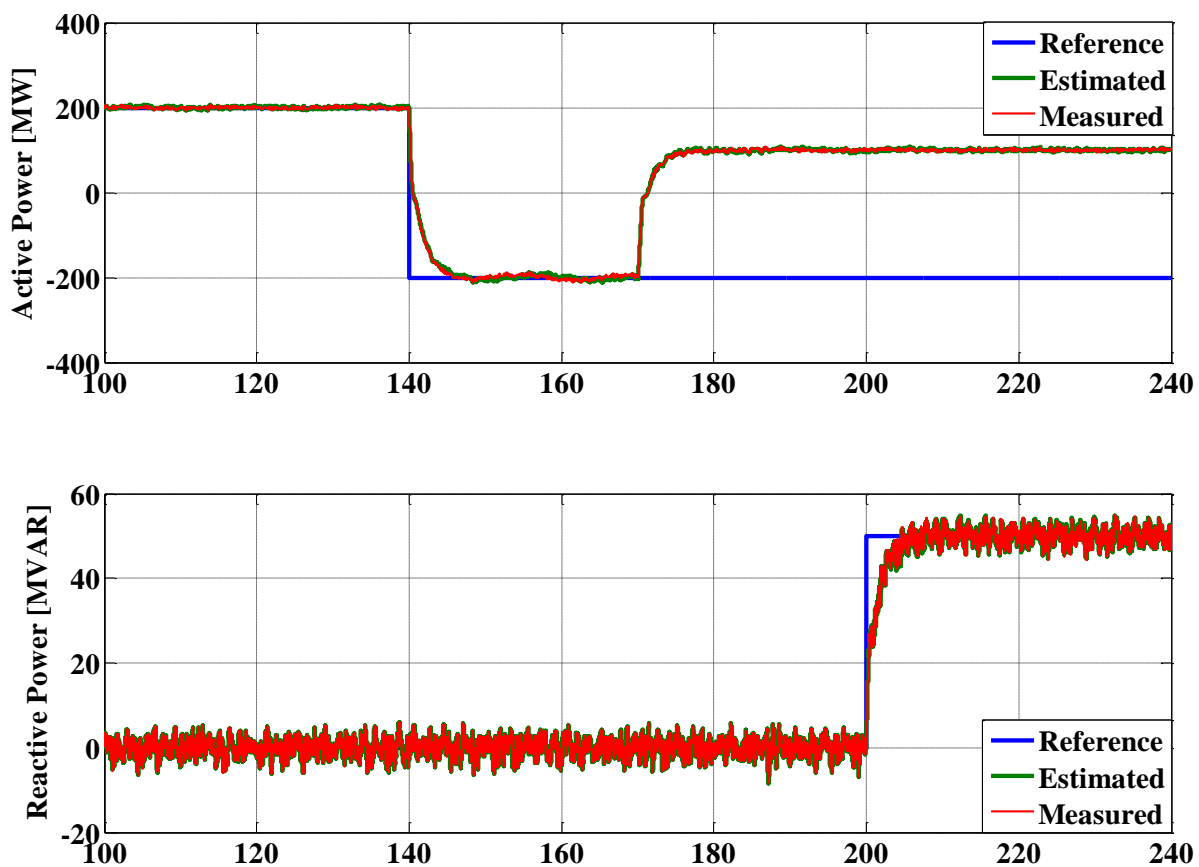


Fig. 5.8. Active power (top) and reactive power (bottom) under ideal grid conditions for a time scale of 20 ms

### 5.4.2 Harmonic-Voltage Pollution Condition

For voltages above 161 kV, IEEE Standard 519-1992 establishes that the voltage THD must be equal or less than 1.5% for the total voltage and equal or less than 1.0% for the individual voltage components. These maximum limits are exceeded for a time frame of 100 ms (250 ms to 350 ms) by considering the 5<sup>-th</sup>- and 7<sup>+th</sup>-order voltage harmonics (5% and 2% of the fundamental, respectively) to get a voltage THD of 5.39% as shown in Fig. 5.9. This is done with the purpose of evaluating the performance of the controller under severe distortion conditions. As illustrated in Fig. 5.9 (bottom), the injected currents are distorted since the controller is designed to track the estimated grid voltages.

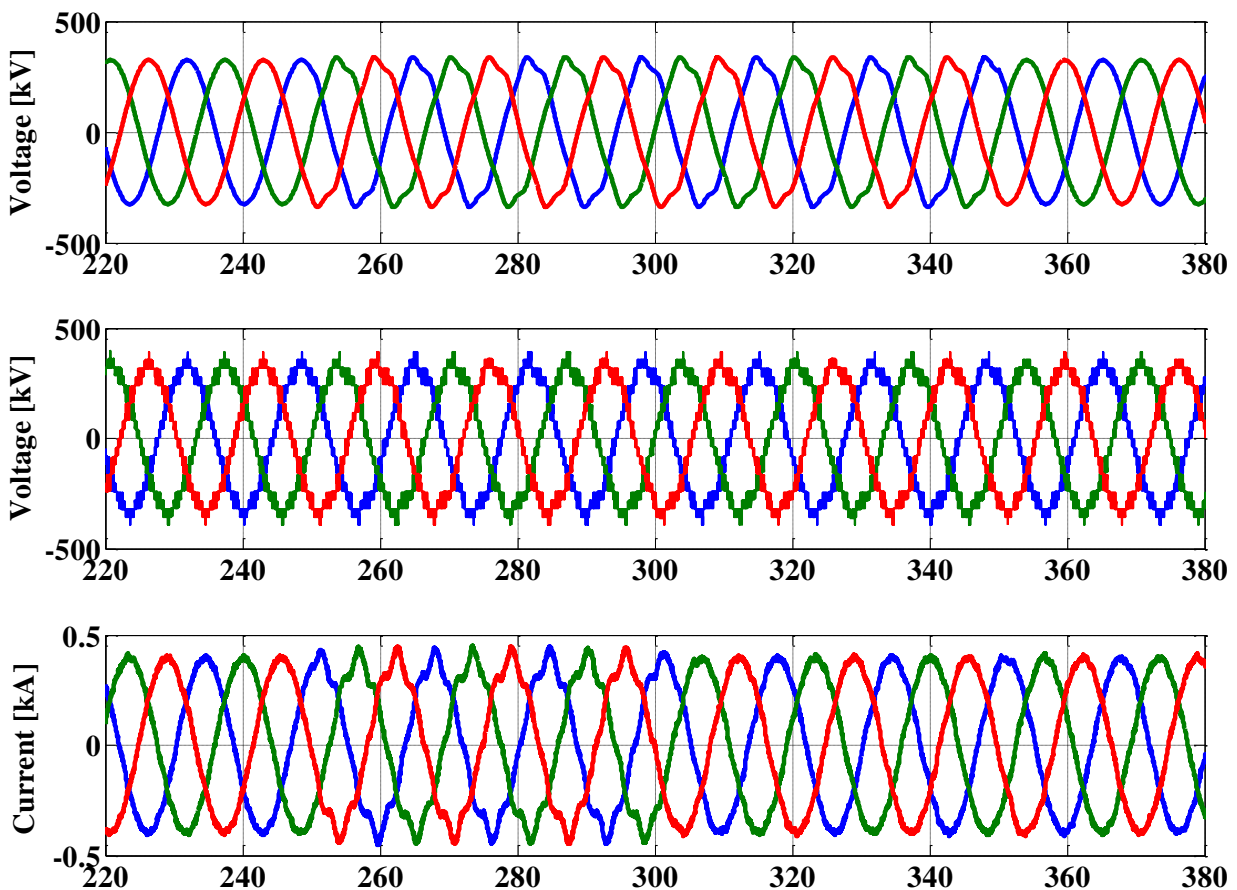


Fig. 5.9. Grid voltages (top), MMC output voltage (middle) and grid current (bottom) under harmonic pollution for a time scale of 20 ms

Between 250 ms and 300 ms the current THD is calculated as 8.28%, which exceeds the current distortion limits set in the IEEE Standard 519-1992 for grids with a short-circuit ratio lower than 50 and at this voltage level. The standard has more strict limits for lower short-circuit ratios at the point of common coupling.

At  $t = 300$  ms a SOGI tuned at  $+6\omega_0$  in the  $dq$  reference frame is introduced to reject the two harmonic current components providing zero steady-state errors for the 5<sup>th</sup>- and 7<sup>th</sup>-order voltage harmonics in the  $abc$  frame. Under this condition the current THD gets reduced to 1.67%. Thus, it is not required to add any additional filtering or control technique to cancel out harmonic effects. Having such a high requirement on the THD for this voltage level makes the controller feasible for interfacing with a HVac grid without any extra modifications to the proposed technique.

#### 5.4.3 Grid-Frequency Variation Condition

To evaluate the controller under grid-frequency variations, the grid frequency is changed from 60 Hz to 59 Hz at  $t = 410$  ms and then changed back to 60 Hz at  $t = 450$  ms. Furthermore, the active power injected into the grid increases from 200 MW to 400 MW at  $t = 420$  ms. From Fig. 5.10, there is no considerable difference between the estimated (green) and actual (red) active powers. Therefore, the proposed controller is able to keep injecting the commanded active power with minimum error during grid-frequency changes. Similar results are obtained when the grid frequency changes from 60 Hz to 61 Hz using the same time frame, which indicates the robustness of the proposed controller when the reactance changes around  $\pm 2\%$  its nominal value. Once the frequency returns to 60 Hz at  $t = 460$  ms, the controller has no transient during the frequency recovery.

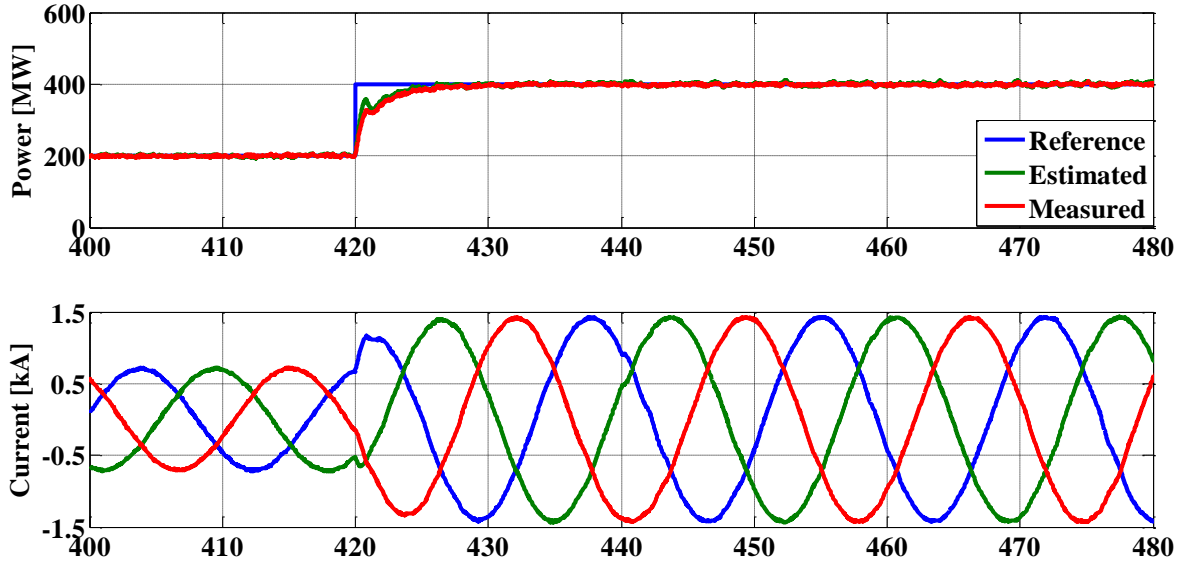


Fig. 5.10. Active power (top) grid currents (bottom) under grid-frequency variations for a time scale of 10 ms

#### 5.4.4 Grid Voltage-Magnitude Variation Condition

In this case, the grid voltage magnitude drops by 5% from  $t = 520$  ms to  $t = 620$  ms. During the voltage drop, the reference in the active power increases from 200 MW to 400 MW. The blue line at the top of Fig. 5.11 is the actual grid voltage and the green one is the estimated grid voltage  $\hat{v}_g^d$ . The middle graph shows the active power injected into the grid. The transients observed at  $t = 570$  ms and  $t = 620$  ms (with an 8.5% overshoot as the worst case scenario) are produced by the changes in the estimated grid voltages; however, the controller is able to keep tracking the active power reference.

Despite the overshoot observed in the estimated grid voltage  $\hat{v}_g^d$  during the change in the active power reference, no overshoots are present in the active power and current waveforms.

The estimated grid voltage  $\hat{v}_g^d$  for 5% voltage magnitude increase as shown at the top of Fig. 5.12. The blue line represents the actual grid voltage and the green line is the grid voltage estimated by the controller.

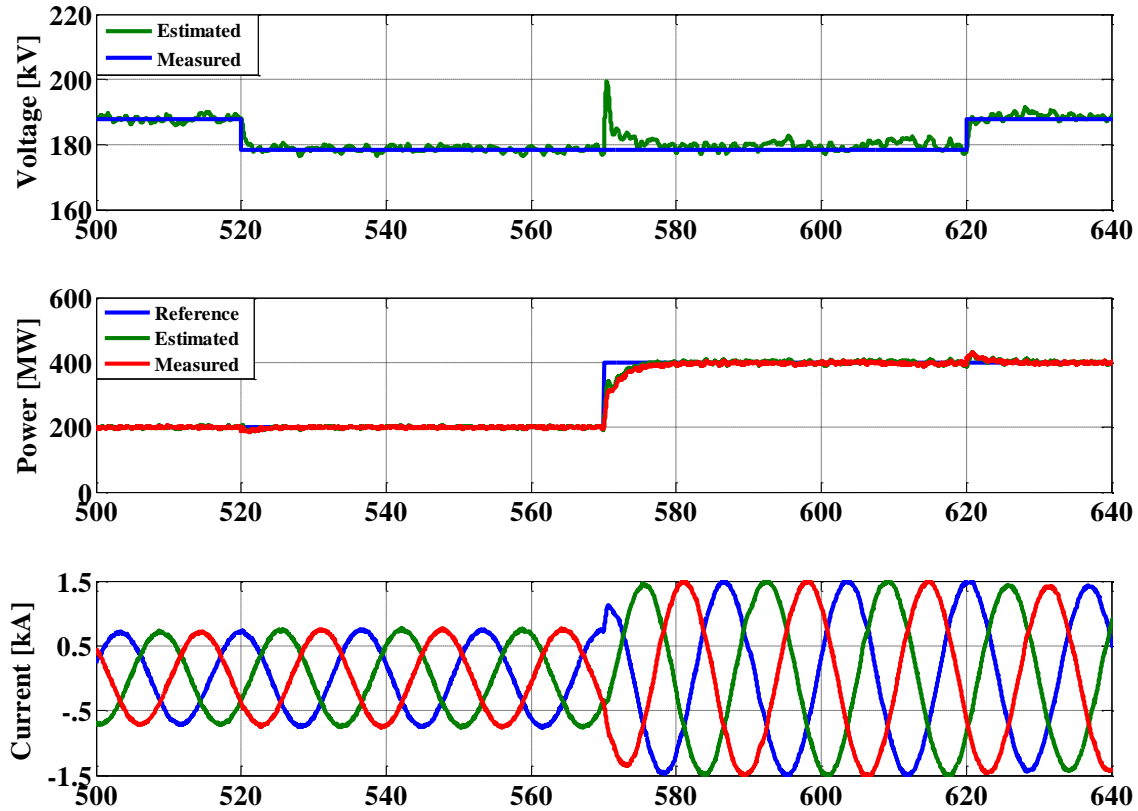


Fig. 5.11. Grid voltage decreases by 5%: voltage in the  $d$  axis (top), active power (middle) and grid currents (bottom) for a time scale of 20 ms

At  $t = 570$  ms, there is an increase in the active power reference that produces a 20% voltage overshoot on  $\hat{v}_g^d$ . Nevertheless, this overshoot does not cause any grid current or any active power overshoot. The middle graph presents the commanded active power reference (blue) and the active power estimated by the controller (green). The controller is able to follow the commanded reference and accurately detect when the grid voltage is increased. The bottom graph shows the currents injected into the grid. There are no transients when the grid voltage increases.

The previous results demonstrate the capability of the controller to accurately detect changes in the grid voltages without the use of any voltage sensors on the grid side. The controller is able to follow the commanded reference for the active power by increasing or decreasing the injected current to compensate for the grid voltage changes.

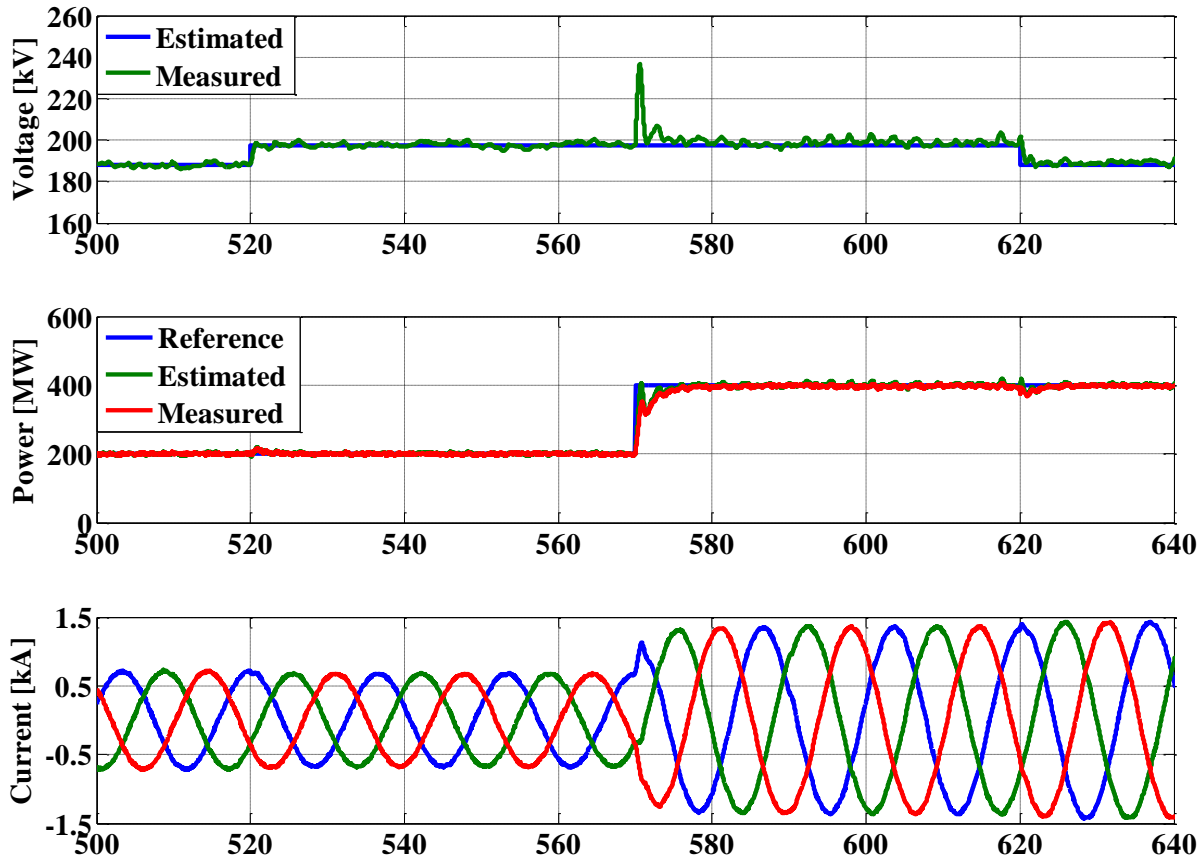


Fig. 5.12. Grid voltage increases by 5%: voltage in the  $d$  axis (top), active power (middle), grid currents (bottom) for a time scale of 20 ms

## 5.5 Conclusions

A sensorless control technique was proposed to independently control the active and reactive powers injected into a grid by a MMC-based HVdc terminal. The proposed control technique evaluated through Matlab/Simulink™ simulations under different grid voltage conditions was capable of maintaining system stability.

The proposed technique accurately detected grid voltage and frequency changes without sensing the grid voltages. When the grid frequency or voltage changed, there were no evident current transients that affected the controller normal operation since the system remained stable



and the commanded references were accurately tracked. In case of existing voltage sensors, the proposed controller can be implemented to increase reliability in case of voltage-sensor failure.

Resonant controllers in the  $d - q$  reference frame achieve double harmonic compensation in the stationary frame facilitating the injection of pure sinusoidal currents. The implementation of the SOGI tuned at  $-2\omega_0$  in the  $d - q$  reference frame mitigates the effect of the negative component at fundamental frequency due to unbalances. This helps to reduce the voltage ripple in the dc link.

Summarizing, the feasibility of the proposed control technique to synchronize and connect an MMC-based HVdc terminal with a grid was validated via Matlab/Simulink™ simulations. The proposed sensorless technique should reduce the implementation complexity of the MMC-terminal controller, and could also be implemented as a backup technique in case of sensor failure, increasing the reliability of the MMC terminal.

## References

- [1] E.K. Amankwah, J.C. Clare, P.W. Wheeler, A.J. Watson, "Multi carrier PWM of the modular multilevel VSC for medium voltage applications," in *Proceedings of the 27<sup>th</sup> IEEE Applied Power Electronics Conference and Exposition, APEC 2012*, pp. 2398–2406, February, 2012.
- [2] R. Adapa, "High-wire act: HVdc technology: The state of the art," in *Proceedings of the IEEE Power and Energy Magazine*, vol. 10, no. 6, pp. 18–29, November, 2012.
- [3] R. Feldman, M. Tomasini, E. Amankwah, J.C. Clare, P.W. Wheeler, D.R. Trainer, R.S. Whitehouse, "A hybrid modular multilevel voltage source converter for HVDC power transmission," *IEEE Transactions on Industry Applications*, vol. 49, no. 4, pp. 1577–1588, July-August, 2013.
- [4] O. Vestergaard, B. Westman, G. McKay, P. Jones, J. Fitzgerald, B. Williams, "HVDC - Enabling the transition to an energy system based on renewables," in *Proceedings of the 9<sup>th</sup>*

- IEEE International Conference on AC and DC Power Transmission*, pp. 1–6, October, 2010.
- [5] D. Jovicic, N. Strachan, “Offshore wind farm with centralised power conversion and DC interconnection,” in *Proceedings of the IEEE Generation, Transmission & Distribution*, IET, vol. 3, no. 6, pp. 586–595, June, 2009.
- [6] L. Zhang, L. Harnefors, H.P. Nee, “Modeling and control of VSC-HVDC links connected to island systems,” *IEEE Transactions on Power Systems*, vol. 26, no. 2, pp. 783–793, May, 2011.
- [7] —, “Interconnection of two very weak AC systems by VSC-HVDC links using power-synchronization control,” *IEEE Transactions on Power Systems*, vol. 26, no. 1, pp. 344–355, February, 2011.
- [8] J. Graham, G. Bileedt, J. Johansson, “Power system interconnections using HVDC links,” in *Proceedings of the IX Symposium of Specialists in Electric Operational and Expansion Planning*, May, 2003, [Online]. Available: [http://library.abb.com/GLOBAL/SCOT/SCOT289.nsf/VerityDisplay/98CD010BE5F77419C1256EA6002BD87A/\\$File/Interconnections%20HVDC%20web.pdf](http://library.abb.com/GLOBAL/SCOT/SCOT289.nsf/VerityDisplay/98CD010BE5F77419C1256EA6002BD87A/$File/Interconnections%20HVDC%20web.pdf). [Accessed July 2014].
- [9] N. Ahmed, A. Haider, D. Van Hertem, L. Zhang; H.-P. Nee, “Prospects and challenges of future HVDC SuperGrids with modular multilevel converters,” in *Proceeding of the 14<sup>th</sup> IEEE European Conference on Power Electronics and Applications*, EPE 2011, pp. 1–10, August-September, 2011.
- [10] R. Marquardt, “Stromrichterschaltungen Mit Verteilten Energiespeichern,” German Patent DE10103031A1, January 24, 2001.
- [11] A. Lesnicar, R. Marquardt, “An innovative modular multilevel converter topology suitable for a wide power range,” in *Proceedings of the IEEE Power Tech Conference*, vol. 3, pp. 1–6, June, 2003.
- [12] B. Gemmell, J. Dorn, D. Retzmann, D. Soerangr, “Prospects of multilevel VSC technologies for power transmission,” in *Proceedings of the IEEE Transmission and Distribution Conference and Exposition*, IEEE/PES 2008, pp. 1–16, April, 2008.

- [13] N. Flourentzou, V.G. Agelidis, G.D. Demetriades, "VSC-Based HVDC power Transmission systems: An overview," *IEEE Transactions on Power Electronics*, vol. 24, no. 3, pp. 592–602, March, 2009.
- [14] H.-J. Knaak, "Modular multilevel converters and HVDC/FACTS: A success story," in *Proceedings of the 14<sup>th</sup> IEEE European Conference on Power Electronics and Applications*, EPE 2011, pp. 1–6, August-September, 2011.
- [15] M. Glinka, R. Marquardt, "A new AC/AC multilevel converter family," *IEEE Transactions on Industrial Electronics*, vol. 52, no. 3, pp. 662–669, June, 2005.
- [16] J. Strauss, "MMC design aspects and applications," [Online]. Available: [http://www.ptd.siemens.de/CIGRE\\_MMC\\_DesignAspects.pdf](http://www.ptd.siemens.de/CIGRE_MMC_DesignAspects.pdf). [Accessed July 2014].
- [17] M. Glinka, "Prototype of multiphase modular-multilevel-converter with 2 MW power rating and 17-level-output-voltage," in *Proceedings of the 35<sup>th</sup> IEEE Annual Power Electronics Specialists Conference*, PESC 2004, vol. 4, pp. 2572–2576, June, 2004.
- [18] G. Congzhe, X. Jiang, Y. Li, Z. Chen, J. Liu, "A DC-link voltage self-balance method for a diode-clamped modular multilevel converter with minimum number of voltage sensors," *IEEE Transactions on Power Electronics*, vol. 28, no. 5, pp. 2125–2139, May, 2013.
- [19] A. Timbus, M. Liserre, R. Teodorescu, P. Rodriguez, F. Blaabjerg, "Evaluation of current controllers for distributed power generation systems," *IEEE Transactions on Power Electronics*, vol. 24, no. 3, pp. 654–664, March, 2009.
- [20] M. Hagiwara, H. Akagi, "Control and experiment of pulsewidth-modulated modular multilevel converters," *IEEE Transactions on Power Electronics*, vol. 24, no.7, pp. 1737–1746, July, 2009.
- [21] M.A. Pérez, J. Rodríguez, E.J. Fuentes, F. Kammerer, "Predictive control of AC–AC modular multilevel converters," *IEEE Transactions on Industrial Electronics*, vol. 59, no. 7, pp. 2832–2839, July, 2012.
- [22] M. Hagiwara, R. Maeda, H. Akagi, "Control and analysis of the modular multilevel cascade converter based on double-star chopper-cells (MMCC-DSCC)," *IEEE Transactions on Power Electronics*, vol. 26, no. 6, pp. 1649–1658, June, 2011.

- [23] Q. Tu, Z. Xu, L. Xu, "Reduced switching-frequency modulation and circulating current suppression for modular multilevel converters," *IEEE Transactions on Power Delivery*, vol. 26, no. 3, pp. 2009–2017, July, 2011.
- [24] T. Noguchi, H. Tomiki, S. Kondo, I. Takahashi, "Direct power control of PWM converter without power-source voltage sensors," *IEEE Transactions on Industry Applications*, vol. 34, no. 3, pp. 473–479, May-June, 1998.
- [25] I. Agirman, V. Blasko, "A novel control method of a VSC without AC line voltage sensors," *IEEE Transactions on Industry Applications*, vol. 39, no. 2, pp. 519–524, March-April, 2003.
- [26] Y.A.-R.I. Mohamed, E.F. El-Saadany, M.M.A. Salama, "Adaptive grid-voltage sensorless control scheme for inverter-based distributed generation," *IEEE Transactions on Energy Conversion*, vol. 24, no. 3, pp. 683–694, September, 2009.
- [27] M. Saeedifard, R. Iravani, "Dynamic performance of a modular multilevel back-to-back HVDC system," *IEEE Transactions on Power Delivery*, vol. 25, no. 4, pp. 2903–2912, October, 2010.
- [28] Y. Zhou, D. Jiang, J. Guo, P. Hu, Y. Liang, "Analysis and control of modular multilevel converters under unbalanced conditions," *IEEE Transactions on Power Delivery*, vol. 28, no. 4, pp. 1986–1995, October, 2013.
- [29] Q. Tu, Z. Xu, Y. Chang, L. Guan, "Suppressing dc voltage ripples of MMC-HVDC under unbalanced grid conditions," *IEEE Transaction on Power Delivery*, vol. 27, no. 3, pp. 1332–1338, July, 2012.
- [30] Z. Li, P. Wang, Z. Chu, H. Zhu, Y. Luo, Y. Li, "An inner current suppression method for modular multilevel converters," *IEEE Transactions on Power Electronics*, vol. 28, no. 11, pp. 4873–4879, November, 2013.
- [31] C.A. Busada, S. Gomez, A.E. Leon, "Current controller based on reduce order generalized integrators for distributed generation systems," *IEEE Transactions on Industrial Electronics*, vol. 59, no. 7, pp. 2898–2909, July, 2012.
- [32] J. Gomez, C.A. Busada, J.A. Solsona, "Frequency-adaptive current controller for three-phase grid-connected converters," *IEEE Transactions on Industrial Electronics*, vol. 60, no. 10, pp. 4169–4177, October, 2013.

- [33] M. Liserre, R. Teodorescu, F. Blaabjerg, "Multiple harmonics control for three-phase grid converter systems with the use of PI-RES current controller in a rotating frame," *IEEE Transactions on Power Electronics*, vol. 21, no. 3, pp. 836–841, May, 2006.
- [34] A. Yazdani and R. Iravani, "Space phasors and two-dimensional frames" in *Voltage-Sourced Converters in Power Systems - Modeling, Control and Applications*, 1<sup>st</sup> Edition, Wiley, 2011, chapter 4, pp. 69–114.
- [35] M.P. Kazmierkowski, L. Malesani, "Current control techniques for three-phase voltage-source PWM converters: a survey," *IEEE Transactions on Industrial Electronics*, vol. 45, no. 5, pp. 691–703, October, 1998.
- [36] M. Guan, Z. Xu, "Modeling and control of a modular multilevel converter-based HVDC system under unbalanced grid conditions," *IEEE Transactions on Power Electronics*, vol. 27, no. 12, pp. 4858–4867, December, 2012.
- [37] A. Escobar, J.C. Balda, C. A. Busada, and D. Christal, "An indirect matrix converter for CCHP microturbines in data center power systems," in *Proceedings of the 34<sup>th</sup> IEEE International Telecommunications Energy Conference*, pp. 1–6, October, 2012.
- [38] A. Yazdani, R. Iravani, "A unified dynamic model and control for the voltage-sourced converter unbalanced grid conditions," *IEEE Transactions on Power Delivery*, vol. 21, no. 21, pp. 1620–1629, July, 2006.
- [39] X. Yuan, W. Merk, H. Stemmler, J. Allmeling, "Stationary-frame generalized integrators for current control of active power filters with zero steady-state error for current harmonics of concern under unbalanced and distorted operating conditions," *IEEE Transactions on Industry Applications*, vol. 38, no. 2, pp. 523–532, March/April, 2002.
- [40] P. Rodriguez, A. Luna, I. Candela, R. Teodorescu, F. Blaabjerg, "Grid synchronization of power converters using multiple second order generalized integrators," in *Proceedings of the 34<sup>th</sup> IEEE Annual Conference in Industrial Electronics, IECON 2008*, pp. 755–760, November, 2008.
- [41] Inter-American Development Bank "Colombia-Panama Interconnection" [Online] Available: <http://www.iadb.org/en/projects/project-description-title,1303.html?id=rs%2Dt1241> [Accessed: July 2014].



**Department of Electrical Engineering**

1 University Avenue, 3217 Bell Engineering Center, Fayetteville, AR 72701, (479) 575-3005, (479) 575-7967 (fax)

August 3, 2014

To whom it may concern,

This letter is to verify that Mr. Andrés Escobar Mejía, ID number: 010533274, is the first author and did at least 51% of the work for the paper titled "A SENSORLESS GRID SYNCHRONIZATION METHOD FOR MODULAR MULTILEVEL CONVERTERS IN HVDC SYSTEMS".

Kind Regards,

Dr. Juan Carlos Balda

University Professor and Major Advisor to Mr. Escobar Mejía

Department Head

## CHAPTER SIX

### CONCLUSIONS AND SUGGESTIONS FOR FUTURE WORK

#### 6.1 Conclusions

Besides the conclusions provided at the end of each chapter, the activities in this doctoral dissertation have also led to the following novel conclusions:

##### *6.1.1 BBC and IMC Efficiency Comparison*

An analytical comparison between the BBC and the IMC in terms of conduction and switching losses was presented in Chapter Two. As indicated in Figure 2.3, the efficiency of both converters was about 98.34% for a switching frequency of 10 kHz. Above this frequency the IMC becomes more efficient. For instance, at 40 kHz its efficiency was about 97.52% whereas the BBC had an efficiency of 95.84%. Despite the fact that the number of semiconductor devices in the rectifier stage doubles, its ability to switch under zero current is beneficial at high switching frequencies. Analysis showed that the switching losses of the BBC rectifier stage at 40 kHz account for 17% of the total converter losses.

From this analysis it can be concluded that wide bandgap devices such as SiC MOSFETs are more attractive for IMC realizations since they have superior thermal properties. This allows high switching frequencies while reducing the requirements for thermal management systems. Results also show that the IMC could be used as a standard PEI for small-scale DG units, such as microturbines connected to a 480 V bus in a data center.

### 6.1.2 IMC New Sensorless Controller

A new method to synchronize a microturbine-based DG unit to the power grid was introduced in Chapter Two. As shown in Figure 2.5, the method was developed in the  $d - q$  frame and did not require the implementation of voltage sensors. Instead, the information from current sensors was used to accurately estimate the grid conditions to regulate the active power injected into the grid. Simulation results in the time domain validated the proposed controller for different operating conditions. As illustrated in Figure 2.6, the settling time was around 7 ms and the current overshoot is under 25% when the reference changed from zero to its rated value. No significant changes in the reactive power were detected, indicating the ability of the proposed sensorless algorithm to decouple the  $d$  and  $q$  reference frames. As shown in Figure 2.8, there was a 5% and 24% overshoots in two of the output phase currents when the converter locked onto the grid. The magnitude and duration of the overshoots are function of the instantaneous values of the grid voltages at the instant the connection is made and the series inductor, along with the time that the controller took to identify the grid voltages. When the commanded current reference changed in  $t=50$  ms, the current overshoot was 12% for one of the phases.

### 6.1.3 IMC in Boost Operation Mode

The IMC operating in the “reverse”<sup>1</sup> configuration is presented in Chapter Three. As illustrated in Figure 3.1, this configuration allowed operation of the IMC in the boost mode, overcoming the voltage ratio limitation typical of MCs.

A laboratory test setup comprising of a 5 kVA Si IGBT-based VSC (generating 50 Vrms at 100 Hz) and a 5 kVA SiC JFET-based IMC (accomplishing a power density of 5.7 kVA/liter)

---

<sup>1</sup> Initially proposed for grid-connected DG units in [1].



operating in the reverse configuration was built to experimentally validate the sensorless controller. The IMC comprises of four stages: the CSI and VSR power stage, input and output filters, gate driver board and DSP-based control board. The guidelines presented in [2] were followed to minimize power stage trace parasitic inductances that may lead to harmful overvoltages across the SiC devices.

The selection of the switching frequency  $f_{sw}$  was a compromise between the IMC efficiency and size, and the DSP processing time. From the power semiconductor device point of view,  $f_{sw}$  may be selected according to the maximum power that the device is able to dissipate without exceeding its maximum junction temperature; theoretically the SiC JFET can be switched up to 500 kHz without damage. Similar Si-based semiconductor devices (e.g., IGBTs) are usually switched up to 8 kHz in the case of medium-power converters and less than 3 kHz for high-power converters. Considering that the control algorithm runs in 35  $\mu$ s and that the IMC becomes more efficient than the BBC for frequencies above 10 kHz, as demonstrated in [3], the  $f_{sw}$  is selected as 30 kHz, allowing the control algorithm to run in one switching period, while leaving a 5  $\mu$ s dead-time to compensate for any delays in the execution of the algorithm.

A method to accurately calculate the controller parameters  $A$  and  $B$  (forward direct and indirect gain respectively) was presented to synchronize the DG unit and the grid in the Chapter Three. The proper selection of the controller gains were calculated to minimize the duration of current transients (i.e., less than 20% as illustrated in Figure 3.5), achieve a fast and reliable lock with the DG unit, and guaranteeing system stability during steady-state operation (the poles of the characteristic equation (3.3) were located in the left-hand side of the  $s$ -plane). It was established that a good practice is to select values of  $A$  to be larger than  $|Lg|$  since both generation and motor conditions are included above this limit. The selection of the gain  $B$  determines the

location of the zero in the controller transfer function. Small values for this gain reduce overcurrents caused by the change in the reference, but cause the zero to move far from the origin, thus making the system's response time very slow.

As expected, the boost inductor (input inductor) plays an important role in the performance of the IMC in terms of boost ratio, input current harmonic content and switching frequency. According to the results presented in Figure 3.6, it was established that to guarantee a current waveform THD within the IEEE 519 limits, the input inductor must be selected between 0.7 p.u ( $f_{sw} = 10$  kHz) and 0.2 p.u ( $f_{sw} = 40$  kHz).

The experimental results presented in Figure 3.7 and Figure 3.8 proved the effectiveness of the proposed controller and the ability of the IMC to boost the voltage to 75 Vrms (50% boost). Even though the inverter and the rectifier stages were synchronized to switch the latter under zero current, errors associated with delays caused small currents to flow in the dc-link during this state. The inherent  $di/dt$  of these currents interacting with the partial parasitic inductances of the current path in the IMC power stage caused spikes in the virtual dc-link. The duration and magnitude of these spikes are determined by volt-seconds applied to these partial inductances over the switching period.

One advantage for this sensorless controller is that it can be used as a back-up control strategy in the case of DG unit output voltage sensor failure.

#### *6.1.4 New PEI Involving the IMC*

In Chapter Four, the IMC was combined with MMCs and MF-XFMRs interfaces (as given in Figure 4.1) to develop a new bidirectional ac-ac PEI topology, demonstrating further that the IMC could be a standard PEI for particular applications where space is a constraint.

A practical application was identified to show the potential feasibility of the proposed PEI. As shown in Figure 4.3, the new PEI could be used to deliver electric power to future oils and gas subsea facilities. To this end, the potential advantages of the involved stages were described. The size requirements of the MMC capacitance and arm inductance were evaluated for different fundamental frequencies. From an analysis of the Figure 4.4, the capacitor size in each SM was significantly reduced when the MMC fundamental frequency increased from 60 Hz to 1 kHz. The same analysis was performed for the MF-XMFR. The results showed that among amorphous, ferrite and nanocrystalline materials, amorphous demands less space for different fundamental frequencies. For the considered case study, the target was to achieve a 90% system efficiency. Under this consideration, the fundamental frequency in the MF-XMFR was set to 250 Hz, which led to a 76% reduction in the capacitance requirements in the MMC terminal and 71.64% reduction in the transformer volume when compared to a transformer operating at a fundamental frequency of 60 Hz. At a fundamental frequency of 500 Hz the capacitor size is reduced up to 88% and the transformer volume up to 66%. However, the penalty was a 2.24% reduction in the desired efficiency at the system level.

#### *6.1.5 Proposed Sensorless Controller for a High Power Rating Converter*

The sensorless controller proposed in the Chapter Two was successfully extended to a 400 MW,  $\pm 200$  kV MMC-based HVdc terminal in Chapter Five. Two new functionalities were added to this controller. First, the controller was capable of regulating the reactive power flows between

the dc and ac grids. Second, resonant controllers were added to counteract the effect of grid imbalances. The controller was extensively simulated in the time domain for different operating points. The results illustrated that the current transient during the initial synchronization reached a maximum of 700 A and then reduced to zero in less than a quarter cycle. The  $di/dt$  was calculated as  $3.5 \times 10^{-3}$  A/ $\mu$ s, which is much smaller than the maximum change in current that a commercially available 6.5kV, 800A IGBT can withstand (3200 A/ $\mu$ s). Disturbances such as grid frequency and voltage variations were introduced to validate the controller robustness during severe grid conditions. The results indicated that no large current transients were present during the initial grid synchronization or changes in the power reference.

## 6.2 Recommendations for Future Work

The following improvements are suggested for future work:

- Explore increasing the IMC switching frequency by improving the control board architecture. The DSP must execute the analog-to-digital conversion process as well as the closed-loop control algorithm within one switching period to avoid errors in the gate driver signals. An FPGA that performs the lower level functions (e.g., generating the space vector) in conjunction with the DSP, which perform the main control algorithm, can be used to enable higher switching frequencies and increase functionalities (e.g., temperature sensing), of the entire system [4].
- Reduce computational overhead of the proposed sensorless controller by moving it from the rotating  $d - q$  frame to the stationary  $\alpha - \beta$  reference frame. This eliminates the need to transform the sensed signals, and anti-transform the generated control signals, reducing the

computational time per sample [5]. This might lead to an increase in the switching frequency.

- Explore the capability of the IMC operating in the “reverse” configuration to overcome grid disturbances such as voltage sags.
- Analyze the performance of the proposed PEI for motor drives under different operating conditions such as regeneration during motor deceleration, startup and torque variations.
- Evaluate the power density of the IMC considering input and output filters for different switching frequencies.

## References

- [1] X. Liu, P. C. Loh, P. Wang, F. Blaabjerg, Y. Tang, E.A. Al-Ammar, “Distributed generation using indirect matrix converter in reverse power mode,” *IEEE Transactions on Power Electronics*, vol. 28, no. 3, pp. 1072–1082, March 2013.
- [2] C. Stewart, A. Escobar-Mejia, J.C. Balda, “Guidelines for developing power stage layouts using normally-off SiC JFETs based on parasitics analysis,” in *Proceedings of the IEEE Energy Conversion Congress and Exposition, ECCE 2013*, pp. 948–955, September, 2013.
- [3] A. Escobar, J.C. Balda, C.A. Busada, D. Christal, “An indirect matrix converter for CCHP microturbines in data center power systems,” in *Proceedings of the IEEE 34<sup>th</sup> International Telecommunications Conference, INTELEC 2012*, pp. 1–6, October, 2012.
- [4] S.-H. Hwang, X. Liu, J.-M. kim, H. Li, “Distributed digital control of modular-based solid-state transformer using DSP+FPGA,” *IEEE Transactions on Industrial Electronics*, vol. 60, no. 2, pp. 670–680, February, 2013.
- [5] C.A. Busada, J.S. Gomez, A.E. Leon, J.A. Solsona, “Current controller based on reduced order generalized integrators for distributed generation systems,” *IEEE Transactions on Industrial Electronics*, vol. 59, no. 7, pp. 2898–2909, July, 2012.